Optical Amplification for Terabit-per-Second Ultra-high Speed Communication Systems

Zohreh Lali-Dastjerdi

Ph. D. Thesis

August 2013

DTU Fotonik
Department of Photonics Engineering

Optical Amplification for Terabit-per-Second Ultra-High Speed Communication Systems

Ph.D. Thesis

Zohreh Lali-Dastjerdi

August 2013

DTU Fotonik
Department of Photonics Engineering

DTU Fotonik
Department of Photonics Engineering
Technical University of Denmark
Building 343
DK-2800 Kgs. Lyngby
Denmark

Abstract

The present thesis is concerned with fiber optical parametric amplification and regeneration for high-speed optical communication systems. Fiber optical parametric amplifiers (FOPAs) have multi-functional applications depending on their implementation in optical systems. Based on a few femtosecond amplification response time and flexible operation spectral range, FOPAs are able to simultaneously operate as amplifiers and all-optical signal processors in high-speed Tbaud networks. In this thesis, we study the performance of FOPAs in detail in the linear and nonlinear (saturated) regimes where they can be utilized as all-optical regenerators. The optical gain and amplitude regeneration properties of FOPAs are investigated for monochromatic waves, short optical pulses and data modulated signals up to 640 Gbit/s.

In the fundamental study part of the thesis, an original physical explanation behind an observed asymmetry in gain saturated single-pump FOPAs is presented. The proposed theory is able to explain the origin of gain asymmetries in single-pump FOPAs based on the interplay between third-order dispersion and radiation of dispersive waves in the saturation regime. Furthermore, it predicts the strength of the asymmetric gain in saturated single-pump FOPAs.

Pump-to-signal intensity noise transfer has been recognized as one of the major noise sources in FOPAs as it leads to modulation of the signal gain. The conversion of intensity noise from pump to signal is quantified in detail in terms of modulation frequency and saturation effect in order to assess the degradation of the amplified signal. In a very good agreement with the performed experiments, it is shown that the noise transferred to the signal can be effectively suppressed by operating in the saturation regime.

The amplification of short few picosecond and subpicosecond optical pulses is explored using the chirped-pulse amplification scheme in FOPAs. The dynamics of the chirped-pulse amplification and pulse distortion are studied for differently chirped few-picosecond pulses in transition between the linear and the nonlinear regime. Amplification of short

pulses compatible with Tbaud systems is experimentally carried out for the first time where 400 fs pulses are amplified in a single-pump FOPA.

Finally, the first experimental demonstrations of the performance of FOPAs both in long transmission links as well as in high-capacity systems are presented in the last part of this thesis. FOPAs are cascaded as in-line amplifiers using a recirculating loop transmission and error-free transmission of 40 Gbit/s is successfully achieved. On the other hand, error-free parametric amplification for high serial data rates on a single-wavelength channel is demonstrated for an optical time division multiplexed signal at 640 Gbit/s with no power penalty. At last, all-optical phase-preserving amplitude regeneration based on a saturated-FOPA at 640 Gbit/s is demonstrated for phase modulated signals.

Resumé

Denne afhandling fokuserer på fiber optiske parametriske forstærkere samt regeneration i højhastigheds optiske kommunikations systemer. Fiber optiske parametriske forstærkere (FOPA) kan benyttes til adskillige applikationer baseret på hvorledes de implementeres i et optisk kommunikations system. Med afsæt i femto sekund forstærkningsresponsen samt deres fleksible spektrale operationsområde, kan FOPAer benyttes samtidigt både som forstærkere samt som optiske signal processorer i højhastigheds Tbaud netværk. I denne afhandling vil vi studere ydelsen af FOPAer i detaljer, både i det lineære samt i det ikke-lineære mættede område hvor de benyttes som rent optiske regeneratorer. Den optiske forstærkning samt amplitude regenererings egenskaberne af FOPAer bliver undersøgt for monokromatiske bølger, korte optiske pulser samt data modulerede signaler op til 640 Gbit/s.

I det grundlæggende teoristudie i denne afhandling vil en ny fysisk forklaring af den observerede forskel i det mættede forstærkningsspektrums opførsel for en enkelt-pumpe FOPA blive præsenteret samt sammenlignet med den konventionelle fasetilpasnings beskrivelse. Den foreslåede teori kan forklare årsagen til asymmetrien i forstærkningsprofilen for enkelt-pumpe FOPAer som et sammenspil mellem tredje ordens dispersion samt udstråling af dispersive bølger i det mættede område. Desuden kan teorien benyttes til at forudsige styrken af asymmetrien i forstærkningen i den mættede enkelt-pumpe FOPA.

Overførslen af intensitetsstøj fra pumpe til signal er blevet identificeret som en af de vigtigste støj bidragsydere i en FOPA idet det medfører modulation af signal forstærkningen. Overførslen af intensitetsstøj fra pumpe til signal er fastlagt i detaljer som funktion af modulation frekvens samt mætningseffekter for at afdække degraderingen af det forstærkede signal. I særdeles god overensstemmelse med de udførte eksperimenter er det eftervist at støjoverførslen til signalet kan undertrykkes ved at operere i det mættede område.

I dette studie bliver forstærkningen af korte pikosekund samt endnu kortere optiske pulser undersøgt ved at benytte chirped-puls forstærkn-

ingsprincippet i FOPAer. Dynamikken af princippet samt pulsforvrængningen bliver studeret for forskellige chirped pikosekund pulser i overgangen fra det lineære til det ikke-lineære område. Forstærkningen af korte pulser kompatible med Tbaud systemer er eksperimentelt eftervist for første gang idet 400 fs pulser er blevet forstærket i en enkelt-pumpe FOPA.

Endelig vil den første eksperimentelle demonstration af FOPA ydelsen i lang distance transmissions forbindelser så vel som i høj-kapacitets systemer blive præsenteret i den sidste del af denne afhandling. FOPAer er kaskadekoblet som in-line forstærkere ved hjælp af en recirkulerende transmissionsløkke og fejlfri transmission ved 40 Gbit/s er succesfuldt demonstreret. Yderligere er fejlfri parametrisk forstærkning for højhastigheds seriel data på en enkelt bølgelængde blevet demonstreret for et optisk tids sammenflettet signal ved 640 Gbit/s uden nogen forøgelse i den nødvendig modtagne optisk effekt. Til sidst er en rent optisk fase bevarende amplitude regenerering baseret på en mættet FOPA ved 640 Gbit/s fase moduleret signal demonstreret.

Acknowledgment

First and foremost I would like to sincerely thank my supervisors Christophe Peucheret, Karsten Rottwitt and Michael Galili (DTU Fotonik) who I learned from and worked with in this Ph.D. project. Among all, the regular progress meetings and the inspiring discussions are highly appreciated. My greatest thanks goes to Christophe Peucheret for continuously supporting and assisting me from the start and all the way until the completion of this thesis. His leadership, support, attention to details and hard work have set an example, I hope to match some day.

I am grateful to all my colleagues in high-speed communication group, DTU Fotonik, that I have had the pleasure to work with in a friendly and professional atmosphere. Special thanks to Valentina Cristofori, Ning Kang, Francesco Da Ros, Toke Lund-Hansen, Oskars Ozolins for our collaboration and useful discussions from time to time. I am grateful to the Technical University of Denmark who financed the project, OFS Fitel Denmark for providing highly nonlinear fibers, Otto Mønsted and Oticon funds for their generous travel supports.

I would like to thank my examiners Peter Andrekson (Chalmers University of Technology, Sweden), Arnaud Mussot (University Lille 1, France) and Jesper Lægsgaard (DTU Fotonik), who provided encouraging and constructive feedback. I am grateful for their thoughtful and detailed comments.

My family receives my deepest gratitude for all their endless love, encouragement and support. For my beloved parents who raised me with love, have taught to never give up and to follow my dreams and gave me life's real education and always supported me during the long years of my education. For my loving, supportive, and patient husband Feisal whose understanding and unconditional support during the past three years are so appreciated. Thank you.

Ph.D. Publications

This Ph.D. project has resulted in the following publication list:

Articles in peer-reviewed journals:

[J-1] **Z. Lali-Dastjerdi**, M. Galili, H. C. H. Mulvad, H. Hu, L. K. Oxenløwe, K. Rottwitt, and C. Peucheret, "Parametric amplification and phase preserving amplitude regeneration of a 640 Gbit/s RZ-DPSK signal," submitted to *Optics Express*.

[J-2] V. Cristofori, **Z. Lali-Dastjerdi**, L. S. Rishłj, M. Galili, C. Peucheret, and K. Rottwitt, "Dynamic characterization and amplification of sub-picosecond pulses in fiber optical parametric chirped pulse amplifiers," submitted to *Optics Express*.

[J-3] V. Cristofori, **Z. Lali-Dastjerdi**, T. Lund-Hansen, C. Peucheret, and K. Rottwitt, "Experimental investigation of saturation effect on pump-to-signal intensity modulation transfer in single-pump phase-insensitive fiber optic parametric amplifiers," *Journal of the Optical Society of America B: Optical Physics*, vol. 30, no. 4, pp. 884-888, Apr 2013.

[J-4] **Z. Lali-Dastjerdi**, K. Rottwitt, M. Galili, and C. Peucheret, "Asymmetric gain-saturated spectrum in fiber optical parametric amplifiers," *Optics Express*, vol. 20, no. 14, pp. 15530-15539, Jul 2012.

[J-5] **Z. Lali-Dastjerdi**, V. Cristofori, T. Lund-Hansen, K. Rottwitt, M. Galili, and C. Peucheret, "Pump-to-signal intensity modulation transfer characteristics in FOPAs: Modulation frequency and saturation effect," *Journal of Lightwave Technology*, vol. 30, no. 18, pp. 3061-3067, Sep 2012.

Articles in peer-reviewed conferences:

[C-1] **Z. Lali-Dastjerdi**, M. Galili, H. C. H. Mulvad, H. Hu, L. K. Oxenløwe, K. Rottwitt, and C. Peucheret, "All-optical phase-preserving amplitude regeneration of a 640 Gbit/s RZ-DPSK signal," in *European Conference on Optical Communicatio*n, *ECOC* 2013, London, UK, paper P.3.24.

[C-2] V. Cristofori, **Z. Lali-Dastjerdi**, L. S. Rishøj, M. Galili, C. Peucheret, and K. Rottwitt, "Dynamic characterization of fiber optical chirped pulse amplification for sub-ps pulses," *Nonlinear Optics Topical Meeting*, *NLO 2013*, Hawaii, USA, paper NW4A.07.

[C-3] V. Cristofori, **Z. Lali-Dastjerdi**, F. Da Ros, L. S. Rishøj, M. Galili, C. Peucheret, and K. Rottwitt, "Fiber optical parametric chirped pulse amplification of sub-picosecond pulses," in *OptoElectronics and Communications Conferenc*e, *OECC 2013*, Kyoto, Japan, paper TuS2-3.

[C-4] **Z. Lali-Dastjerdi**, M. Galili, H. C. H. Mulvad, H. Hu, L. K. Oxenløwe, K. Rottwitt, and C. Peucheret, "Parametric amplification of a 640 Gbit/s RZ-DPSK signal," in *Optical Fiber Communication Conference*, *OFC/NFOEC 2012*, Anaheim, California, USA, paper JW2A.21.

[C-5] **Z. Lali-Dastjerdi**, O. Ozolins, Y. An, V. Cristofori, F. D. Ros, N. Kan, H. Hu, H. C. H. Mulvad, K. Rottwitt, M. Galili, and C. Peucheret, "Demonstration of cascaded in-line single-pump fiber optical parametric amplifiers in recirculating loop transmission," in *European Conference on Optical Communicatio*n, *ECOC* 2012, Amsterdam, The Netherlands, paper Mo.2.C.5.

[C-6] **Z. Lali-Dastjerdi**, F. Da Ros, K. Rottwitt, M. Galili, and C. Peucheret, "Pulse distortion in saturated fiber optical parametric chirped pulse amplification," in *Conference on Lasers and Electro-Optics*, *CLEO 2012*, San José, California, USA, paper JW2A.82.

[C-7] **Z. Lali-Dastjerdi**, K. Rottwitt, M. Galili, C. Peucheret, "Asymmetric gain-saturated spectrum in one-pump fiber optical parametric amplifiers," in *IEEE Photonics Conference*, *IPC 2011*, Arlington, Virginia, USA, paper TuO3.

[C-8] V. Cristofori, **Z. Lali-Dastjerdi**, T. Lund-Hansen, M. Galili, C. Peucheret, and K. Rottwitt, "Saturation effect on pump-to-signal intensity modulation transfer in single-pump phase-insensitive fiber optic parametric amplifiers," in *IEEE Photonics Conference*, *IPC 2011*, Arlington, Virginia, USA, paper TuO2.

[C-9] **Z. Lali-Dastjerdi**, T. Lund-Hansen, K. Rottwitt, M. Galili, and C. Peucheret, "Pump-to-signal intensity modulation transfer in saturated-gain fiber optical parametric ampliers," in *Conference on Lasers and Electro-Optics Pacific Rim*, *CLEO PR 2011*, Sydney, Australia, paper C971.

[C-10] **Z. Lali-Dastjerdi**, T. Lund-Hansen, N. Kang, K. Rottwitt, M. Galili, and C. Peucheret, "High-frequency RIN transfer in fiber optic parametric amplifiers," in *Conference on Lasers and Electro-Optics*, *CLEO/Europe 2011*, Munich, Germany, paper CI25.

Patent application

[P-1] L. K. Oxenløwe, H. C. H. Mulvad, M. Galili, **Z. Lali-Dastjerdi**, F. Da Ros, E. Palushani, C. Peucheret, H. Hu, "All-optical regeneration system for optical wavelength division multiplexed communication systems," European patent application No. 13159278.4-1860, 2013.

The following work was published during the Ph.D. project but is outside the scope of the thesis:

[O-1] O. Ozolins, Y. An, **Z. Lali-Dastjerdi**, Y. Ding, V. Bobrovs, G. Ivanovs, and C. Peucheret, "Cascadability of silicon microring resonators for 40-Gbit/s OOK and DPSK optical signals," in Asia Communications and Photonics Conference, ACP 2012, Guangzhou, China, paper AS1G.1.

Contents

Chapter 1

Introduction

1.1 Background and Perspective

Fiber optical parametric amplifiers (FOPAs) can be ideal candidates for optical amplification and signal processing applications. Fiber optical parametric amplification relies on the third-order non-linear susceptibility of silica glass that induces the four-wave mixing (FWM) process. An intense pump wave at frequency ω_p co-propagates with a signal at frequency ω_s through the fiber and amplifies it. A phase conjugated replica of the signal, called idler, which has the same modulation information as the signal is also generated at $\omega_i = 2\omega_p - \omega_s$ along with amplification of the signal. Signal and idler can be amplified during propagation through the fiber provided the pump power is high enough and phase matching is fulfilled. The first parametric amplification in optical fibers based on stimulated FWM was experimentally demonstrated by Stolen in 1975 [1]. The technological development of highly non-linear fibers (HNLFs) as the gain medium, as well as the exploration of efficient ways of suppression of back-scattered stimulated Brillouin scattering in fibers have made FOPAs an attractive research topic for ultra-fast optical communication and signal processing. Many impressive performances have been demonstrated so far using FOPAs which are detailed in the following.

As parametric processed are based on the energy exchange between the involved waves in FOPAs, unlike in fiber optical Raman amplifiers and erbium-doped fiber amplifiers (EDFAs), no energy is stored in the medium and very high gains are achievable in this type of amplifier. Amplification of more than 60 dB has been realized in a single piece or two pieces of HNLF [2, 3]

The gain profiles of FOPAs are determined by the dispersion profile of the fiber, so the gain flatness and amplification bandwidth can be greatly

tailored by the wavelength allocation of the interacting waves. Unlike EDFAs, FOPAs can amplify signals over many spectral bands, similarly to Raman amplifiers, but with the possibility of wide-band amplification as the parametric process does not rely on energy transitions between energy states. Using only a single stage FOPA, a gain bandwidth as broad as 100 nm with $\sim$ 12 dB gain and $\pm$2 dB gain variation has been demonstrated using single-pump FOPA [4]. Achieving gain flatness over a wider spectral range is also possible by using two pumps. Amplification over 150 nm with $\sim$ 23 dB gain and 4.7 dB gain ripple has been reported in a dual-pump amplifier [5]. The Raman effect and dispersion fluctuations should be controlled in order to achieve gain flatness over a wide range of wavelengths. A parametric gain of 40 dB with 3 dB gain bandwidth of 81 nm has also been demonstrated [6].

A particularly interesting characteristic of FOPAs is their low noise figure (NF), when the phases of the input waves to the FOPA are controlled, i.e. in phase-sensitive FOPAs (PS-FOPAs). The ideal noise figure of 0 dB, i.e. noiseless amplification, is possible in PS-FOPAs . Noise figure of 1.1 dB, below the quantum limit of phase-insensitive FOPAs (PI-FOPAs), has been measured by implementing a PS-FOPA with 26.5 dB gain [7]. The simply designed standard PI-FOPAs, compared to PS-FOPAs which are consisting of two stages (one for phase-locking and phase control of the input waves and the second for parametric amplification), have a quantum limited NF of 3 dB. Noise figures as low as 4.2 dB with 27 dB phase-insensitive parametric gain have been achieved [8] which is comparable with the NF of other phase-insensitive optical amplifiers, i.e. EDFAs and Raman fiber amplifiers.

1.2 Applications of Parametric Amplifiers in High-Speed Optical Signal Processing

Beyond amplification, FOPAs are also capable of many signal processing applications. A phase conjugated copy of the signal, usually at another frequency, is always generated in the FWM process[1]. The wavelength converted copy of the signal has the same modulation as the signal (only with inverted spectrum) and can be used for changing the signal wave-

[1]Signal and idler may overlap in frequency in non-degenerate FWM where the interaction is between two pumps and a signal located at the pumps mean frequency. In this case, the generated idler overlaps with the signal at the mean-frequency of the pumps. If the two pumps have orthogonal polarizations, the idler will have an orthogonal polarization to the signal. This has applications in frequency-preserving parametric dispersion compensators [9] and frequency-preserving optical serial-to-parallel conversion [10].

length in optical communication systems while its conversion efficiency is as high as the signal gain.

The converted wavelength has the inverted spectrum of the input signals which can also be simultaneously used for compensating chromatic dispersion and loss of the transmission fiber . By placing a FOPA in the middle of a fiber span, a wavelength converted signal with compensated dispersion is automatically available at the end of the span. In [11], simultaneous compensation of loss and chromatic dispersion for 10 Gbit/s transmission over 90 km of standard fiber using mid-span phase conjugation with a FOPA has been realized with 9.4 dB gain over a bandwidth of 17 nm. At a higher data rate, a 640 Gbit/s return-to-zero on-off keying (RZ-OOK) signal has been transmitted over 100 km standard single-mode fiber (SSMF) based on mid-span all-optical dispersion compensation [12].

Since the non-linear response of the optical fiber is quasi-instantaneous, parametric processes have found a variety of applications in high-speed signal processing. If the pump wave in a FOPA is modulated, the modulation of the pump will result in instantaneous modulation of signal and idler which can be used for high-speed all optical short pulse generation, optical demultiplexing of optical time multiplexed (OTDM) signals and regeneration of data signals.

OTDM demultiplexing can be realized in a pulsed-pump FOPA by synchronized propagation of a train of pulsed-pump at the base repetition rate of the OTDM signal. The signal pulses temporally coinciding with the pump pulses, at the base repetition rate of the OTDM signal, are amplified and extracted. Using a sinusoidally modulated pump, demultiplexing from a 40 Gbit/s to 10 Gbit/s data has been demonstrated with more than 30 dB gain [13, 14]. It is also possible to use the wavelength converted signal (idler) as the output of the demultiplexer. As only the desired pulses are present at the idler frequency, a higher optical signal-to-noise ratio (OSNR) is expected at the converted wavelength. All-optical time demultiplexing of a 160 Gbit/s OTDM signal to 10 Gbit/s has also been demonstrated with more than 12 dB conversion efficiency in both polarization-dependent [15] and polarization-independent [16] FOPAs.

A sinusoidally modulated pump propagating with a continuous wave signal through a FOPA results in the generation of short pulses at the signal frequency with the same repetition rate as the modulation frequency of the pump and controllable pulse width depending on the applied pump power. Nearly transform-limited pulses can be achieved [17, 18, 19]. Return-to-zero (RZ) pulses ($\sim$ 2 ps) has been generated at bit rates of 40, 80 and 160 Gbit/s data transmission has been generated using

FOPAs [17].

Due to the effects of fiber non-linearity, dispersion, and noise added by optical amplifiers in long-haul optical communication systems, signals may become distorted and need to be regenerated. All-optical signal regeneration that does not need conversion to the electrical domain is highly desirable for high-speed optical transmission systems. When a FOPA works in the saturation regime, it can be utilized for optical level equalization and noise suppression which can be used as a regenerator providing amplification and reshaping of the distorted signal. Only amplification of a distorted signal is referred to as 1R-regeneration. If reshaping is included, it is referred to as 2R-regeneration. If furthermore retiming is provided, it is referred to as 3R-regeneration. CW-pump FOPAs are suitable for 2R-regeneration while pulsed-pump FOPAs can work as 3R-regenerators [20]. Optical regeneration based on FOPAs is due to the instantaneous pump power dependence of the parametric gain [21, 22]. PI-FOPAs are able to regenerate the amplitude of intensity encoded signals directly while phase-preserving amplitude regeneration of phase encoded data signals is able to mitigate accumulation of nonlinear phase noise in phase modulated systems [23]. Phase-preserving amplitude regeneration based on FOPAs has been experimentally verified for 40 Gbit/s differential phase-shift keying (DPSK) signals [24], 80 Gbit/s polarization multiplexed RZ-DPSK [25], 160 Gbit/s DPSK [26] and 10 Gbit/s differential quadrature phase-shift keying (DQPSK) [27] systems.

Phase regeneration of phase encoded signals is directly achievable using PS-FOPAs. Phase and amplitude regeneration of DPSK at 40 Gbit/s [28] and quadrature phase-shift keying (QPSK) for 10 Gbaud [29] and 50 Gbaud [30] signals has been demonstrated.

As the wavelength converted signal is tunable with the pump frequency, a wide range of wavelength tunable signal processing application is also possible. Uniformly tunable wavelength conversion without spectral inversion over 30 nm [31] has been demonstrated by cascading two pieces of HNLF. A parametric tunable dispersion compensator (PTDC) via parametric wavelength conversion was proposed in [32], which is free from the trade off between the bandwidth and the amount of tunable dispersion. Based on this concept wideband generation of picosecond pulses using FOPAs [33] and wavelength tunable optical parametric regenerators with wavelength tunable range covering over 20 nm [34, 35] have been reported for modulated signals up to 43 Gbit/s.

1.3 Practical Challenges in Implementation of FOPAs

Performances and applications of FOPAs indicate that they have great potential to be used in optical communication networks. However, there are several practical challenges needed to be overcome before implementing them in real optical links.The following lists some of the challenging aspects, which are being discussed later in this thesis.

High pump power with high OSNR Parametric gain depends on the pump power propagating together with the signal inside the HNLF. The pump wave needs to be amplified to Watt levels, which in the telecommunication window can be achieved thanks to high-power EDFAs followed by a narrow-band optical bandpass filter in order to remove the out-of-band amplified spontaneous emission (ASE) noise. The residual ASE left limits the OSNR of the pump and imposes some relative intensity noise (RIN) to it. Apart from this, there may be other sources of RIN for the pump. In order to propagate the high-power pump through the fiber, one needs to combat the back-scattered stimulated Brillouin scattering (SBS). The most efficient and common way to suppress the back-scatted power is to make the pump spectrum broader than the Brillouin gain bandwidth (about 50 MHz). This can be done by phase modulation of the pump wave up to several GHz. Phase modulation of the pump in return has some adverse effects on the signal and idler. The phase modulation applied to the pump can be transferred to intensity modulation through filtering or dispersion and will modulate the gain/conversion efficiency through the pump power dependence of the gain/conversion efficiency. It also can broaden the spectrum of the idler to twice that of the pump in single-pump FOPAs. In pulsed-pump FOPAs, SBS can cease, which indeed demands a more complex setup and also needs the pump to be synchronized with the signal.

In order to assess the effect of pump intensity modulation on the performance of FOPAs, one needs to know the mechanism of this pump-to-signal intensity modulation transfer (IMT). Chapter 4 of this thesis is concerned with this effect and thoroughly discusses it theoretically as well as experimentally.

Gain flatness The amplification of short pulses in high-speed OTDM or multi-channel densed wavelength division multiplexed (WDM) systems require optical amplifiers with a fairly uniform gain spectrum. The amplification bandwidth of FOPAs is governed by the dispersion pro-

file and non-linearity of the fiber. Gain flatness is manageable by a proper balance between the dispersion and the involved non-linearities in FOPAs, in which the phase-matching between the waves is preserved over a wide spectral range. Chapter 7 discusses the design of a single-pump FOPA for amplification of short pulses for high-speed signals where amplification and regeneration of a 640 Gbit/s OTDM signal are experimentally carried out.

In-line amplification Since FOPAs can amplify data signals outside the amplification band of EDFAs, they can be an option for extending the transmission bandwidth for long-distance optical links when they are implemented as in-line amplifiers. To determine the performance of FOPAs in an optical transmission link, the noise accumulation, as the most limiting factor, needs to be examined. So far, FOPAs have been mostly used as stand-alone amplifiers and their performance as in-line amplifiers remains largely unexplored. However, cascading FOPAs can be challenging due to several factors that need to be controlled, such as polarization sensitivity and pump-to-signal noise transfer. Chapter 6 tries to find the limit that has been applied from noise accumulation in FOPAs by cascading single-pump FOPAs in a recirculating loop transmission.

1.4 Scope and Structure of This Thesis

The goal of this Ph.D. project is to explore fiber optical parametric amplification for high-speed optical communications. More specifically, it characterize the performance of FOPAs in linear (samll-signal gain) and non-linear (saturated) regimes for continuous wave signals, short pulses and data modulated signals up to 640 Gbit/s.

Chapter 2 starts by reviewing the theory of parametric amplification in optical fibers, which is needed to understand the operation of FOPAs. Phase matching requirements for parametric gain and numerical method used in the simulation carried out in this thesis are presented. Implementation of single- and dual-pump FOPAs and experimentally measured parametric gain are also presented.

Chapter 3 is concerned with the operation of single- and dual-pump FOPAs in the saturation regime. It shows an observed new feature of asymmetry in the saturated gain spectra of single-pump FOPAs. Experimental results and theoretical explanations are presented. The bandwidth limitation of dual-pump FOPA in saturation is also discussed in this chapter.

The subject of Chapter 4 is pump-to-signal intensity modulation transfer in FOPAs and it investigates the mechanism of the IMT in FOPAs and characterizes it in terms of modulation frequency and its behavior in saturation. The mechanism of IMT through the fiber, signal wavelength dependence and a way for minimizing it are discussed. The experimental verification of IMT is also presented.

The amplification of short pulses using FOPAs has been investigated in Chapter 5. In the first section, based on chirped pulse amplification, amplification of few picosecond and sub-picosecond short pulses is experimentally carried out. The pulse distortion for differently chirped pulses, with a few picosecond pulsewidth, under transition from the linear to the saturated gain regime are investigated. In the second section, chirped-pulse amplification of Tbaud-class pulses has been demonstrated for pulses as short as 400 fs.

Chapter 6 examines a single-pump FOPA as an in-line amplifier to asses its performance for long-haul transmission and under noise accumulation. A single-pump FOPA is placed in a recirculating loop for transmission of 40 Gbit/s OOK and DPSK signals.

In Chapter 7, the amplification and regeneration performance of a single-pump FOPA has been investigated in high-capacity systems for an OTDM 640 Gbit/s RZ-DPSK signal. At the end, the summary and outlook to future works are provided in Chapter 8.

1.5 Contributions of This Ph.D. Project

The following are the main results and contributions achieved during this Ph.D. project. They are summarized in the same order as they appear in the chapters:

Asymmetric gain-saturated spectra in FOPAs The first experimental observation of gain asymmetry in single-pump FOPAs under strong saturation is reported [C-7]. The original physical mechanism leading to this gain asymmetry is explained in terms of interaction between higher-order four-wave mixing products and dispersive waves radiated as an effect of third-order dispersion. Numerical simulations are used to confirm the experimental results and prove the validity of the proposed theory [J-4].

Characteristics of pump-to-signal intensity modulation transfer in FOPAs A comprehensive study of pump-to-signal intensity modulation transfer (IMT) in single-pump FOPAs is reported. In particular,

the IMT is studied for the first time for high-frequency fluctuations of the pump [C-10] as well as in the saturated gain regime [C-9, J-5]. The IMT cut-off frequency in typical single-pump FOPAs is around 100-200 GHz. The possibilities to shift this frequency based on dispersion and non-linearities involved in the parametric gain are discussed. Minimization of severe IMT to the signal at low modulation frequencies is assessed. Experimental results confirm the validity of the numerical study [C-8, J-3].

Fiber optical parametric chirped pulse amplification (FOPCPA) of picosecond and and sub-picosecond pulses FOPCPA has been experimentally studied for few picosecond short pulses with different chirped signals in the linear and non-linear gain regime. The signal distortion after recompression has been investigated experimentally for the first time [C-6]. Chirped pulse amplification of pulses as short as 400 fs using FOPAs has been experimentally demonstrated [C-2, C-3, J-2].

First demonstration of cascaded in-line FOPAs The first experimental demonstration of single-pump FOPAs as an in-line amplifier is presented for 40 Gbit/s RZ-OOK and RZ-DPSK modulated signals by placing FOPA in a recirculating loop transmission [C-5].

First demonstration of parametric amplification and all-optical phase-preserving amplitude regeneration of a 640 Gbit/s RZ-DPSK signal A gain-flattened single-pump FOPA has been designed for amplification and regeneration of pulses as short as 620 fs. Based on these results parametric amplification of a 640 Gbit/s RZ-DPSK OTDM signal has been demonstrated and characterized for the first time [C-4, J-1]. The first demonstration of all optical phase-preserving amplitude regeneration for different levels of degraded 640 Gbit/s RZ-DPSK signal is reported [C-1, J-1].

Chapter 2

Fiber Optical Parametric Amplification

2.1 Introduction

This chapter serves as an introduction to fiber optical parametric amplifiers (FOPAs). The principle of parametric amplification in optical fibers is base on parametric mixing of waves with different frequencies, called four-wave mixing. Section 2.2 describes the four-wave mixing and the amplitude evolution of the participating waves in an optical fibers. Modulation instability, as a spontaneous process of parametric amplification, is introduced in section 2.3. The stimulated process of modulation instability, which leads to parametric amplification is discussed in section 2.4. Parametric gain and the amplification bandwidth of FOPAs are discussed in section 2.6. The simulation method that has been used in this thesis is explained in section 2.5. Section 2.7 discusses the suppression of the back-scattered power in optical fibers and the polarization sensitivity of FOPAs as two practical points to implement the FOPAs. At last this chapters is summarized in section 2.8.

2.2 Four-Wave Mixing and Coupled Amplitude Equations

We consider the interaction of four monochromatic waves with angular frequencies ω_1, ω_2, ω_3 and ω_4. It is assumed that all the waves are linearly co-polarized along the same axis and propagate along the z axis. The total electric field can be represented as

$$\mathbf{E}(x,y,z,t) = \frac{1}{2}F(x,y)\left\{\sum_{j=1}^{4} A_j(z)\exp\left[i(\beta_j z - \omega_j t)\right] + c.c.\right\}, \quad (2.1)$$

where $F(x,y)$ is the transverse modal profile which is assumed to be identical for all the waves along the fiber, $A_j(z)$ is the slowly varying envelope of the wave at frequency ω_j and β_j is its propagation constant. The slowly varying envelope approximation (SVEA) is valid when the envelope of the wave changes much slower than the period of the optical carrier and is satisfied in many case of practical interest [36].

Propagation constant Propagation constant is a function of frequency and determines the group delay and chromatic dispersion of the fiber. One can expand it as a Taylor series about a reference angular frequency ω_0

$$\beta(\omega) = n(\omega)\frac{\omega}{c} = \beta_0 + \beta_1(\omega-\omega_0) + \frac{1}{2!}\beta_2(\omega-\omega_0)^2 + \frac{1}{3!}\beta_3(\omega-\omega_0)^3 + \cdots \quad (2.2)$$

where $n(\omega)$ represents the frequency dependent refractive index, c is the speed of light in vacuum and

$$\beta_m = \left(\frac{d^m\beta}{d\omega^m}\right)_{\omega=\omega_0} (m = 0, 1, 2, \ldots). \quad (2.3)$$

The group velocity of an optical wave at which the envelop of the optical wave propagates, υ_g, is inversely related to the first order dispersion β_1

$$\upsilon_g = \frac{d\omega}{d\beta} = \frac{1}{\beta_1}. \quad (2.4)$$

The second order dispersion β_2 indicates the dispersion of the group velocity and is known as *group-velocity dispersion* (GVD) parameter.The *Dispersion parameter*, D, is a parameter commonly used in the specification of the fiber parameters and defined as

$$D = \frac{d\beta_1}{d\lambda} = -\frac{2\pi c}{\lambda^2}\beta_2 \quad (2.5)$$

and its dimension is commonly expressed in ps·nm^{-1}·km^{-1}. The wavelength at which $\beta_2 = 0$ is known as *zero-dispersion wavelength* (ZDW) and the wavelength region where $\beta_2 > 0$ (i.e. $D < 0$) is called *normal*

dispersion region and the region where $\beta_2 < 0$ (i.e. $D > 0$) is called *anomalous dispersion* region. Even though the second-order dispersion vanishes at ZDW the dispersive effects do not completely disappear. The third-order dispersion, β_3, becomes the dominant term close to the ZDW and needs to be considered especially for the propagation of short pulses in fiber.

The third-order dispersion is related to the slop of the dispersion $dD/d\lambda$ and is a parameter which is usually provided at the ZDW by fiber manufacturers. The *dispersion slope*,$S = dD/d\lambda$, depends on both β_2 and β_3

$$S = \frac{\omega}{\lambda^2}(2\beta_2 + \omega\beta_3), \tag{2.6}$$

which it has dimension of ps·nm^{-2}·km^{-1} and this value for SSMF typically is $\sim$ 0.07 ps·nm^{-2}·km^{-1} and for standard HNLF is $\sim$ 0.01-0.03 ps·nm^{-2}·km^{-1}. Fourth-order dispersion, β_4, can be extracted from $dS/d\lambda$ and so on for the higher orders of dispersion.

In order to see the influence of different terms of dispersion on the propagation constant, $\beta(\omega)$ for a standard highly non-linear fiber (HNLF), including different frequency-dependent dispersion terms in the expansion of the propagation constant, is plotted in Fig. 2.1.

The HNLF has a ZDW at 1550 nm, $S = 0.0185$ ps·nm^{-2}·km^{-1} and $dS/d\lambda = -1\times10^{-4}$ ps·nm^{-3}·km^{-1}. The propagation constant is expanded around the reference frequency 1555 nm where $\beta_2 < 0$. As it can be seen, the fourth-order dispersion has insignificant impact over a 100 nm bandwidth around the reference frequency. The effect of the fourth-order dispersion, however, can be observed for bandwidths over several hundreds of nanometers. The parametric gain and amplification bandwidth of FOPAs are strongly dependent on the dispersion terms, as it will be discussed in section 2.4.

Kerr non-linearity The total induced polarization $\mathbf{P}$ induced by an electric field has the general form of

$$\mathbf{P} = \varepsilon_0 \left[\chi^{(1)} \cdot \mathbf{E} + \chi^{(2)} : \mathbf{EE} + \chi^{(3)} \vdots \mathbf{EEE} + \cdots \right], \tag{2.7}$$

where $\chi^{(j)}, (j = 1, 2, 3, \ldots)$ is jth order susceptibility. The first term represents the linear response of the medium to the applied optical field. The response of the medium is non-linear when the induced polarization depends on the higher orders of the optical field. The first term including the first order susceptibility, $\chi^{(1)}$, has the dominant contribution in the induced polarization and shows its effect through the linear refractive

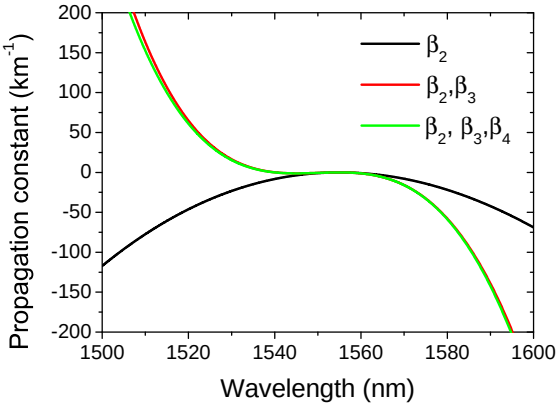

Figure 2.1: Expansion of the propagation constant for a standard HNLF considering different frequency-dependent dispersion terms.

index and attenuation coefficient, which are dependent on the real and imaginary parts of $\chi^{(1)}$, respectively. The second order susceptibility, $\chi^{(2)}$, exists in non-centrosymmetric media and vanishes in fused silica glass because of the symmetry of the SiO_2 molecule. Therefore, non-linear effects in optical fibers originate from third-order susceptibility, $\chi^{(3)}$. Nolinearities associated with $\chi^{(3)}$ can be classified into two different types, one related to the real part of $\chi^{(3)}$, and the other one with the imaginary part of $\chi^{(3)}$. The former is known as *Kerr non-linearity*, while the later is related to inelastic scattering in the fiber. Unlike for inelastic scattering in the fiber, i.e. Raman and Brillouin scattering, no energy is transferred to the medium in the effects originating from the Kerr non-linearity.

The Kerr non-linearity results in the intensity-dependent part of the refractive index. The refractive index can be represented as

$$\tilde{n}(\omega, |\mathbf{E}|^2) = n(\omega) + n_2 |\mathbf{E}|^2, \tag{2.8}$$

where $n(\omega)$ is the linear refractive index and n_2 is called the *non-linear refractive index* and depends on the real part of $\chi^{(3)}$

$$n_2 = \frac{3}{8n}\mathrm{Re}(\chi^{(3)}). \tag{2.9}$$

The Kerr non-linearity leads to different effects in an optical fiber, including self-induced phase shift by an optical field itself , known as *self-phase modulation* (SPM), phase shift induced by another field with different frequency, known as *cross-phase modulation* (XPM) and *four-wave mixing* (FWM).

Four-wave mixing Considering the interaction of three electric fields through the third-order non-linearity in silica glass fiber, one can calculate that the induced polarization will consist of 21 non-zero terms based on the following interactions:

$$\begin{array}{lccc}
\text{SPM} & \omega_1+\omega_1-\omega_1 & \omega_2+\omega_2-\omega_2 & \omega_3+\omega_3-\omega_3 \\
\text{XPM} & \omega_1+\omega_2-\omega_2 & \omega_1+\omega_3-\omega_3 & \\
 & \omega_2+\omega_1-\omega_1 & \omega_2+\omega_3-\omega_3 & \\
 & \omega_3+\omega_1-\omega_1 & \omega_3+\omega_2-\omega_2 & \\
\text{FWM} & 2\omega_1-\omega_2 & 2\omega_1-\omega_3 & \\
 & 2\omega_2-\omega_1 & 2\omega_2-\omega_3 & \\
 & 2\omega_3-\omega_1 & 2\omega_3-\omega_2 & \\
 & \omega_1+\omega_2-\omega_3 & \omega_1+\omega_3-\omega_2 & \omega_3+\omega_1-\omega_2 \\
\text{THG} & \omega_1+\omega_1+\omega_1 & \omega_2+\omega_2+\omega_2 & \omega_3+\omega_3+\omega_3
\end{array} \tag{2.10}$$

Third-order non-linear interactions among four waves, which lead to generation of new frequencies, includes third-harmonic generation (THG) and FWM. In the case of THG, three photons transfer their energy to a single photon ($\omega+\omega+\omega=3\omega$) while in the FWM process two photons at the same or different frequencies are annihilated and two photons at different frequencies are simultaneously created ($\omega_1+\omega_2=\omega_3+\omega_4$). The efficiency of THG is very low in standard single-mode fibers as the phase-matching for THG is difficult to be realized. In this case, the values of the refractive index at ω and 3ω differ enough for the fundamental mode in standard single-mode fibers so that the THG process cannot be phase-matched in them. i.e.

$$\Delta\beta=\beta(3\omega)-3\beta(\omega)=\frac{3\omega}{c}\left[n(3\omega)-n(\omega)\right]\neq 0. \tag{2.11}$$

The phase-matching requirement for FWM can be expressed as

$$\Delta\beta=\beta(\omega_1)+\beta(\omega_2)-\beta(\omega_3)-\beta(\omega_4)=0. \tag{2.12}$$

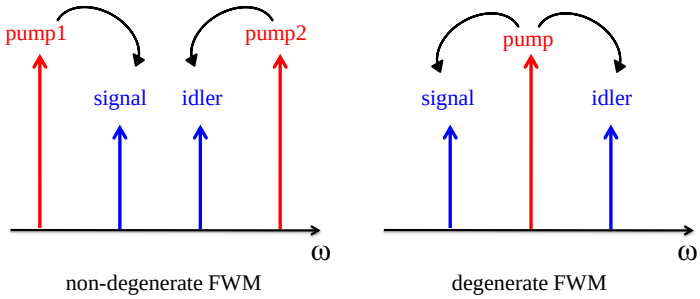

Figure 2.2: Nomenclature of waves interacting in non-degenerate and degenerate FWM.

The frequency allocation of FWM is shown in Fig. 2.2. When $\omega_1 \neq \omega_2$ the FWM is known as *non-degenerate* FWM and two photons with different frequencies, from two pumps, annihilate to generate a signal and an idler photon simultaneously, which are down-shifted (*Stokes* band) and up-shifted (*anti-Stokes* band) in frequency from the mean frequency of the pumps. In *degenerate* FWM, where $\omega_1 = \omega_2$, the pump wave loses two photons to generate a signal and idler simultaneously, which are symmetrically located with respect to the pump frequency.

Coupled amplitude equations Considering the phase-matched condition where $\omega_1 + \omega_2 = \omega_3 + \omega_4$ and $\beta(\omega_1) + \beta(\omega_2) = \beta(\omega_3) + \beta(\omega_4)$, the induced polarization for the generated wave ω_4 can be written as

$$P_4 = \frac{3\varepsilon_0}{4}\chi^{(3)}\Big[|E_4|^2 E_4 + 2|E_1|^2 E_4 + 2|E_2|^2 E_4 + 2|E_3|^2 E_4 \qquad (2.13)$$

$$+2E_1E_2E_3^*\exp(i\Delta\beta z)\Big]$$

The first term determines the SPM while the second to fourth terms determine the XPM between different fields. The last term is responsible for the parametric energy exchange among the waves, i.e. FWM. The polarization for the other waves can be written in the same manner. Substituting the total electric field and polarization in the wave equation, one can derive the coupled equations for the amplitude of the interacting waves as follow

$$\frac{dA_{P1}}{dz} = i\gamma\Big\{\Big[|A_{P1}|^2 + 2\left(|A_{P2}|^2 + |A_S|^2 + |A_I|^2\right)\Big]A_{P1} \qquad (2.14)$$

$$+2A_S A_I A_{P2}^* \exp(-i\Delta\beta z)\Big\}$$

$$\frac{dA_{P2}}{dz} = i\gamma\Big\{\Big[|A_{P2}|^2 + 2\left(|A_{P1}|^2 + |A_S|^2 + |A_I|^2\right)\Big] A_{P2} \tag{2.15}$$

$$+2A_S A_I A_{P1}^* \exp(-i\Delta\beta z)\Big\}$$

$$\frac{dA_S}{dz} = i\gamma\Big\{\Big[|A_S|^2 + 2\left(|A_I|^2 + |A_{P1}|^2 + |A_{P2}|^2\right)\Big] A_S \tag{2.16}$$

$$+2A_I^* A_{P1} A_{P2} \exp(i\Delta\beta z)\Big\}$$

$$\frac{dA_I}{dz} = i\gamma\Big\{\Big[|A_I|^2 + 2\left(|A_S|^2 + |A_{P1}|^2 + |A_{P2}|^2\right)\Big] A_I \tag{2.17}$$

$$+2A_S^* A_{P1} A_{P2} \exp(i\Delta\beta z)\Big\}$$

where γ is the *non-linear coefficient* of the fiber. The coupled equations represent the amplitude evolution of the waves in an optical fiber. From these equation one can derive an analytical equation for the amplitude of the signal and idler, provided the pump power is much higher than the input signal power. We will refer to these equations later in the next sections.

Non-linear coefficient The non-linear coefficient of the fiber is a parameter used to describe the non-linear effects in fibers

$$\gamma = \frac{2\pi n_2}{\lambda A_{eff}}, \tag{2.18}$$

where n_2 represents the non-linear refractive index of the fiber and A_{eff} is the *effective area* of the fiber, which depends on fiber parameters such as the core radius and the core-cladding index difference.

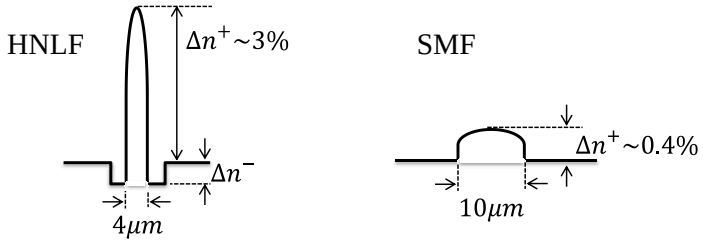

Figure 2.3: Schematic refractive index profiles for HNLF (left) and SSMF (right) [37].

The non-linear coefficient of an optical fibers, γ, is a parameter to express the strength of the Kerr non-linearities in fibers, which in silica fibers can be controlled by A_{eff}.

Fig. 2.3 shows the schematic refractive index profiles of a HNLF and a standard single-mode fiber (SSMF). In typical HNLFs, the relative refractive index difference between the core and the outer cladding (Δn^+) is around 3%, while the core diameter is around 4 µm. The W-cladding profile with a relative refractive index difference of Δn^- is employed to realize single-mode operation as well as flexibilities in designing of chromatic dispersion [37]. Typical HNLFs used for FOPAs have a non-linear coefficient of 10-20 $W^{-1}{\cdot}km^{-1}$, while typical SSMFs have a non-linear coefficient $\sim$ 1.3 $W^{-1}{\cdot}km^{-1}$.

2.3 Modulation Instability

Modulation instability (MI) is based on degenerate FWM and is the basis of parametric amplification. In this effect, an intense wave at an angular frequency ω_p in the anomalous dispersion region of the optical fiber interacts with the noise photons (vacuum fluctuations) at sideband frequencies $\omega_p \pm \Delta\omega$ and transfers energy from the pump to these two frequency bands, known as anti-Stokes and Stokes frequency bands. This effect was observed in optical fibers in 1980 by K. Tai et al. [38] and then in 1984 presented by A. Hasegawa as a method of generation periodic trains of short optical pulses with a controllable pulse width and repetition rate for telecommunications applications [39]. MI is a result of the interplay between the non-linear and dispersive effects in the fiber, which results into break up of the CW pump into a train of short pulses.

The growth of the sidebands can be treated in terms of amplification of a weak modulation imposed on the harmonic wave. Amplification is maximum for the frequencies components which satisfy the phase mis-

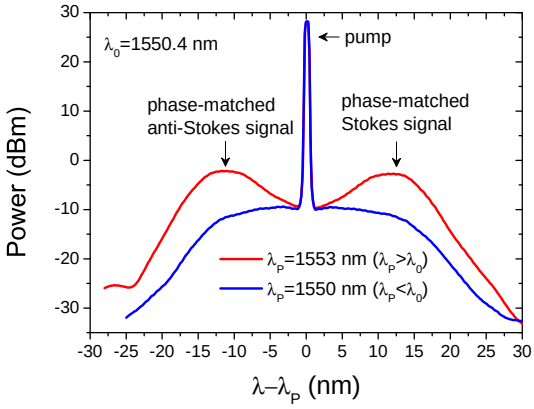

Figure 2.4: Measured modulation instability spectra, in a 500 m HNLF and $P_p = 28$ dBm, for two different pump wavelengths.

match condition

$$2\beta(\omega_p) = \beta(\omega_p + \Delta\omega) + \beta(\omega_p - \Delta\omega). \tag{2.19}$$

Fig. 2.4 shows two measured MI spectrum in a 500 m HNLF for 28 dBm launched pump power at two different wavelengths $\lambda_p = 1550$ nm and 1553 nm; one below and one above the ZDW which is at 1550.4 nm. Noise photons originate from the ASE noise generated by an EDFA used to amplify the pump laser. Amplification of the noise around the pump can be clearly observed especially for $\lambda_p = 1553$ nm, where the pump is located above the ZDW, i.e. in anomalous dispersion, and ensures the phase-matching condition, which will be discussed in the next section. Two side lobes are indeed formed as the result of the modulation from the noise source applied on the pump signal.

2.4 Parametric Gain

Parametric amplification is a result of stimulated MI when a weak signal is launched to the optical fiber together with an intense pump wave. In order to find the signal gain, we need to refer to the FWM coupled equations, which govern the energy transfer between the waves. The coupled equations, Eq. (2.14, 2.15, 2.16, 2.17), include SPM, XPM and FWM and one can solve these coupled equations analytically under the undepleted pump assumption. This assumption is valid when the pumps are much more intense than the signal. Under this assumption an analytical

solution for the output power of the signal, $P_s(L)$, and idler, $P_i(L)$, can be derived from the coupled equations [36]

$$P_s(L) = P_s(0)\left[1 + \left(\frac{\gamma P_0 r}{g}\sinh(gL)\right)^2\right], \tag{2.20}$$

$$P_i(L) = P_s(0)\left(\frac{\gamma P_0 r}{g}\sinh(gL)\right)^2, \tag{2.21}$$

where L is the fiber length and g is the *parametric gain coefficient*

$$g = \sqrt{(\gamma P_0 r)^2 - \left(\frac{\kappa}{2}\right)^2}, \tag{2.22}$$

where $r = 2(P_1P_2)^{1/2}/P_0$, $P_0 = P_1 + P_2$ and κ is *total phase-mismatch factor*

$$\kappa = \Delta\beta + \gamma(P_1 + P_2), \tag{2.23}$$

which consists of two terms. The first term is the *linear phase-mismatch*, $\Delta\beta$, which depends on the propagation constants of the waves, more specifically on the dispersion profile of the fiber. The second term is the *non-linear phase-mismatch* which is always positive.

Considering a single-pump FOPA, based on degenerate FWM, where $P_1 = P_2 = P_p$, Fig. 2.5 shows its signal gain spectrum. The signal gain, $G_s = P_s(L)/P_s(0)$, depend on the phase-mismatch factor, κ, and shows two maxima around the pump frequency corresponding to the perfect phase-matched frequencies.

At the maximum gain $\kappa = 0$, which necessitate $\Delta\beta < 0$. For degenerate FWM, the power flows from one pump at ω_p to the signal at $\omega_p + \Delta\omega$ and idler at $\omega_p - \Delta\omega$, and the linear phase-mismatch can be written as fallow

$$\Delta\beta = \beta(\omega_p + \Delta\omega) + \beta(\omega_p - \Delta\omega) - 2\beta(\omega_p) = 2\sum_{m=1}^{\infty}\frac{\beta_{2m}(\omega_p)}{(2m)!}(\Delta\omega)^{2m}. \tag{2.24}$$

It appears that the linear phase-mismatch, $\Delta\beta$, depends on the even orders of dispersion and even powers of the pump-signal frequency separation. Considering the first term as the dominant term

$$\Delta\beta = \beta_2(\omega_p)(\omega_s - \omega_p)^2, \tag{2.25}$$

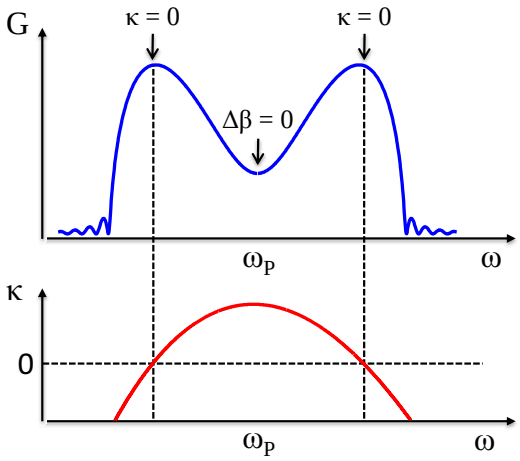

Figure 2.5: Parametric gain and and phase-mismatch factor spectrum for a single-pump FOPA.

it can be seen that $\beta_2(\omega_p)$ should be negative in order to satisfy the phase-mismatch condition

$$\kappa = \Delta\beta + 2\gamma P_p = 0. \tag{2.26}$$

It is thus essential that the pump is located in the anomalous dispersion region of the fiber, i.e. where $\beta_2(\omega_p) < 0$. The linear phase-mismatch, $\Delta\beta$ is zero at the pump frequency and its absolute value increases for the frequencies further away from the pump. When its value cancels out the positive non-linear phase-mismatch, then $\kappa = 0$ and maximum gain occurs, as it is illustrated in Fig. 2.5, for the two wavelength located at the frequencies $\omega_p \pm \sqrt{(2\gamma P_p)/|\beta_2|}$.

For the perfect phase-matched frequencies , $\kappa = 0$, and for $\gamma PL \gg 1$, the signal gain can be estimates by

$$G_s \simeq \sinh^2(gL) \simeq \frac{1}{4}\exp\left(2\gamma P_p L\right), \tag{2.27}$$

which shows that the signal gain increases exponentially with $\gamma P_p L$.

The gain spectrum of the signal is symmetric, as can be seen from Fig. 2.5 which is due to the fact that the linear phase-mismatch factor in Eq. 2.24 depends only on even-order dispersion as well as on the even powers of the pump-signal frequency separation. The gain spectrum remains symmetric under the assumption of undepleted pump, while it may turn out to be asymmetric in depleted pump conditions. Details of the this asymmetry feature of the gain spectrum will be discussed in Chapter 3.

Amplification bandwidth The amplification bandwidth in FOPAs, is defined here as the frequency separation between the two phase-matched signals showing maximum gain, depends on the relative contributions of the linear and non-linear phase-mismatch factors in the total phase-mismatch factor, κ. This sections describes the effect of the dispersion profile of the fiber on the gain bandwidth.

In order to maximize the amplification bandwidth, one needs to maximize $\Delta\omega$ in 2.24. Considering up to fourth-order dispersion (FOD)

$$\Delta\beta = \beta_2(\omega_p)(\Delta\omega)^2 + \frac{1}{12}\beta_4(\omega_p)(\Delta\omega)^4. \tag{2.28}$$

The signs and values of β_2 and β_4 are the determining factors in the phase-matching. The phase-matching requirement is $\Delta\beta < 0$. Since the first term, containing the second-order dispersion (SOD), β_2, is the dominant term, pumping the amplifier in anomalous dispersion can ensure us this term is negative. If the FOD, β_4, is negative as well, then the two terms of the dispersion act in the same direction that can narrow the amplification bandwidth for a fixed value of non-linear phase-mismatch. In order to clarify the effect of FOD on the parametric amplification bandwidth, the total phase-mismatch factor, κ, is plotted for different values of β_4 in Fig. 2.6. The non-linear phase-mismatch considered here is $2\gamma P_p = 10\ \mathrm{km}^{-1}$, reference frequency is at 1551 nm, ZDW is at 1550 nm and $S = 0.0185\ \mathrm{ps{\cdot}nm^{-2}{\cdot}km^{-1}}$. As it can be seen, for negative values of β_4 as well as $\beta_4 = 0$, only two phase-matched wavelengths exist. For positive values of β_4, two other phase-matched wavelengths are available which are located much farther than from the center, i.e the pump wavelength. Therefore, FOD can affect the phase-matching, which can, for low positive values of β_4, result in amplification bandwidths several times broader and flatter than the situations in which FOD becomes negligible or negative.

In most standard HNLFs, the FOD is of the order of $10^{-4}\ \mathrm{ps^4{\cdot}km^{-1}}$ [37], which has a negligible contribution over a bandwidth of less than 100 nm. In this case, based on the SOD parameter one can calculate the amplification bandwidth for single-pump FOPAs as

$$\Delta\omega = 2\sqrt{\frac{2\gamma P_p}{|\beta_2|}}. \tag{2.29}$$

In all the experiments carried out throughout this thesis, standard HNLFs have been used, for which the amplifier bandwidth for single-pump FOPAs can be fairly accurately estimated by 2.29.

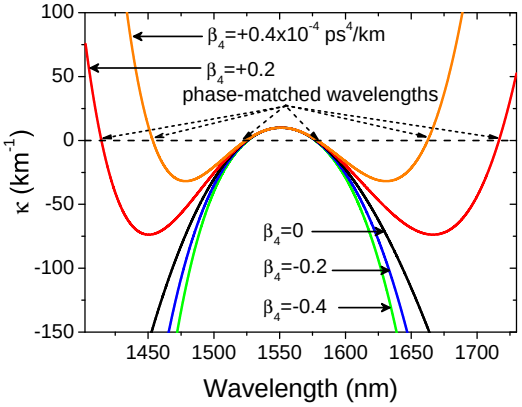

Figure 2.6: Effect of β_4 on total phase-mismatch factor.

2.5 Simulation Method

In order to model FOPAs, one need to solve the non-linear Schrödinger equation (NLSE). When a large number of waves are interacting in the HNLF, a situation that specifically arises when the amplifier operates in its saturation mode and many idlers exist, it usually turns out to be cumbersome and even impossible to use a model based on coupled equations. Since the NLSE is a partial differential equation, a numerical approach is needed to solve it. This section focuses on the numerical method used for simulations throughout this thesis.

2.5.1 Non-Linear Schrödinger Equation

The NLSE governs the propagation of the electromagnetic field in optical fibers [36]. In a time frame moving with the signal group velocity, the NLSE for propagation of a slowly varying envelope in a single-mode fiber can be written as

$$\frac{\partial A}{\partial z} + \frac{\alpha}{2}A + \frac{i}{2}\beta_2\frac{\partial^2 A}{\partial t^2} - \frac{1}{6}\beta_3\frac{\partial^3 A}{\partial t^3} = i\gamma\left|A\right|^2 A, \tag{2.30}$$

where A is the solution depending on initial conditions and can be either a single wave or the sum of a couple of waves. This equations includes all the effects considered in the simulations throughout this thesis. FOD and Raman effects are not included as the FOPAs studied in this thesis have amplification bandwidths of $\sim$ 50 nm. As it was discussed in the previous section, the FOD has an insignificant influence within a 100 nm wavelength range. The peak gain of stimulated Raman scattering is bout

100 nm above the pump wavelength, which is far out of the amplification bandwidth of the considered FOPAs.

2.5.2 The Symmetrized Split Step Fourier Method

The split step Fourier method (SSFM) is the method typically used to solve the NLSE, which is based on independently applying the non-linear and dispersion effects over very short segments of fiber length h. By defining the linear and non-linear operators as

$$\hat{D} = -\frac{\alpha}{2} - \frac{i}{2}\beta_2\frac{\partial^2}{\partial t^2} + \frac{1}{6}\beta_3\frac{\partial^3}{\partial t^3}, \tag{2.31}$$

$$\hat{N} = i\gamma\left|A\right|^2, \tag{2.32}$$

Eq. (2.30) can be written as

$$\frac{\partial A}{\partial z} = (\hat{D} + \hat{N})A. \tag{2.33}$$

In a small step from z to $z+h$, Eq. (2.30) is solved one time with $\hat{D} = 0$ where the non-linearity alone is applied and second time with $\hat{N}$=0 where only dispersion is applied. An approximate solution for $A(z+h,t)$ can be obtained as

$$A(z+h,t) \approx \exp(h\hat{D})\exp(h\hat{N})A(z,t). \tag{2.34}$$

The accuracy of the SSFM depends on the procedure according to which the linear and non-linear operators are applied to propagate the electric field over a step from z to $z+h$. The symmetrized SSFM is a way to increase the accuracy of this method. In this way the non-linear operator is applied in the middle of the segment rather than at the boundaries of each segment, as shown in the Fig. 2.7,

$$A(z+h,t) \approx \exp(\frac{h}{2}\hat{D})\exp(h\hat{N})\exp(\frac{h}{2}\hat{D})A(z,t). \tag{2.35}$$

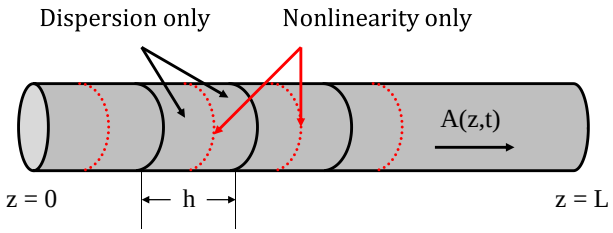

Figure 2.7: Schematic illustration of the symmetrized split-step Fourier method.

The symmetrized SSFM can be implemented as follows:

1. The fiber length is divided into a large number of equally spaced segments.

2. The optical field propagates over a distance $h/2$ with only dispersion. This needs to be carried out in the frequency domain and necessitates to transfer the optical field and the dispersion operator to the frequency domain. The linear operator in the frequency domain can be written as

$$\tilde{\hat{D}}(i\omega) = -\frac{\alpha}{2} + \frac{i}{2}\beta_2(\omega - \omega_0)^2 + \frac{i}{6}\beta_3(\omega - \omega_0)^3, \tag{2.36}$$

   where $\partial/\partial t$ is replaced by $-i\omega$. The final optical field at $z + h/2$ needs to be converted back to the time domain for the next step:

$$A(z + \frac{h}{2}, t) = F^{-1}\left[\exp\left(\frac{h}{2}\tilde{\hat{D}}(i\omega)\right)\tilde{A}(z,\omega)\right], \tag{2.37}$$

   where $\tilde{A}(z,\omega)$ is the Fourier transfer of $A(z,t)$.

3. At the point $z + h/2$, the non-linear operator acts over a distance h in the time domain

$$A(z + \frac{h}{2}, t) = \exp\left(h\hat{N}\right)A(z + \frac{h}{2}, t). \tag{2.38}$$

4. At last, the linear operator acts at the second half of the segment

$$A(z + h, t) = F^{-1}\left[\exp\left(\frac{h}{2}\tilde{\hat{D}}(i\omega)\right)\tilde{A}(z + \frac{h}{2}, \omega)\right]. \tag{2.39}$$

This method implies that the non-linearity is effectively considered at the middle of each segment. The step size in the SSFM depends on the complexity of the problem. If both dispersion and non-linearity are

significant, higher accuracy by choosing smaller step sizes is required, otherwise the error in splitting the dispersive and the non-linear step increases [40, 41]. Specifically about FOPAs, the larger the number of waves interacting, the smaller step size is needed. This point needs to be especially ensured in the saturated condition where intense waves are launched to the fiber and a large number of FWM products are generated during propagation through the fiber. All the simulations in this thesis have been carried out using the symmetrized SSFM with a constant step size[1]. The choice of step size was based on comparing the results simulated by a coarse step size with the ones obtained from a fine step size. The optimum step size was chosen the one that the simulated results based on that shows no difference with compare to the fine step size.

The following advantages can be counted for SSFM over solving the coupled equations: 1. The SSFM is time dependent, which this means that it can be used for CW as well as intensity modulated waves. 2. It is easy to insert higher-order dispersion terms; by adding more terms into the linear operator. 3. It is easy to increase the number of input fields by adding more terms to the initial global field. 4. Access to the wave evolution in time and frequency domain is possible.

2.6 Measured Parametric Gain and Amplification Bandwidth

This section presents measured parametric gain spectra in both single- and dual-pump FOPAs. More specifically, it discusses the effect of the pump power and pump wavelengths on the gain bandwidth of FOPAs.

2.6.1 Single-Pump FOPA

Single-pump FOPAs work based on degenerate FWM where an intense pump is tuned within the wavelength range where the dispersion of the fiber is anomalous. The pump transfers energy to the signal and idler located symmetrically around the pump frequency. From Eq. (2.26) one can find that the phase-matched frequency with maximum gain can be adjusted by modifying either the linear or non-linear phase-mismatch factor. Here we study the effect of both factors in practice. It should be noted that the undepleted-pump condition (unsaturated regime) has

[1] The step size in SSFM can also be adaptive according to the changes in the balance between dispersion and nonlinearity which can happen during propagation [40].

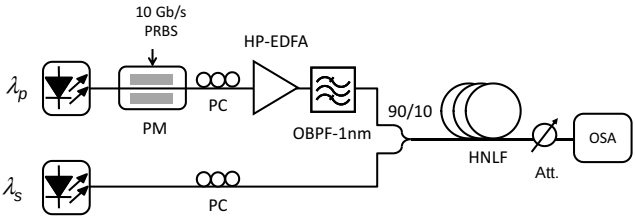

Figure 2.8: Experimental setup for a single-pump FOPA.

been assumed so far throughout this chapter. Therefore, in the following experiments the signal power is considered much lower (by at least 30 dB) than the pump power to ensure operation of the amplifiers in the undepleted-pump regime.

Experimental Setup

The experimental setup to characterize the gain spectrum of a single-pump FOPA is represented in Fig. 2.8. The pump signal originates from a continuous wave (CW) laser that is phase modulated using a 10 Gbit/s $2^7 - 1$ pseudorandom binary sequence (PRBS) to increase the threshold of the stimulated Brillouin scattering (the need for this will be discussed in the next section), amplified by a high-power erbium-doped fiber amplifier (HP-EDFA) and filtered by a 1 nm bandwidth optical band pass filter (OBPF) to reduce the produced out-of-band amplified spontaneous emission (ASE) noise. The pump is coupled with the signal, originating from a CW laser, using a 90/10% coupler to a 500 m HNLF with $\gamma = 10.7$ W^{-1}·km^{-1}, $S = 0.0185$ ps·nm^{-2}·km^{-1}, $\lambda_0 = 1550.4$ nm, and $\alpha = 0.7$ dB·km^{-1}. Two polarization controllers (PCs) are used to align the polarization states of the pump and signal by maximizing the signal gain. The gain spectra are measured using an optical spectrum analyzer (OSA).

Experimental Results

For a fiber with a fixed dispersion profile, the pump power and pump wavelength are the parameters able to modify the gain spectrum via non-linear and linear phase-mismatch, respectively. Higher values of the pump power demand higher values of $\Delta\beta$ at the phase-matched signal frequency. This means that $\kappa = 0$ for larger values of $|\omega_s - \omega_p|$, which implies a wider band amplifier. Fig. 2.9 shows the parametric gain spectra measured for different input pump powers launched to the HNLF. The pump wavelength is set at 1557.5 nm. The gain spectra are mea-

sured by sweeping the CW signal in wavelength, for different values of the pump power. The peaks located in the middle of the gain spectra are the pump waves which are not removed from the swept spectra.

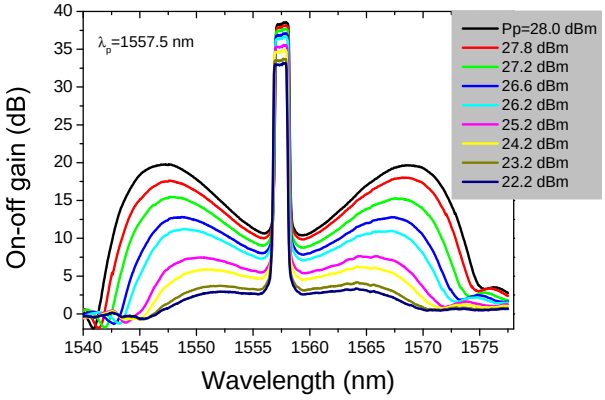

Figure 2.9: Measured parametric gain spectra for different input pump powers.

As it can be seen from Fig. 2.9, increasing the pump power has two effects: increasing the gain as well as broadening the gain spectrum. For a certain value of non-linear phase-mismatch ($2\gamma P_p$), $\Delta\beta$ can be adjusted by the choice of pump frequency, which can modify the value of $\beta_2(\omega_p)$. The closer the pump wavelength to the ZDW, the lower is $\beta_2(\omega_p)$ and the phase-matching can be fulfilled for a signal wavelength further from the pump frequency, which indeed makes the gain spectrum broader. The effect of the pump wavelength on the gain spectrum is depicted in Fig. 2.10. The ZDW is located at 1550.4 nm and the pump wavelength varies from 1548 nm to 1559 nm. For λ_p=1559 nm, the spectrum is the narrowest one and parametric gain vanishes for $\lambda_p = 1548$ nm where the pump is located in the normal dispersion region and the phase-matching is not fulfilled.

As long as the pump wavelength is located above the ZDW, one expects from the theory that changing the pump wavelength just affects the phase-matched signal frequency and is not supposed to change the value of the gain. It means that, by detuning the pump wavelength, we expect to see all the gain spectra with the same amount of maximum gain but with different bandwidths. However, one can observe from the measured spectra that the gain is lower for the phase-matched signal of the wider band amplifiers, i.e. when the pump wavelength is closer to the ZDW. This is attributed to longitudinal fluctuations of the ZDW throughout the fiber, which modify the phase-matching [42]. For a few kilometers of

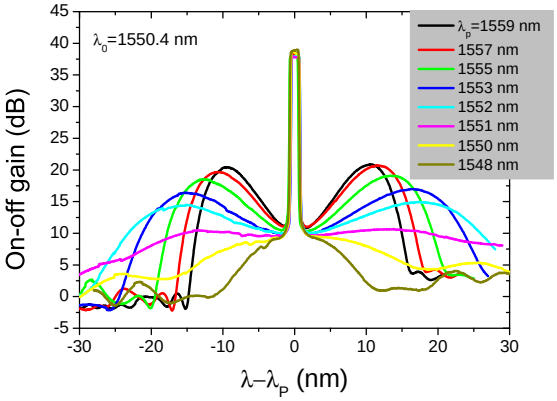

Figure 2.10: Measured parametric gain spectra for different separations of the pump wavelength from the ZDW.

HNLF, a fluctuation of ±1 nm has been measured for the ZDW, which originates from the fabrication process of the fiber [37]. Even though the wide gain spectra, i.e. the one corresponding to λ_p=1551 nm, has a lower gain value it has instead a fairly flat spectrum which can be sought for applications such as short pulse amplification. Therefore, in the vicinity of the ZDW, there is a trade off between the gain and the gain spectrum flatness.

Gain Flatness In order to amplify a large number of WDM channels or short-pulsed high-speed signals, one would like a flat gain amplifier. As we saw from theory and experiments, dispersion and non-linear phase shift are the two options one can modify to tailor the gain spectrum. Generally speaking, the gain spectrum in a single-pump FOPA is not as uniform as one would like. For a determined HNLF, one may increase the pump power to broaden the spectrum. This solution is mainly limited by the stimulated Brillouin scattering (SBS) threshold. However this can be eased by choosing shorter lengths of HNLF which increase the SBS threshold and allows for an increase of the launched pump power. In [43] 26 WDM channels are simultaneously amplified by 20 dB using a single-pump FOPA. This has been achieved by choosing a 114 m length standard HNLF and 35 dBm launched pump power.

Another way to modify the gain spectrum is tuning the pump wavelength with respect to the ZDW when the launched pump power to the HNLF is limited by the output of the EDFA or the SBS threshold. Even though locating the pump wavelength very close to the ZDW, less than

$\sim$ 2 nm, limits the signal gain as discussed, it can provide a fairly flat gain spectrum over $\sim$ 10 nm, which can safely amplify sub-picosecond pulses suitable for signals modulated at the order of the 640 Gbit/s [C-1, C4]. Chapter 7 specifically discusses FOPA designs for the amplification of such signals in a single-pump FOPA.

2.6.2 Dual-Pump FOPA

Dual-pump FOPAs work based on non-degenerate FWM. Two pumps at two different frequencies, mostly located symmetrically with respect to the ZDW, transfer energy to the signal and an idler located symmetrically with respect to the mean frequency of the pumps. By using two pumps, phase-matching can be fulfilled over a wider range of wavelengths than in a single-pump amplifier. The total phase-mismatch factor is presented as Eq. (2.23),where the linear phase-mismatch for dual-pump FOPAs will take the form

$$\Delta\beta = 2\sum_{m=1}^{\infty}\frac{\beta_{2m}(\omega_c)}{(2m)!}\left[(\omega_s-\omega_c)^2-\Delta\omega_p^2\right], \tag{2.40}$$

where $\omega_c = (\omega_{p1}+\omega_{p2})/2$ and $\Delta\omega_p = (\omega_{p1}-\omega_{p2})/2$ as schematically shown in Fig. 2.11. The pumps' frequency difference, $\Delta\omega_p$, is a parameter which, independently from the signal frequency, contributes to the phase-matching and can control the phase-matching over a wide spectral range. Locating the pumps far enough from each other, $\Delta\beta$ will have a relatively large negative value, which can be balanced by high values of non-linear phase-mismatch $\gamma(P_{p1}+P_{p2})$ and finally provides broadband amplification. Setting the pump mean frequency, ω_c, at the ZDW one can make $\Delta\beta$ almost constant over a wide spectral range, as it will be dominated by the FOD. Then a constant value of non-linear phase-mismatch can easily cancel out $\Delta\beta$ and broaden the possible amplification bandwidth.

Pump-Pump Interaction

The first interaction in dual-pump FOPA stems from the degenerate FWM between the two pumps themselves, depicted as P_C and P_L in Fig. 2.11, generating two new frequencies, I_C and I_L, which exist independently of a signal being launched together with the pumps to the HNLF or not. The conversion efficiency of these idlers depends on the pump frequency separation, $2\Delta\omega_p$, as well as the pump powers. For a fixed level of power for both pumps, wavelength detuning of the pumps with respect to the ZDW can affect the conversion efficiency of these

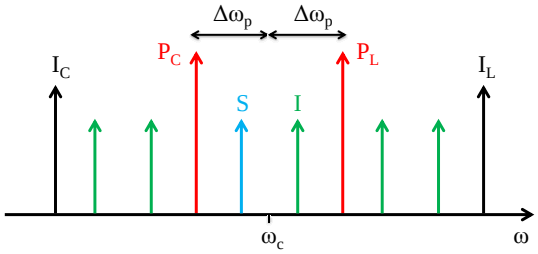

Figure 2.11: Nomenclature of waves interacting in dual-pump FOPA.

idlers. As FWM is a parametric process and all the energy launched to the medium is exchanged between the existing waves, these idlers compete for power transfer from the pump when a signal is launched to the HNLF. In fact, one can find the optimum range of $\Delta\omega_p$ for which the conversion efficiency of these idlers is minimum, which results in more power transfer to the signal. Therefore, the first step in the optimization of a dual-pump FOPA for a given pump power level can be finding the optimum value of $\Delta\omega_p$ by minimizing the conversion efficiencies of the pump generated idlers.

Fig. 2.12(left) shows simulated output power of two the pumps and the generated idlers in a 500 m HNLF, having the parameters listed in the caption of the figure, when no signal exists, for two levels of pump powers $P_C = P_L = 24$ dBm and 26 dBm .

The output power of the idlers is weak for $\Delta\lambda_p = \lambda_C - \lambda_L \sim 20$ nm for $P_C = P_L = 24$ dBm while the generation of the idlers is more efficient for higher pump powers, $P_C = P_L = 26$ dBm, and they become weak for $\Delta\lambda_p \sim 25$ nm. The experimentally measured output spectrum for $P_C = P_L = 26$ dBm is shown in Fig. 2.12(right) for $\Delta\lambda_p = 15.6$ nm and 20 nm. Generation of the idlers can be enhanced by high power pumping as well as small values of $\Delta\omega_p$. Depending on these two factors, the power of the idlers can even exceed the pump powers as can be seen for $\Delta\lambda_p = 15.6$ nm.

Gain spectra for dual-pump FOPAs are simulated and shown in Fig. 2.13 for different values of pump power. The pump wavelength separation is fixed to 40 nm and the pumps are located at 1540 nm and 1580 nm. The gain spectrum is symmetric around the average pump frequency and is flatter for the higher pump powers, i.e. $P_C = P_L = 25$ dBm, when the linear and non-linear mismatches are well balanced.

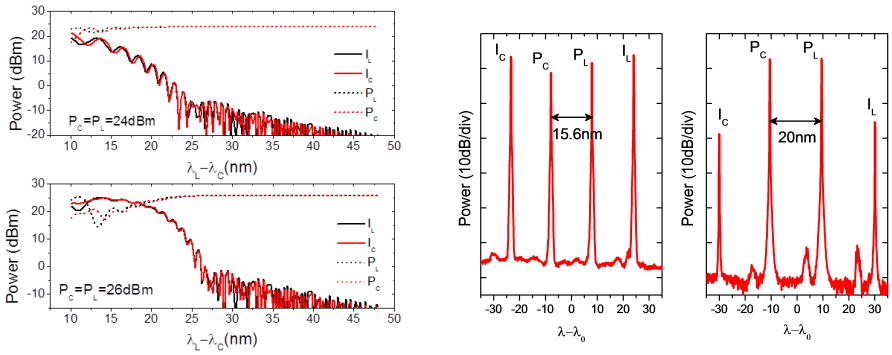

Figure 2.12: Left: simulated output power of the pumps and idlers generated by the pumps. Right: measured output power spectra for two different pump wavelength separations (15.6 nm and 20 nm) when P_C=P_L=26 dBm. γ = 10.7 W^{-1}·km^{-1}, S = 0.017 ps·nm^{-2}·km^{-1}, ZDW=1561 nm, α=0.7 dB·km^{-1}.

Experimental Setup

The experimental setup for a dual-pump FOPA is shown is Fig. 2.14. Two pumps in the C- and L- bands originating from two tunable laser sources are combined, phase modulated by three radio-frequency (RF) tones to broaden their spectra and suppress the back scattered power (this will be clarified later in the next section) then amplified by two high-power EDFAs. The out-of-band ASE noise is filtered by 1 nm OBPFs and the pumps are then combined with the signal into a HNLF that has the same parameters already mentioned. WDM couplers with less than 1 dB coupling loss are used to combine and split the pumps. The polarization of the all waves are alined to obtain the maximum amplification for the signal.

Experimental Results

On-off gain spectra for different pump powers and pump wavelength separations are shown in Fig. 2.15. The local peak in the middle of the spectrum, with 3 dB more power, corresponds to the average pump frequency where the signal overlaps with the generated idler. As it can be observed, the gain spectrum around the pumps is not flat. This is due to the generated idlers which are symmetric of the signal with respect to the pumps adjacent to them. Such structures can be qualitatively understood as resulting from the interaction between the basic two-pump gain mechanism and the two one-pump gain spectra that would exist around each pump if the other one were turned off [44]. Maximum Raman amplification of $\sim$ 1 dB was measured for the pump wave located

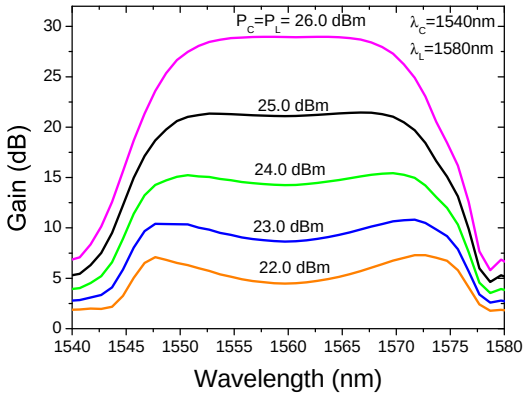

Figure 2.13: Simulated gain spectra for a dual-pump FOPA for different pump input powers.

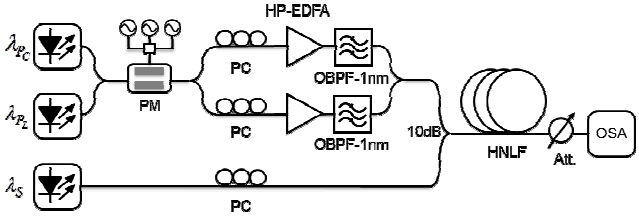

Figure 2.14: Experimental setup for a dual-pump FOPA.

at 1580 nm, gained from the pump wave located at shorter wavelength 1540 nm.

2.7 Implementation of FOPAs

There are some practical points that need to be considered in the implementation of FOPAs. This section discusses two main concerns: one is the back-scattered power in the HNLF and the other one is the polarization sensitivity of FOPAs.

2.7.1 Stimulated Brillouin Scattering

The main constrain in CW pump based FOPAs is SBS, which prevents launching high optical powers into the fiber and limits the efficient pump power transmitted to the HNLF. SBS has a low threshold and high gain, thus it is desirable to increase the SBS threshold of the fiber or decrease the Brillouin gain coefficient.

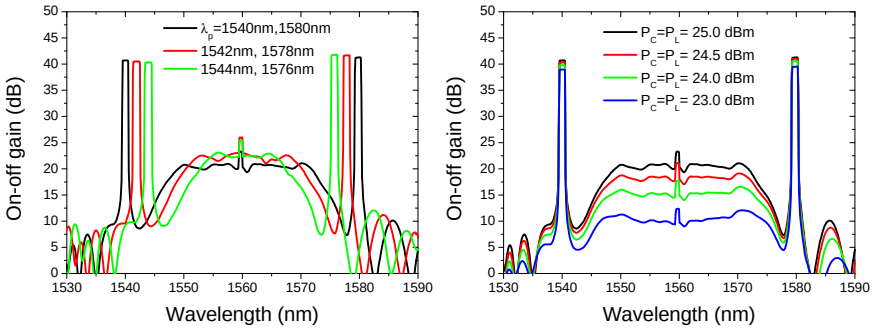

Figure 2.15: Measured dual-pump gain spectra. Left: for different pump powers(λ_C=1540 nm, λ_L=1580 nm). Right: for different pump wavelength separations ($P_C = P_L =$ 25 dBm).

SBS is a non-linear effect which originates from an inelastic scattering process in which a part of the energy of the optical field is transferred to the medium as an acoustic wave, downshifted in frequency. The frequency shift of the the acoustic waves (Brillouin frequency shift) depends on the scattering angle between the incident and scattered light. The frequency shift is zero in the same direction as the incident light (forward scattering) and is maximum in the opposite direction to that of the incident light (backward scattering) . Particularly, in a single-mode optical fiber, SBS can only occur in the backward direction.

The SBS threshold, P_{th}, is defined as the input pump power for which the back-scattered power becomes equal to the pump power at the input of the fiber[2] and can be approximately given by

$$P_{th} = 21 \left(\frac{A_{eff}}{g_B L_{eff}} \right) \left(\frac{\Delta\nu_B + \Delta\nu_p}{\Delta\nu_B} \right), \tag{2.41}$$

where A_{eff} is the effective area of the fiber, g_B is the Brillouin gain coefficient, L_{eff} is the effective length of the fiber, $\Delta\nu_B$ and $\Delta\nu_p$ are Brillouin gain and pump spectral bandwidth, respectively. In practice, there are two techniques used to increase the SBS threshold. One is based on manipulating the physical properties of the fiber, which affects the Brillouin gain bandwidth, $\Delta\nu_B$, and thus the Brillouin gain coefficient g_B, while the other one deals with the launched beam to the fiber resulting in broadening the laser linewidth, $\Delta\nu_p$.

[2]The SBS threshold can be defined in different ways. It might also be defined as the input power where the back-scattered powers from SBS and Rayleigh scattering are equal or the input power at which 1% of the input power is back reflected.

Broadening the Brillouin gain bandwidth One way to mitigate SBS is to change the acoustic guiding of the optical fiber which varies the frequency of the acoustic wave and affects the Brillouin gain bandwidth. This can be done by modifying the core radius, dopant concentration, applying linear or stepwise strain and temperature gradients to the fiber [45, 46, 47, 48, 49], etc. These methods rely on the fact that the Brillouin frequency downshift (the frequency of the longitudinal acoustic mode) can be changed along the fiber. Therefore, the SBS shift can be distributed over a broader frequency rang which in turn results in an increase of the Brillouin gain bandwidth and reduces the effective Brillouin gain of the fiber.

Broadening the laser linewidth The other way to enhance the SBS threshold is broadening the linewidth of the pump laser by phase or frequency modulation beyond the Brillouin gain bandwidth [50, 51]. If the pump spectrum is spread over a frequency range, then the power spectral density is lower which result in less efficient SBS over a broader frequency range. In this case, the pump spectrum needs to be broadened more than the Brillouin gain bandwidth in order to efficiently decrease the amount of power within the Brillouin gain bandwidth and consequently increase the SBS threshold.

SBS suppression in HNLFs Broadening the pump linewith by phase modulation (PM) more than the SBS bandwidth (which is typically tens of MHz), using discrete sinusoidal radio-frequency (RF), PRBS or white noise source are the most common ways to suppress SBS. Even though this method has been recognized as the most efficient method, it however introduces some undesirable effects to the system. For example, pump phase modulation broadens the linewidth of the converted signal approximately twice compared to the pump linewidth as the electric field of the idler is proportional to the squared electric field of the pump wave. Also pump phase modulation can be transferred to intensity modulation through filtering or dispersion and modulate the signal gain and the conversion efficiency. Specially, this method cannot be applied for phase-sensitive FOPAs where a precise phase control of the pumps, signal and idler is needed.

Temperature or strain control methods can be other options, which do not introduce noise to the pump. On the other hand, these methods may be manageable only over short lengths of fibers or may shorten the life time of the fiber. As a consequence of stretching the HNLF, the core geometry of the fiber is changed, which results in changes in

the dispersion profile of the fiber, including a ZDW gradient along the fiber, or possibly increase the polarization mode dispersion (PMD) of the HNLF. Since precise dispersion characteristics of HNLFs are needed to design FOPAs, this method may not applicable in many cases.

Aluminum doping instead of germanium doping can increase the SBS threshold by raising the refractive index and lowering the acoustic index. However, Al-doped HNLFs have about 8 times more loss than standard HNLFs which largely limits their effective length [52].

Using a couple of optical isolators along the fiber can help suppressing the back-scattered power. Nevertheless, the loss of the isolators and additional coupling loss added to the system limits the launched power to the fibers. Recently a fiber optic parametric amplifier/wavelength converter has been constructed from four HNLF pieces with applied strain gradients and separated by isolators. The effective total SBS threshold increase using this scheme is about 11 dB which results in 10 dB parametric gain [53].

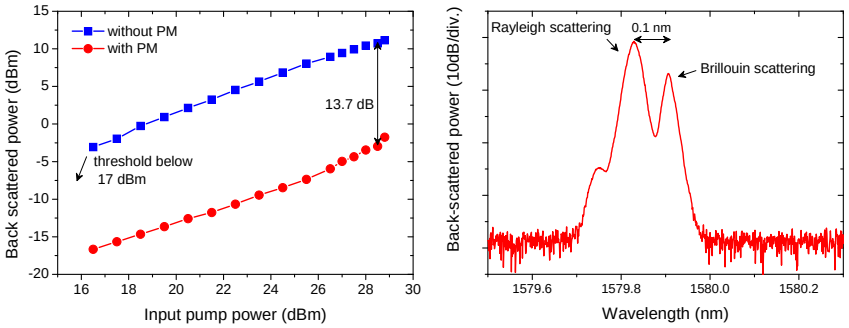

Figure 2.16: Left: Measured Brillouin back-scattered power with and without pump PM at 10 Gbit/s. Right: Back scattered power spectrum corresponding to 28.5 dBm input power into a 500 m standard HNLF.

In the experiments reported in this thesis, SBS is efficiently suppressed through phase modulation of the pump wave, where the phase modulator is driven either by a PRBS or a combination of discrete RF tones. The back-scattered power from a 500 m long HNLF, with the characteristics listed in the caption of Fig. 2.12, with and without pump PM (at 10 Gbit/s using PRBS) is shown in Fig. 2.16(left). Defining the SBS threshold as the input power where the back scattered power deviates from linear behavior, about 12 dB of increase in SBS threshold, from below 17 dBm to 28.5 dBm, is measured. Fig. 2.16(right) shows the back scattered power spectrum corresponding to an input pump power of 28.5 dBm showing the Rayleigh back-scattered power at the pump

frequency and the Brillouin one with a 0.1 nm wavelength shift.

It is worth to mention that the phase-matching in FOPAs is less affected by phase modulating the pump wave using RF tones than PRBS by considering the point that the spectrum of a phase modulated wave is more uniformly broadened using a combined RF tones than a PRBS [54]. Therefore, in the following chapters, in these experiments where data modulated signals have been amplified in FOPAs, SBS is suppressed by pump PM where the phase modulator is driven by three or four combined RF tones.

2.7.2 Polarization Sensitivity

Parametric gain/conversion efficiency strongly depends on the states of polarization (SOP) of the interacting waves as a result of the requirement of angular-momentum conservation among the four interacting photons in the FWM process [55], which can be understood from the full vector theory of the FWM process in optical fibers. This polarization sensitivity can be an issue for the practical implementation of FOPAs in optical communication links where they can be used as in-line amplifiers. Moreover, for amplification and signal processing of polarization multiplexed data signals, polarization independent FOPAs are vital.

There are different techniques to realize a polarization independent FOPA either in single- or dual-pump configurations. In dual-pump FOPAs, polarization insensitive operation can be acheived by employing a polarization diversity loop [56, 57] or by orthogonal linearly polarized pumps [58]. For single-pump FOPAs only the scheme based on polarization diversity loop is applicable. In the following, the polarization independent parametric gain realized in a single-pump FOPA is discussed.

Experimental Setup for Polarization Diversity Scheme in

Fig. 2.17 illustrates the setup for the polarization diversity loop scheme in a single-pump FOPA. In this scheme, the input pump is split equally in power into two orthogonal linearly polarized components, by means of a 4 port polarization beam splitter (PBS). The two pump polarization components propagates in clockwise and counter-clockwise directions inside the HNLF. The input signal, which is randomly polarized using a polarization scrambler (PS), enters the loop at the T port of the PBS and is split into two orthogonal components with a power splitting depending on its input polarization. Each signal component co-propagates with a co-polarized pump beam and as long as the signal power is low

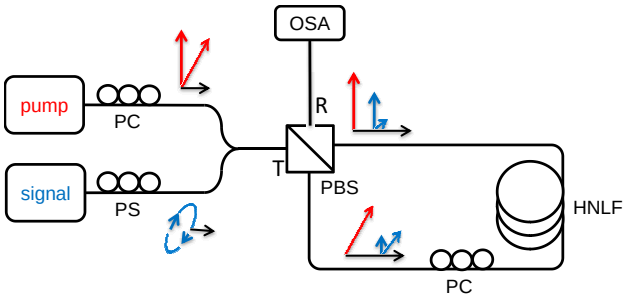

Figure 2.17: Experimental setup for a polarization diversity single-pump FOPA.

enough to ensure small-signal gain operation, the two counter propagating signal components are amplified identically and then recombined at the R port of the PBS. A polarization controller is used inside the loop to ensure that the signal beams exit the loop at port R and no power is reflected to the input port T.

Experimental Result

A polarization independent gain spectrum measured for a single-pump FOPA is shown in Fig. 2.18 and compared with the case when the signal and pump are linearly co-polarized by sending all the pump power in one path and matching the signal SOP in order to maximizing the gain. About 10 dB gain difference can be observed where using the polarization diversity scheme and splitting the pump power. Even though the PBS ensure that the two pump polarization components have the same power, some insertion loss reduces the gain. Splitting the pump power costs the gain 6 dB. Using a PBS with $\sim$ 1 dB insertion loss limits the gain by 4 dB in the FOPA used in this experiment addition to the 6 dB gain reduction from splitting the pump power. Considering co-polarized pump and signal, 1 dB reduction of the pump power from 27.5 dBm to 26.5 dBm reduces the gain by about 4 dB, which can be calculated from the maximum gain for the phase-matched signal, $G_{max} = \exp(2\gamma P_p L)/4$. Fig. 2.18 shows the signal output power fluctuations over time with a residual polarization dependence of less than 0.3 dB where the input signal is scrambled.

Polarization-Independent Dual-Pump FOPA

For a dual-pump FOPA, the same configuration can be used where two pump beams are introduced at the T port of the PBS. If we intent to

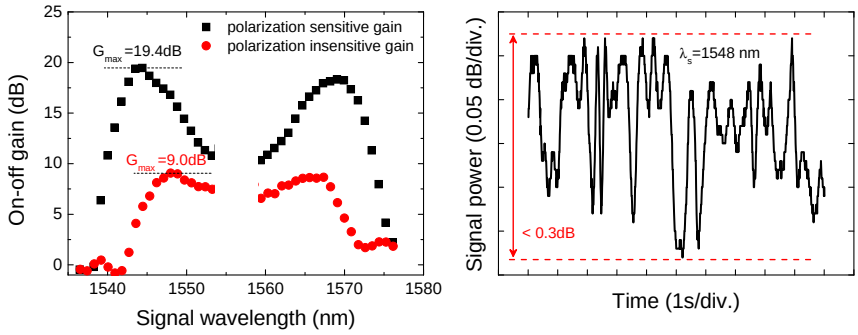

Figure 2.18: Left: polarization-sensitive and polarization-insensitive on-off gain spectra. Right: output signal power when the polarization scrambler is on.

achieve high gain with a dual-pump FOPA, a PBS with high power handling capacity is needed.

Polarization-independent parametric amplification and wavelength conversion of 28 GBd differential quadrature phase-shift keying (DQPSK) signals in dual-polarization has been realized in a polarization-diversity loop [59] with 20 dB on-off gain. Polarization-independent dual-pump FOPAs can also be realized in a unidirectional setup with no loop where two pump beams with orthogonal polarizations are launched along with the signal to the HNLF [58]. In this case the full power of the pumps propagates through the HNLF but with orthogonal polarization. Even though the 6 dB gain reduction is not expected in this configuration, the orthogonality of the pumps reduces the non-linear coupling efficiency.

Polarization-Independent Gain-Saturated FOPA

The discussed polarization diversity scheme, using a single stage of FOAP, works based on the linear gain operation of FOPAs, i.e when the parametric gain is independent of signal input power. It means that the ratio in power spilling of the two polarization states of the signal does not affect the gain, as long as the pump power is split equally for both polarization. However, in non-linear (saturated) regime, amplification depends on the signal power, and an unequal splitting power for the signal results in different gains for each sate of the signal polarization.

Polarization independent amplification in saturated regime can be realized in a two-stage amplification [60]. In this scheme, two stages of FOPA cascaded with 45^{o} polarization rotated alignments. Amplification for the two states of the signal polarization in the second stage is opposite of the first stage, which at the end results in a same amplifica-

tion/saturation for the both states of polarizations. Using this scheme, polarization independent limiter has been demonstrated for level equalization for a waveform deteriorated and polarization scrambled 40 Gbit/s signal [60].

2.8 Summary

In this chapter, the principles of FOPAs under undepleted pump condition were theoretically and experimentally discussed. Phase-matching, as the main requirement for parametric amplification was discussed and its effect on the amplification bandwidth and signal gain was experimentally shown in both single and dual-pump FOPAs. The power and wavelength of the pump (pumps) combined with the dispersion profile of the fiber are the main parameters tailoring the parametric gain spectrum. Practical solutions in order to suppress the unavoidable back-scattered pump power and the advantages and drawbacks were discussed. Polarization insensitive single-pump FOPAs implemented using a polarization diversity scheme have been explained and experimentally measured.

Chapter 3

Gain Saturation in Fiber Optical Parametric Amplifiers

3.1 Introduction

In the previous chapter, the parametric gain was studied under undepleted pump assumption, i.e. $P_s \ll P_p$. In this condition, the signal gain is independent of the signal power launched to the amplifier. The schematic behavior of the pump and signal powers as well as signal gain as a function of input signal power are shown in Fig. 3.1. As the signal input power increases, the pump power depletes, which results in a decrease of the signal gain. At some point, shown in green, the signal output power saturates which is known as saturated regime. Applications such as reduction of intensity fluctuations of the input signal [24, 22] necessitate the fiber optical parametric amplifiers (FOPAs) to operate in their saturated regime and therefore accentuate the need for proper characterization of the saturated gain spectra of FOPAs. This chapter explores the gain saturation behavior of single-pump FOPAs in section 3.2 and dual-pump FOPAs in section 3.2.

3.2 Asymmetric Gain-Saturated Spectrum in Single-Pump FOPAs

Single-pump FOPAs working in the undepleted pump regime (can also be named linear or unsaturated regime) have only one dominant four-wave mixing (FWM) product (idler), which is symmetrically located with

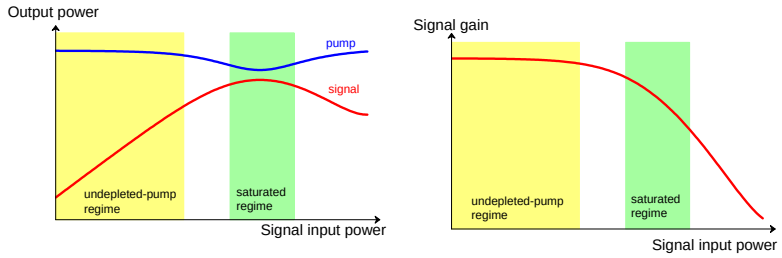

Figure 3.1: Signal power and gain evolutions as a function of signal input power from the undepleted-pump to the saturated regime.

respect to the pump frequency. In the unsaturated gain regime, the gain spectrum is symmetric with two gain peaks corresponding to two phase-matched signal frequencies around the pump. As it was shown in section 2.4, the symmetric feature of the unsaturated gain spectrum originates from the fact that the linear phase mismatch factor, $\Delta\beta$, depends only on even-order dispersion as well as on the even powers of the pump-signal frequency separation.

To study the gain spectrum behavior in the non-linear saturated regime for single-pump FOPAs, one may solve the coupled equations based on the interaction between only three waves (pump, signal and idler) or solve the generalized non-linear Schrödinger equation (NLSE) which takes into account all the waves generated in the parametric processes and their interactions. The unsaturated and saturated gain spectra obtained from each method with and without including third-order dispersion (TOD) are presented in Fig. 3.2. The black curves show the unsaturated spectra, which are the same in the three cases. The red curves show the saturated gain spectra. One can see that the saturated gain spectrum is not symmetric anymore when the TOD is included int the interaction between the waves. The output power spectra in saturation, for the signal tuned to the phase matched frequency for linear regime, is shown in the second row of Fig. 3.2. As it can be seen, the power distribution of the waves around the pump is asymmetric after including the TOD.

In fact, in the non-linear gain regime, the saturated gain spectrum remains symmetric as long as the higher-order FWM products (HFPs defined as the FWM products other than the idler) do not grow significantly. However, under strong saturation conditions, the power of some of the HFPs may reach or even exceed the signal power and therefore those products can no longer be ignored in the analysis of the gain spectrum. The behavior of the gain spectrum of FOPAs in the non-linear

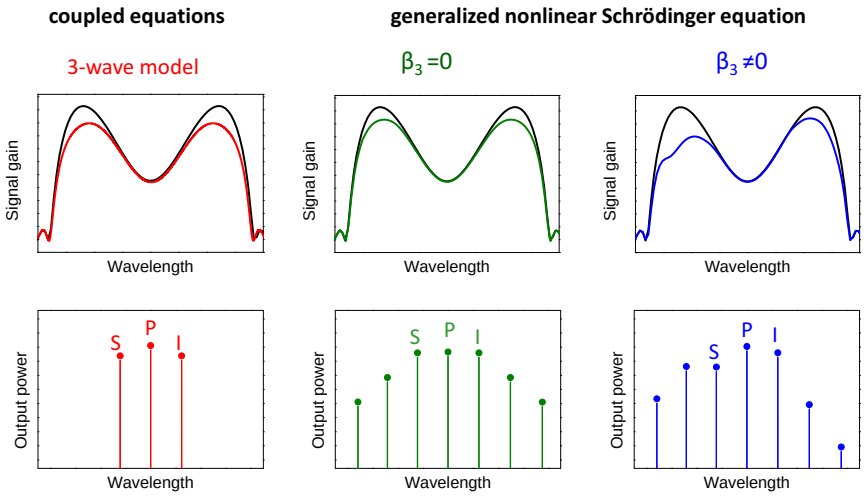

Figure 3.2: Comparison of FOPA gain calculated using coupled equations and the NLSE in linear and saturated gain regime when the TOD is ignored or taken into account in the saturation.

regime (i.e. under gain saturation) has been studied in a few papers [61, 62], whereas in most reported applications using FOPAs in the saturation regime, only some specific wavelengths within the gain spectrum have been selected for operation. So far, the existence of a gain difference between the two sides of the gain spectrum of single-pump FOPAs in saturation has neither been studied nor analyzed. This section discusses the gain asymmetry in gain spectra of single-pump FOPAs under saturation and explains the possible original physical mechanism leading to this new and different gain asymmetry [C-7, J-4].

3.2.1 Experimental Observation

The asymmetric gain spectrum was first observed experimentally. The experimental setup is represented in Fig. 3.3. The pump signal originates from a continuous wave (CW) laser at $\lambda_p = 1557.5$ nm that is phase modulated using a 10 Gbit/s $2^7 - 1$ pseudorandom binary sequence (PRBS) to suppress stimulated Brillouin scattering, amplified by an erbium-doped fiber amplifier (EDFA) and filtered by a 1 nm bandwidth optical band pass filter (OBPF) to reduce the produced amplified spontaneous emission (ASE) noise.

A tunable laser source provides the signal, which is amplified by a flat-gain EDFA swept in wavelength in the range of 1538 nm to 1575 nm. The input signal power is controlled by a variable attenuator (Att.). A

10/90% coupler combines the pump and signal, whose states of polarization are optimized with polarization controllers (PCs), into a 500 m long highly non-linear fiber (HNLF) with zero-dispersion wavelength (ZDW) at $\lambda_0 = 1550.4$ nm, non-linear coefficient of 10.7 $W^{-1}{\cdot}km^{-1}$, dispersion slope of 0.0185 $ps{\cdot}nm^{-2}{\cdot}km^{-1}$, and attenuation of 0.7 $dB{\cdot}km^{-1}$. The pump power at the HNLF input is 28.6 dBm. The gain spectra are measured using an optical spectrum analyzer (OSA). The experimentally measured signal gain spectra for unsaturated gain and signal input powers (P_s) of -3 dBm (modest saturation) and -0.2 dBm (strong saturation) are shown in Fig. 3.6. The experimental unsaturated gain spectrum is symmetric and has 25.4 dB gain at 1546 nm (anti-Stokes side) and 1570 nm (Stokes side). Clearly, one can see that the maximum gain drops differently at the two lobes of the spectrum when the gain enters saturation. The measured gain differences between the wavelengths corresponding to the maximum unsaturated gain are 1.9 dB and 3.5 dB when P_s is -3 dBm and -0.2 dBm, respectively.

3.2.2 Interplay of HFPs and Dispersive Waves

To understand the physical mechanism behind this unexpected gain asymmetry, the interaction between all the waves, present at the input of the amplifier as well as generated during propagation through the HNLF, is considered in both time and frequency domains. In FOPAs, an increase of the signal input power results in a growth of the FWM products. Fig. 3.5(a) represents the nomenclature of the FWM products used throughout this work. The pump P and signal S generate an idler I. In the single-pump FOPAs considered here, HFPs (corresponding to FWM products other than the idler) are generated on an angular frequency grid with spacing $\Delta\omega_{ps} = |\omega_p - \omega_s|$. The nth order HFP, noted nHFP, is at angular frequency $\omega_n = m\omega_s - (m-1)\omega_p$ on the signal

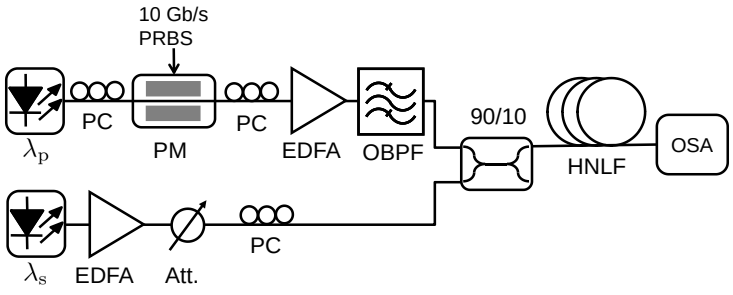

Figure 3.3: Experimental setup for FOPA gain characterization.

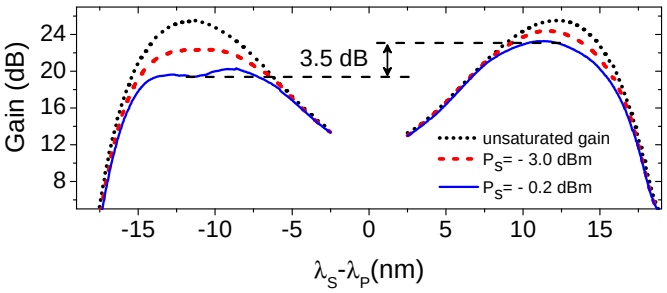

Figure 3.4: Experimental signal gain spectra for different signal input powers.

side when $n = m - 1$ (for integer $m \geq 2$), or on the idler side when $n = m + 1$ (for integer $m \leq -2$). In the time domain, the total (pump, signal, idler and HFPs) power appears as oscillations that transform into a train of short pulses when the number and power of the HFPs increase. Therefore, as the amplifier enters the saturation regime and short pulses are formed, higher order dispersion, and more specifically TOD, affects considerably the dynamics of the propagating waves. Since the pump is located in the anomalous dispersion region of the fiber, the short pulses are perturbed in the presence of TOD and emit dispersive waves (DWs) to become stable as fundamental solitons [63]. DWs are radiated at the anti-Stokes side of the spectrum in the normal dispersion region of the fiber when the phase matching condition between them and fundamental solitons is fulfilled. Similar considerations have been introduced for the interpretation of CW pumping in supercontinuum generation [64] and of symmetry-breaking of modulation instability spectra [65].

Assuming that dispersion orders higher than TOD can be neglected, the generated DWs are separated in frequency from the pump by $\Delta\omega_{DW}$ such that

$$\beta_3 \Delta\omega_{DW}^3 + 3\beta_2 \Delta\omega_{DW}^2 - 3\gamma P_p = 0, \tag{3.1}$$

where β_2 and β_3 are the second order dispersion (SOD) and TOD, respectively, P_p is the pump power and γ is the non-linear coefficient [36]. Energy transfer to shorter wavelengths as DWs disturbs the symmetric FWM efficiency between the two sides of the gain spectrum. If the condition $\Delta\omega_{DW} = (n+1)\Delta\omega_{ps}$ is satisfied, where n is an integer $n \geq 1$ and $\Delta\omega_{ps}$ is the pump-signal angular frequency separation, the DWs will overlap at the anti-Stokes side with the signal (when $\lambda_s < \lambda_p$) or idler (when $\lambda_s > \lambda_p$) for $n = 0$, the first order HFP for n = 1 (1HFP when $\lambda_s < \lambda_p$ or -1HFP when $\lambda_s > \lambda_p$)) and so on.

Frequency matching between the generated DWs and HFPs for $|n| \geq 1$ reduces the energy transfer to the wavelength at $n = 0$ corresponding

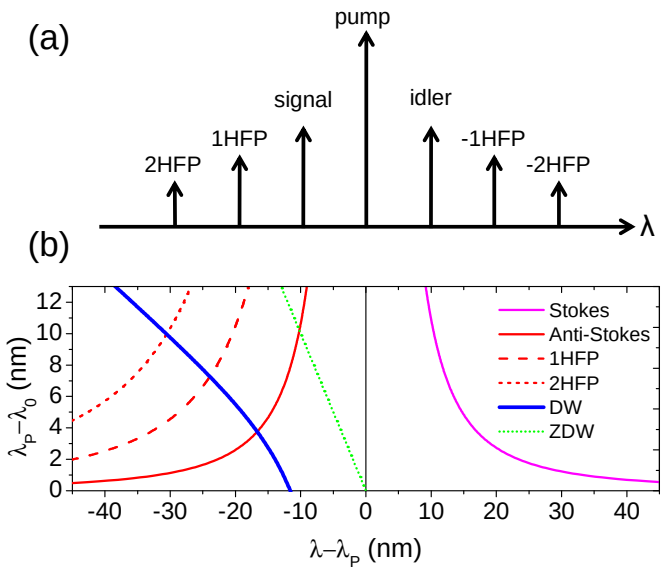

Figure 3.5: (a) Nomenclature of the FWM products . (b) Wavelength positions of the maximum unsaturated gain at the Stokes and anti-Stokes sides of the pump, corresponding 1HFPs, 2HFPs, as well as DWs for different values of the detuning between the pump and the zero-dispersion wavelength $\Delta\lambda_{p0}$.

to the signal (idler) when $\lambda_s < \lambda_p$ ($\lambda_s > \lambda_p$), hence reducing the gain or conversion efficiency at the anti-Stokes side.

The wavelengths of the maximum unsaturated gain at the Stokes and anti-Stokes sides of the pump, corresponding 1HFPs and 2HFPs, and DWs are displayed in Fig. 3.5(b) as a function of the separation between the zero-dispersion and the pump wavelengths ($\Delta\lambda_{p0} = \lambda_p - \lambda_0$). As it can be seen, the wavelengths of the generated DWs overlap with the signal or the HFPs when $\Delta\lambda_{p0}$ is between 3 and 10 nm. In the reported experiment, $\Delta\lambda_{p0} = 7.1$ nm, for which it can be seen from Fig. 3.5(b) that the 1HFP almost overlaps with the DWs, which leads to energy transfer to the 1HFP, which in turn reduces the signal gain at the anti-Stokes side of the spectrum. The growth of the ±1HFP is well confirmed in Fig. 3.6, which shows the experimental output power of the pump, signal, idler and ±1HFPs as a function of the signal input power for signals at 1546 nm and 1570 nm, corresponding to wavelengths of maximum unsaturated gain. For low signal input powers, the signal and idler waves grow identically, but for input powers above -5 dBm, the wave (signal or idler) located on the Stokes side gains more power as a result of the energy transfer to the first order HFP (1HFP for $\lambda_s = 1546$ nm or -1HFP for $\lambda_s = 1570$ nm) coinciding with the DWs on the anti-Stokes

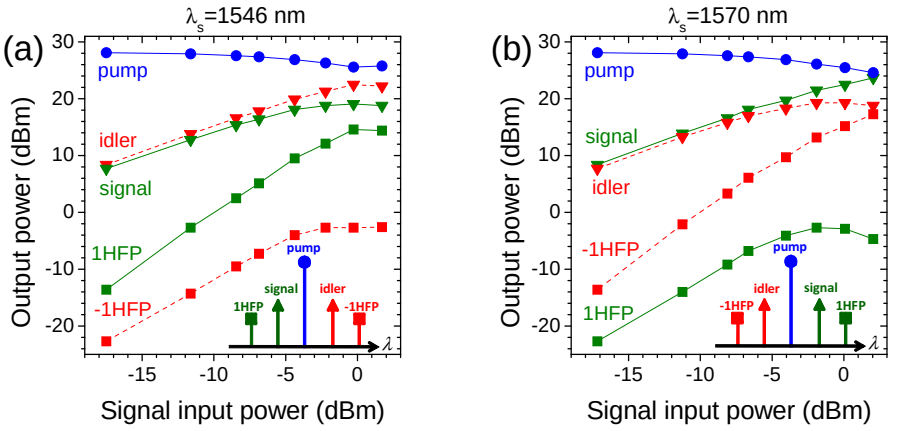

Figure 3.6: Experimentally measured output power of the pump, signal, idler and ±1HFPs for signal wavelengths equal to: (a) $\lambda_s = 1546$ nm (b) $\lambda_s = 1570$ nm.

side. The steep power growth of the first order HFP on the anti-Stokes side is also clearly observed.

3.2.3 Numerical Simulations: Impacts of SOD and TOD

The understanding of the interaction between the HFPs and generated DWs in strong saturation regime is confirmed in this section by simulations, where different values of SOD and TOD have been examined. Simulations are carried out in order to support the proposed mechanism leading to different energy transfers to the waves at the two sides of the saturated gain spectrum. In this section, the gain spectrum of the amplifier implemented experimentally is first simulated. The simulations are then expanded in order to investigate the impact of SOD and TOD on the signal gain or idler conversion efficiency in the linear and non-linear regimes. The gain spectra are simulated by numerically solving the generalized NLSE using the split-step Fourier method [36]. The NLSE used in this work takes the form

$$\frac{\partial A}{\partial z} + \frac{\alpha}{2}A + \frac{i}{2}\beta_2\frac{\partial^2 A}{\partial t^2} - \frac{1}{6}\beta_3\frac{\partial^3 A}{\partial t^3} = i\gamma\left|A\right|^2 A. \tag{3.2}$$

The initial complex envelop is the sum of those of the CW pump and signal

$$A(0,t) = \sqrt{P_p(0,t)}\exp(-i\omega_p t) + \sqrt{P_s(0)}\exp(-i\omega_s t), \tag{3.3}$$

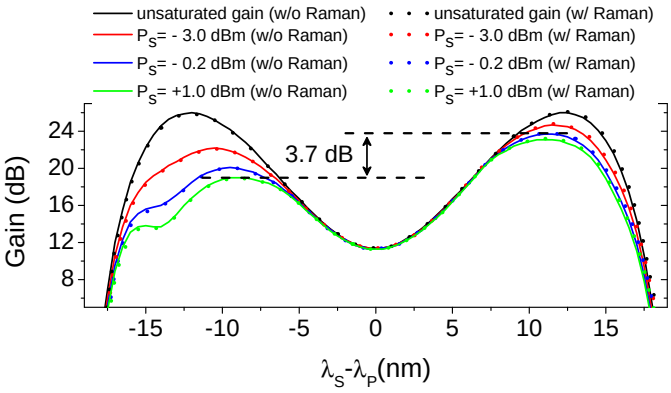

Figure 3.7: Signal gain spectra simulated for different signal input powers with and without taking SRS into account.

where the angular frequencies are expressed relatively to the reference frequency used for baseband transformation. This approach is suitable for the problem under study since it enables to account for all the waves created through all the FWM processes. This is in contrast with the resolution of a system of coupled equations (one for each wave) which limits beforehand the number of waves taken into account and therefore may not be accurate in deep saturation conditions where a potentially large number of HFPs are involved. The calculated gain spectra are shown in Fig. 3.7 for parameters identical to those of the experiment, as well as under stronger saturation with a signal input power of +1 dBm. The solid gain curves have been calculated according to Eq. (3.2) without taking stimulated Raman scattering (SRS) into account in the simulations. The simulation results are in very good agreement with the experiment. The gain differences between the two wavelengths corresponding to the maximum unsaturated gain are 2.1 dB, 3.7 dB and 4.7 dB when the signal input power is -3 dBm, -0.2 dBm, and +1 dBm, respectively. The small discrepancies observed between the simulated and measured gain spectra are believed to be due to the limited accuracy in the determination of the exact dispersive properties of the fiber used in the experiment and their longitudinal variations and to polarization effects.

The FOPA under investigation has a rather limited bandwidth, with a maximum unsaturated gain offset from the pump wavelength by 12 nm. Therefore one would not expect SRS, with a gain peak at about 100 nm above the pump wavelength, to significantly affect the gain spectrum and result in gain asymmetry for such a narrow bandwidth FOPA. This is confirmed when examining both measured and calculated unsaturated

gain spectra in Fig. 3.4 and Fig. 3.7, respectively, which appear symmetric. In order to further confirm that the observed asymmetry is not related to SRS, the gain calculations are repeated by taking SRS into account. In these simulations, the SRS effect is modeled conventionally by adding a delayed non-linear response term to Eq. (3.2) corresponding to a single-Lorentzian approximation of the Raman gain [36]. The corresponding FOPA gain spectra are also represented in Fig. 3.7. It clearly appears that SRS has very little impact on the calculated gain spectra and therefore does not contribute significantly to the reported spectral asymmetry.

As the wavelengths of the DWs, hence $\Delta\omega_{DW}$, depend on both SOD and TOD, their overlaps with the HFPs can be tuned by adjusting either the SOD or TOD of the fibre. Modification of the SOD can modify both the wavelength of the phase matched signal and that of the DWs, while variations of TOD has an impact only on the wavelength of the DWs as the phase matched signal wavelength depends only on SOD. Here we investigate the effect of both dispersion terms.

Impact of SOD

The bandwidth of FOPAs depends on the fulfillment of the phase matching condition, which under the assumption that dispersive effects higher than β_3 can be neglected, and in the unsaturated regime (i.e. the pump power dominates over the power of the signal and idler), is expressed as

$$\Delta\beta + 2\gamma P_p = \beta_2(\omega_p)\Delta\omega_{ps}^2 + 2\gamma P_p = 0, \tag{3.4}$$

where $\Delta\beta$ is the linear phase mismatch parameter. In what follows, the bandwidth of the FOPA is defined as the frequency separation between the two phase matched signal frequencies, i.e.

$$2\Delta\omega_{ps} = 2\sqrt{\frac{2\gamma P_p}{|\beta_2(\omega_p)|}}. \tag{3.5}$$

The amplifier bandwidth can be tuned by tuning the pump wavelength, hence changing the value of SOD at this wavelength. The wavelength of the radiated DWs in deep saturation can be subsequently tuned as well. Consequently, the signal at the maximum unsaturated gain or corresponding HFPs on the short wavelength side of the spectrum can be made to overlap with DWs, as can be seen in Fig. 3.5(b), depending on the dispersion value at the pump wavelength or, equivalently, $\Delta\lambda_{p0}$. In order to evaluate the effect of amplifier bandwidth, or equivalently

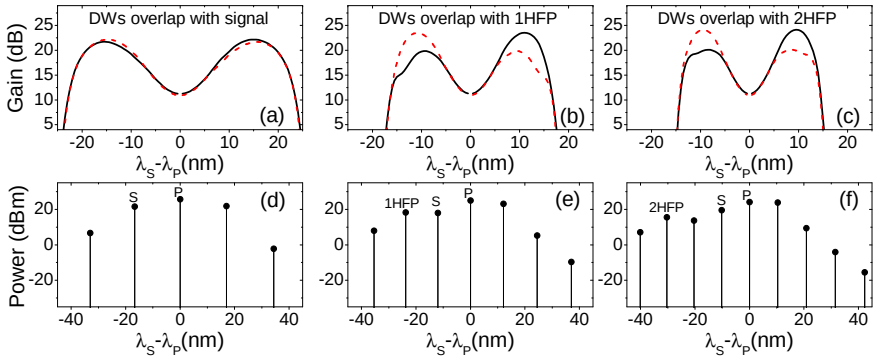

Figure 3.8: Top: Simulated signal gain (solid black curve) and idler conversion efficiency (dashed red curve) spectra for three different amplifier bandwidths corresponding to overlap of the DW with the phase-matched signal wavelength on the short wavelength side (a), 1HFP (b) and 2HFP (c). Bottom: Corresponding output spectra when the signal is tuned to the phase-matched wavelength on the short wavelength side.

SOD, on the saturated gain, the signal gain and idler conversion efficiency spectra are simulated for three bandwidths obtained with three different values of $\Delta\lambda_{p0}$ corresponding to emitted DWs overlapping with the phase matched signal, 1HFP and 2HFP, respectively. Fig. 3.8(a)-(c) show the saturated signal gain and idler conversion efficiency spectra and Fig. 3.8(d)-(f) show the output spectra for signals tuned to the maximum unsaturated gain on the short wavelength side of the spectrum. The signal input power is -0.2 dBm and all other parameters are the same as those in the experiment. The idler conversion efficiency spectra are mirror images of the signal spectra as they are plotted as a function of the signal-pump wavelength separation. The significant growth of the 1HFP and 2HFP are obvious in Fig. 3.8(b),(e) and Fig. 3.8(c),(f), respectively, when the HFPs are resonant with the emitted DWs. The saturated gain difference between the two sides of the spectrum is 0.2 dB, 5.1 dB and 4.4 dB for the broad, relatively narrow and narrow-band amplifiers in Fig. 3.8(a)-(c), respectively.

In order to quantify the difference in power transfer to the signal and the idler (or equivalently the gain difference between two signals located symmetrically around the pump frequency) in the saturation regime, the asymmetry factor is defined as the ratio between the output idler power,

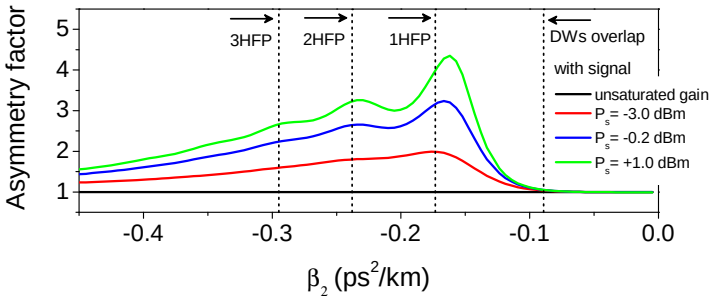

Figure 3.9: Asymmetry factor (idler to signal output power ratio) as a function of $\beta_2(\omega_p)$ (corresponding to different amplifier bandwidths) for different signal input powers.

$P_i(L)$, and the signal output power, $P_s(L)$

$$\text{Asymmetry factor} = \frac{P_i(L)}{P_s(L)}. \tag{3.6}$$

For a signal on the anti Stokes side of the gain spectrum, the larger the asymmetry factor (≥ 1), the larger the spectral asymmetry. Fig. 3.9 shows the asymmetry factor as a function of $\beta_2(\omega_p)$ for different saturation levels. In the small signal gain regime, the asymmetry factor is equal to one for all the amplifier bandwidths (corresponding to different values of $\beta_2(\omega_p)$ or equivalently $\Delta\lambda_{p0}$). The asymmetry factor becomes larger than one when the signal input power is increased to the saturation regime, indicating different energy transfers at the two sides of the spectrum. The wavelength positions of DWs coinciding with the signal and HFPs are depicted by dashed lines in Fig. 3.9. The noteworthy feature in Fig. 3.9 is the presence of peaks when the DWs are in the vicinity of the HFPs wavelengths and local minima in-between. Overlaps of DWs with HFPs closer to the signal cause less energy transfer to the signal. In particular the overlap of the DW with 1HFP corresponds to the largest power ratio between the signal and idler. As seen in Fig. 3.9, the overlaps of DWs with HFPs are not exactly matched to the maximum signal-idler asymmetries. In fact, the DWs wavelengths cannot be exactly predicted from Eq. (3.1) as the HFPs generated during propagation through the fiber are continuously affecting the formed solitons. Furthermore, it can be seen that the asymmetry is more pronounced for small-bandwidth amplifiers, i.e. for those with larger values of $\Delta\lambda_{p0}$, or equivalently higher absolute values of $\beta_2(\omega_p)$.

Impact of TOD

From the well-known analytical solution of the signal gain in the linear regime, only even orders of the dispersion contribute to the signal gain or idler conversion efficiency. It means that all the amplifiers with the same SOD value and different TOD values (i.e. dispersion slope) have the same gain spectra for small signal input powers. On the other hand, according to Eq. (3.1), for a fixed value of SOD the wavelength of the DW depends on the TOD and its phase matching with a fundamental soliton is only valid for nonzero values of TOD. Therefore, the effect of TOD and existence of DWs in the saturation regime can be examined by comparing the asymmetry factor of amplifiers with the same SOD (i.e. same bandwidth) but different TOD parameters. Furthermore, the value of TOD for a given coincidence between the DW wavelength and the phase matched signal, 1HFP or 2HFP can be determined from Eq. (3.1) according to

$$\beta_3 = \frac{3\gamma P_p - 3\beta_2 \Delta\omega_{DW}^2}{\Delta\omega_{DW}^3}, \tag{3.7}$$

where the dispersive wave coincidence with different waves can be calculated from

$$\Delta\omega_{DW} = (n+1)\Delta\omega_{ps} = (n+1)\sqrt{\frac{2\gamma P_p}{|\beta_2(\omega_p)|}}. \tag{3.8}$$

As earlier, the coincidence occurs at the anti-Stokes side of the spectrum with the phase-matched wavelength for $n = 0$, its corresponding 1HFP for $n = 1$, and 2HFP for $n = 2$. The asymmetry factor is plotted as a function of dispersion slope for different signal input power levels in Fig. 3.10. In this figure the SOD is fixed and equal to 0.169 $\text{ps}^{-2}\cdot\text{km}^{-1}$. This value corresponds to the dispersion at the pump wavelength of the experimental FOPA. Therefore all FOPAs obtained by varying the dispersion slope in Fig. 3.10 have the same unsaturated gain spectrum as in Fig. 3.7. The asymmetry factor is equal to one for unsaturated gain, which indicates that the signal and idler have the same output powers independently of the dispersion slope magnitude, as expected.

When increasing the signal input power, some gain asymmetry is created and the asymmetry factor exhibits now different magnitudes for different dispersion slopes. As predicted by our theory, the asymmetry factor shows dominant peaks when the dispersion slope value is in the vicinity of the values calculated from Eq. (3.7) and corresponding to overlaps of the dispersive wave with HFPs. The most interesting point

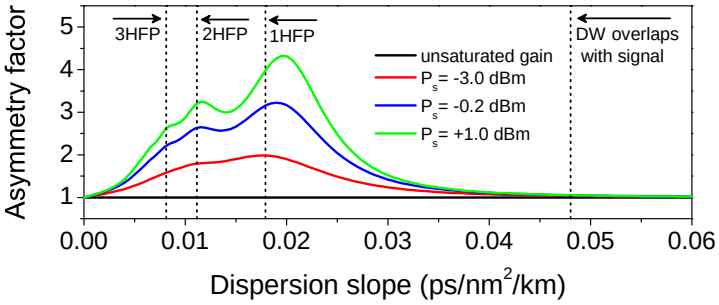

Figure 3.10: Asymmetry factor (idler to signal output power ratio) as a function of dispersion slope for different signal input powers and for amplifiers having the same unsaturated gain spectrum.

of this figure is that the maximum of the asymmetry factor corresponds to the coincidence of the DW with 1HFP, which is located beside the signal, and causes the least energy transfer to the signal in saturation, similarly to the situation shown in Fig. 3.9.

3.2.4 Discussion

In this section, the originality of our results and their relation to previous work is further clarified. The interpretation of an unexpected asymmetry observed in modulation instability spectra in term of interaction between solitons and dispersive wave has been proposed in [65]. Parametric amplification and modulation instability are obviously intricately related and our work builds on the original physics proposed in [65]. However, the key point of our work is the study of the effect of saturation of the parametric gain in single-pump amplifiers. To this respect, the interpretation of the observed gain asymmetry as a consequence of the interaction between dispersive waves and HFPs is novel. Inoue and Mukai [66] have reported the observation of spectral holes located around the signal wavelength in the ASE spectrum of single pump FOPAs. It is believed that the effect described in this chapter is different from the one leading to these spectral holes for a number of reasons. First, our work focuses on spectral asymmetry in the signal gain, which indeed may lead to spectral holes in strong saturation. However these holes appear only on the short wavelength side of the signal gain spectrum. In contrast, the spectral holes in the ASE spectrum observed in [66] occur for both sidebands of the gain spectrum, i.e. for both the signal and idler. No signal gain asymmetry is clearly visible in [66]. Second, in order to account for the observation in [66], a 9-wave model is implemented, including signal,

pump and idler (spaced by $\Delta\nu$), as well as symmetric waves representing ASE components around those with a frequency spacing with the signal, pump and idler (Δf) smaller than that between the signal and pump (i.e. $\Delta f < \Delta\nu$). Using this model, the authors successfully reproduce the behavior of their experimental observations, i.e. the occurrence of a spectral hole in the ASE component power around the signal. In contrast, in our simulations, we need to include HFPs spaced from the pump by multiples of $\Delta\nu$ in order to account for the observed gain asymmetry. Clearly, the transfer of photons between the waves has to be different in the two cases. We highlight again that only 3 "signal" waves (signal, pump and idler) are sufficient to model the observations in [66], indicating that the presence of strong HFPs does not play a significant role in the effect described in this reference, while our interpretation of the gain asymmetry in strongly saturated FOPAs requires to take a number of HFPs into account.

3.3 Dual-Pump FOPAs in Saturation

In this section, a dual-pump FOPA under saturation is experimentally analyzed. As dual-pump FOPAs offer flatter and broader gain spectra, one may wonder about their capability for regeneration of WDM systems or short-pulse amplification where the data signal occupies a wide spectral range. Generally, the behavior of dual-pump FOPAs under saturation is more complicated than in single-pump FOPAs as more waves interact with each other. This section discusses the potential of dual-pump FOPAs for amplitude regeneration in terms of amplification bandwidth.

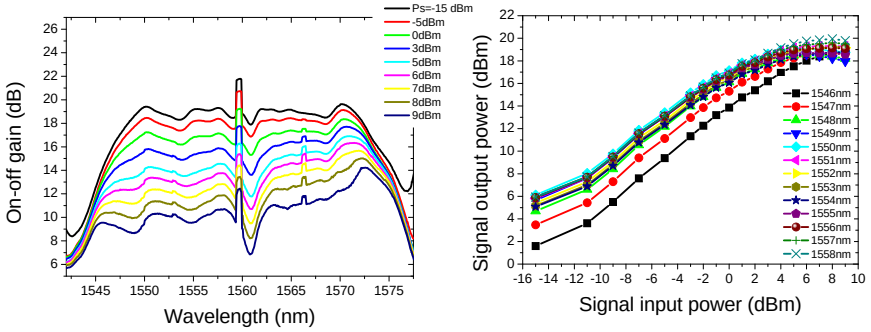

Figure 3.11: Left: measured dual-pump FOPA gain spectra in saturation (pumps are located at 1540 nm and 1580 nm). Right: transfer power of the FOPA for signal wavelength in the range of 1546 nm to 1558 nm.

Fig. 3.11(left) shows the gain spectra of the dual-pump FOPA used in section 2.6.2 under saturation for different levels of the signal input power to the FOPA. Two pumps located at 1540 nm and 1580 nm each of them with 25 dBm power at the input to the HNLF are used. If we divide the spectrum between the two pumps into two regions with respect to the pump mean wavelength, a fairly uniform unsaturated gain spectrum can be seen from 1548 nm to 1558 nm, which remains almost uniform when increasing the signal input power. The power transfer function for this wavelength range is indeed the same as can be seen from Fig. 3.11(right). The same trend is also visible on the other side of the spectrum. It should be noticed that the two spectral regions are not considered as a single here as the two cannot be used for the allocation of data signal at the same time. If the signal is located in one region then the other region is allocated for the generated idler.

3.3.1 Bandwidth Limitation

Increasing the signal input power to the FOPA increases the generation of the HFPs within the region between the pumps as well as outside of it. Generation of the HFPs in a dual-pump FOPAs can limit the useable bandwidth for allocation of data signals. The generated HFPs may fall within the frequency slot for a channel carrying data and can thus be a potential source of crosstalk. Since the crosstalk increases with the increase of signal power, there is a limit on the gain and output power of the signal in dual-pump FOPAs before the crosstalk becomes unacceptable [67]. However, if the amplifier is limited to moderate gains and output powers, the power of HFPs would be very low. The measured output power spectrum of the amplifier for some selected wavelengths in unsaturated regime (with -15 dBm input power) are shown in Fig. 3.12(left). All the signals and generated idlers have the same output power when the amplifier is in linear regime. The output power spectrum for two selected wavelengths at 1553 nm and 1555 nm in saturation (when the signal input power is +6 dBm) are shown in Fig. 3.12(right). Unlike the signal at 1555 nm, the generated HFPs overlap with the signal at 1553 nm.

In order to see the effect of this crosstalk on amplitude regeneration, a noisy 50% RZ-OOK modulated signal[1] at 40 Gbit/s is sent to the amplifier at these two wavelengths i.e. 1553 nm and 1555 nm. The eye diagram for both signals in the linear (first column) and saturation regime (second column) are depicted in Fig. 3.13. The expected behavior

[1]The noise on the modulated signal is obtained from sub-optimal operation of the transmitter.

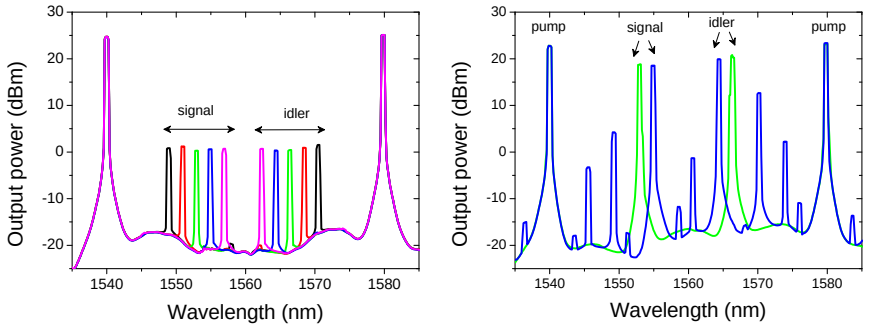

Figure 3.12: Left: output spectra of dual-pump FOPA for some selected wavelengths in the linear regime. Right: output spectra for two selected wavelengths at 1553 nm and 1555 nm in saturation.

of amplitude regeneration which is accompanied with compression of the "1" bits and amplification of the "0" bits can be clearly seen for the signal at 1555 nm. However, for the signal at 1553 nm in saturation a sign of beating between the signal and the generated HFP due to its overlap with the signal can be observed.

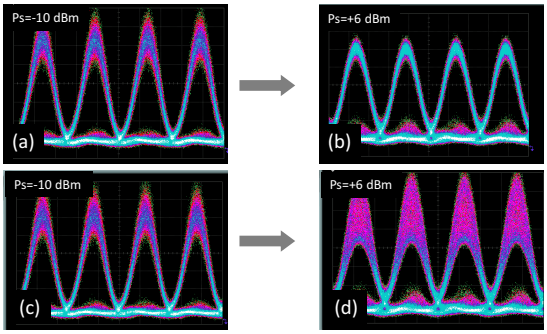

Figure 3.13: Eye diagrams of the amplified signal in linear and saturated regimes for the signal at 1555 nm ((a) and (b)) and at 1553 nm ((c) and (d)).

The overlap of the first HFP generated from FWM between the pump and adjacent signal/idler which falls within the amplification bandwidth between two pumps, i.e. S_1 and I_1 in Fig. 3.14, needs to be controlled. In particular, for the signal located at $(\omega_{P_C} + 2\Delta\omega_p/3)$, or $(\omega_{P_L} - 2\Delta\omega_p/3)$, the first HFP generated from the idler, i.e. I_1, falls on the signal frequency. For amplification of short pulses with frequency width $\Delta\omega_{data}$, one needs to ensure that there is no overlap of HFPs within the bandwidth of the data signal, i.e. the spectral range of $(\omega_{P_C} + 2\Delta\omega_p/3) \pm \Delta\omega_{data}/2$ needs be avoided for location of the signal

center frequency.

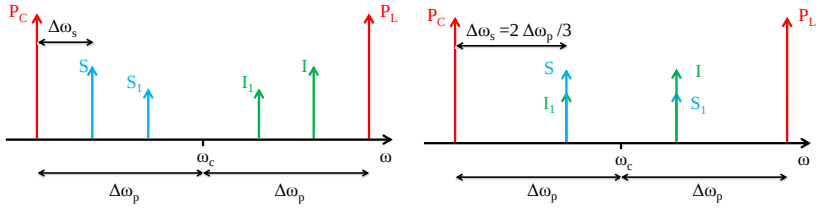

Figure 3.14: Schematic of bandwidth limitations for amplitude regeneration in saturated dual-pump FOPAs.

3.4 Summary

In conclusion, gain saturation in single- and dual-pump FOPAs has been studied. In single-pump FOPAs, an unexpected asymmetry from conventional phase matching considerations has been observed experimentally. The resulting asymmetric gain spectrum is believed to be due to the interplay between the excited HFPs in strong saturation conditions and the DWs emitted at the short-wavelength side of the spectrum. The asymmetry is pronounced when the wavelength of the DWs falls on the HFPs and shows a maximum for overlap with first HFP. Detailed numerical simulations have been shown that dispersion plays an important role in the asymmetry feature of the saturated gain spectrum, such that the asymmetry factor exhibits local maxima for particular dispersion values.

In dual-pump FOPA , the gain spectra maintain their flatnesses in saturation while the generation of HFP limits the applicable bandwidth for signal allocation. When the signal is located between the two pumps in 1/3 of the pump frequency separation, the most powerful generated HFP falls on the signal.

Chapter 4

Pump-to-Signal Intensity modulation Transfer in Fiber Optical Parametric Amplifiers

4.1 Introduction

In practical situations, the pump wave in fiber optical parametric amplifiers (FOPAs) may be affected by some intensity modulation (IM), which can be transferred to the amplified signal instantaneously due to the ultra-fast nature of the Kerr non-linearity involved in the parametric process. The pump IM originates from various sources, resulting in intensity fluctuations in different parts of the frequency spectrum. Low frequency fluctuations may arise from the relative intensity noise (RIN) of the pump laser source or from amplified spontaneous emission noise (ASE) generated in the pump amplification process, typically in erbium doped fiber amplifiers (EDFAs) for pumps in the C- or L-bands. Intensity modulation at higher frequencies (up to a few gigahertz) may also be introduced from phase-to-intensity conversion of the phase modulation (PM) typically imposed on the pump to suppress stimulated Brillouin scattering (SBS). The intensity of the pump may even be modulated at several tens or even hundreds of GHz or Gbit/s for high-speed signal processing applications. For instance, in some pulsed pump FOPA applications [68, 69] where the pump is modulated at repetition rates higher than twice the signal bit rate, the amplified signal can strongly suffer from small residual intensity fluctuations in the 10's to 100's of GHz range on top of the pump pulse train.

So far, the pump-to-signal intensity modulation transfer (IMT) has only been theoretically and experimentally investigated in single-pump FOPAs in the unsaturated (linear) gain regime and for low modulation frequencies (MFs) [70, 71, 72, 73, 74]. At those frequencies, the IMT is frequency independent and the resulting intensity modulation of the signal could reach 10 times that of the pump, depending on the amplifier gain. However, when the MF of the pump is of the order of the inverse of the walk-off delay induced by group velocity mismatch between the pump and signal, the effect of walk-off can no longer be neglected.

It has also been experimentally shown that the excess noise and beat noise of the signal induced by ASE can be suppressed in FOPAs operated in gain saturation [22]. It means that the fast response of the parametric gain can lead to suppression of the intensity noise transferred to the signal when the amplifier operates in the saturated (non-linear) gain regime. In this chapter, we extend for the first time to our knowledge the investigations of the pump to signal IMT in single pump FOPAs to the regimes of high pump modulation frequencies and gain saturation. We explore the mechanism of the IMT along the fiber and furthermore study numerically and experimentally the IMT to the signal over the entire gain bandwidth in the linear and non-linear gain regimes. Parameters affecting the IMT in FOPAs are reviewed in section 4.2. Section 4.3 describes the formalism that has been applied to the simulations. The frequency dependence of the IMT is presented in section 4.4 [C-10, J-5]. Section 4.5 numerically investigates the IMT evolution along the fiber [J-5] and the effect of gain saturation on the IMT over the gain spectrum [C-9, J-5], while section 4.6 focuses on the experimental demonstration of the pump to signal IMT in saturation and comparison with the simulations [C-8, J-3, J-5]. Finally, the conclusions are drawn in section 4.7.

4.2 Parameters Affecting Pump-to-Signal IMT

Considering some IM is imposed to the pump with the modulation frequency ν_m and modulation depth m_p, this modulation transfers to the signal during amplification with the same modulation frequency but different modulation depth depending on the the gain characteristics of the FOPA at the signal wavelength, as it is shown schematically in Fig. 4.1. In the following those characteristics of FOPAs which lead to effective pump-to-signal IMT are reviewed.

Ultra-fast nature of the Kerr non-linearity Due to the ultra-fast nature of the Kerr non-linearity involved in the parametric process,

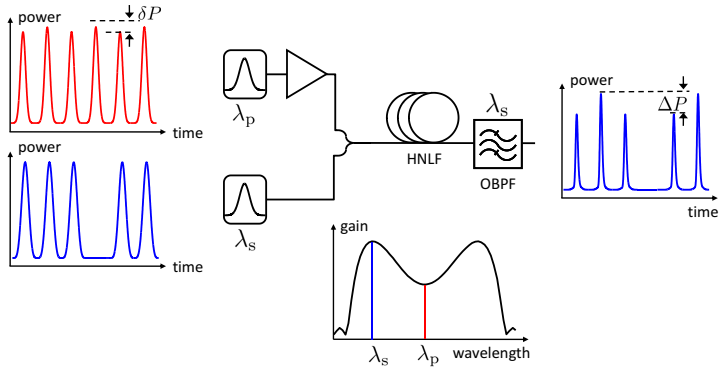

Figure 4.1: Schematic configuration of pump-to-signal IMT.

FOPAs are attractive for high speed signal processing applications. An adverse effect is that the intensity fluctuations of the pump are transferred to the signal instantaneously.

Pump power The pump-to-signal IMT in FOPAs depends on the gain characteristics of this type of amplifier. The parametric gain at the phase-matched signal wavelength is approximately equals to

$$G_s \backsimeq \frac{1}{4}\exp\left(2\gamma P_p L\right). \tag{4.1}$$

As a consequence of the exponential dependence of the parametric gain on the input pump power, the gain and bandwidth of FOPAs increases by increasing the pump power. However, any small intensity noise superimposed on the pump will heavily transfer to the signal and be magnified in the output signal.

Pump-signal walk-off The pump and signal co-propagate in FOPAs, where they typically experience less than 1 km interaction length in highly non-linear optical fibers. Consequently, the dispersion-induced walk-off between the pump and signal is small, which results in efficient IMT from the pump to the signal even at high MFs.

4.3 Theory

The pump-to-signal IMT is modeled by considering an intensity modulated pump combined with a continuous wave (CW) signal at the input of the highly non-linear fiber (HNLF), as schematically shown in Fig. 4.2. The intensity modulation transferred to the signal is evaluated at the

output of the amplifier after filtering the signal by an optical bandpass filter (OBPF). The IMT magnitude can be evaluated by applying a small amount of intensity modulation to the input pump power

$$P_p(0,t) = P_{p0}\left(1 + m_p \cos\left(2\pi\nu_m t\right)\right) \tag{4.2}$$

where P_{p0} is the average input pump power, m_p is the modulation depth and ν_m is the modulation frequency. The pump to signal IMT is defined as the ratio between the modulation depth of the amplified signal $m_s(L)$ and that of the input pump $m_p(0)$

$$IMT = \frac{m_s(L)}{m_p(0)}. \tag{4.3}$$

The modulation depth at each point of the fiber is calculated based on the temporal power fluctuations

$$m(z) = \frac{P_{max}(z,t) - P_{min}(z,t)}{2P_{avg}(z)}, \tag{4.4}$$

where $P_{max}(z)$, $P_{min}(z)$ and $P_{avg}(z)$, are the maximum, minimum and average values of the power, respectively. In the numerical simulations, the split step Fourier method [36] is used to solve the generalized non-linear Schrödinger equation (NLSE):

$$\frac{\partial A}{\partial z} + \frac{\alpha}{2}A + \frac{i}{2}\beta_2\frac{\partial^2 A}{\partial t^2} - \frac{1}{6}\beta_3\frac{\partial^3 A}{\partial t^3} = i\gamma\left|A\right|^2 A, \tag{4.5}$$

where β_2 and β_3 are the second and third order dispersion coefficients, respectively, γ is the non-linear coefficient and α is the fiber loss. The initial complex envelop is considered as the sum of the intensity modulated pump and the CW signal and can be expressed as

$$A(0,t) = \sqrt{P_p(0,t)}\exp(-i\omega_p t) + \sqrt{P_s(0)}\exp(-i\omega_s t), \tag{4.6}$$

where ω_i $(i = p, s)$ is the angular frequency of the pump or signal and $P_s(0)$ is the input power of the CW signal. Solving the generalized NLSE enables to include all relevant non-linear effects as well as to accurately predict the saturation behavior by taking into account all waves generated in the parametric processes and their interactions. The IM of the signal is then evaluated in the time domain by characterization of the temporally varying output signal waveform obtained after bandpass filtering.

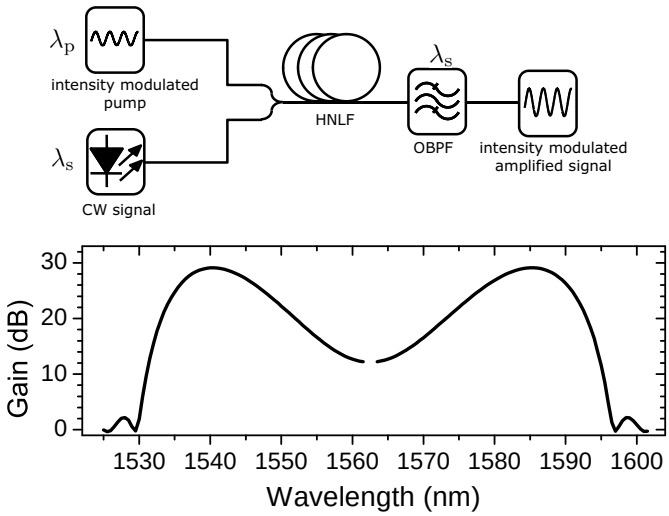

Figure 4.2: Schematic configuration of the setup (top) and signal gain spectrum (bottom). Simulation parameters are: $\gamma = 17\ \mathrm{W^{-1}{\cdot}km^{-1}}$, $P_p = 27$ dBm, $L = 500$ m, $\lambda_p = 1562.5$ nm, $D_\lambda = 0.03\ \mathrm{ps{\cdot}nm^{-2}{\cdot}km^{-1}}$, ZDW = 1561.1 nm, and $\alpha = 0.7\ \mathrm{dB{\cdot}km^{-1}}$.

4.4 Frequency Dependence of the IMT

The small signal gain spectrum of the FOPA considered in the simulations is presented in Fig. 4.2 with parameters listed in the caption of the figure. The maximum gain for a pump power of 27 dBm is 29.1 dB at the two phase matched wavelengths of 1540.5 nm and 1585.5 nm. In the simulations we focus on the signal wavelength at the maximum gain on the short wavelength side of the spectrum (1540.5 nm). Considering the pump wavelength close to the zero dispersion wavelength (ZDW) in the anomalous dispersion region, the walk-off delay τ between the pump and signal can be expressed as

$$\tau \approx D_\lambda L(\lambda_p - \lambda_s)^2, \tag{4.7}$$

where D_λ is the dispersion slope of the fiber, L is the fiber length and $\lambda_i (i = p, s)$ is the wavelength of the pump or the signal, respectively. The walk-off delay for the signal tuned to the maximum gain of our example FOPA is about 3.6 ps as a consequence of the short interaction length of 500 m, as well as the small pump signal wavelength separation of 22 nm.

The frequency dependence of the IMT has been characterized and is plotted together with the IM period in Fig. 4.3. The modulation depth is set to 5%. The behavior of the IMT can be analyzed by comparing the two time scales involved, namely the IM period and the pump

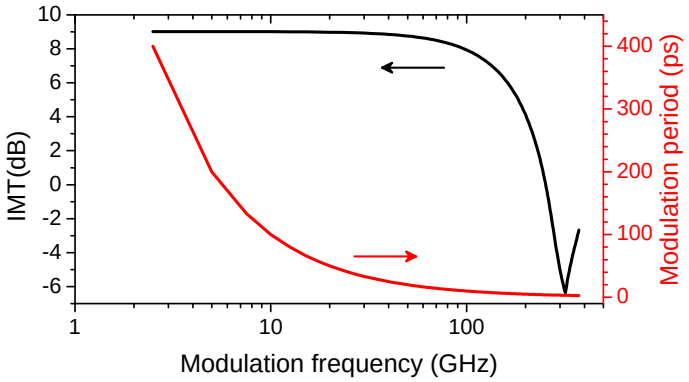

Figure 4.3: Modulation frequency dependence of the IMT for the signal at 1540.5 nm (left axis) and corresponding pump IM period (right axis).

signal walk-off delay. The walk-off time between the pump and signal is about 3.6 ps while the period of oscillations of the modulated pump changes from 400 ps to 2.5 ps when the MF varies between 2.5 GHz and 400 GHz. For low MFs (less than about 50 GHz) the modulation index of the amplified signal is almost constant and independent of the MF, in agreement with [72], with an enhancement by a factor 8 compared to that of the input pump, which corresponds to an IMT of 9 dB. In fact, the small walk-off leads to efficient IMT from the pump to the signal. The dominant contribution of pump IM in this range of frequencies may originate from the PM of the pump at several GHz in view of SBS suppression. Bandpass filtering of the amplified pump in order to suppress out-of-band ASE may result in phase-to-intensity modulation conversion due to the filter transfer function in a frequency region where the most efficient pump to signal IMT occurs. The impact of the group velocity mismatch can be observed at high MFs that are comparable to the reciprocal walk-off delay between the pump and signal. At high MFs the signal can indeed spatially overlap with a pump having different instantaneous power at different locations along the fiber, thus effectively resulting in an averaging of the pump intensity fluctuations seen by the signal and consequently a reduction of the IMT to the signal compared to the walk-off free case. Defining the IMT cut-off frequency as the frequency for which the IMT decreases to half of its maximum, values as high as 161 GHz are obtained at the maximum gain. A modification of the walk-off delay enables to shift the cut-off frequency. The maximum gain angular frequency is shifted from the pump by $\sqrt{2\gamma P_p/|\beta_2|}$ where β_2 is the second order dispersion at the pump wavelength. Hence, the

walk-off between the pump and the signal tuned to the maximum gain is given by $\tau \approx \gamma P_p L \beta_3 / |\beta_2|$, and thus depends on the pump non-linear self phase shift, $\gamma P_p L$, and the fiber dispersion properties through the $\beta_3 / |\beta_2|$ ratio.

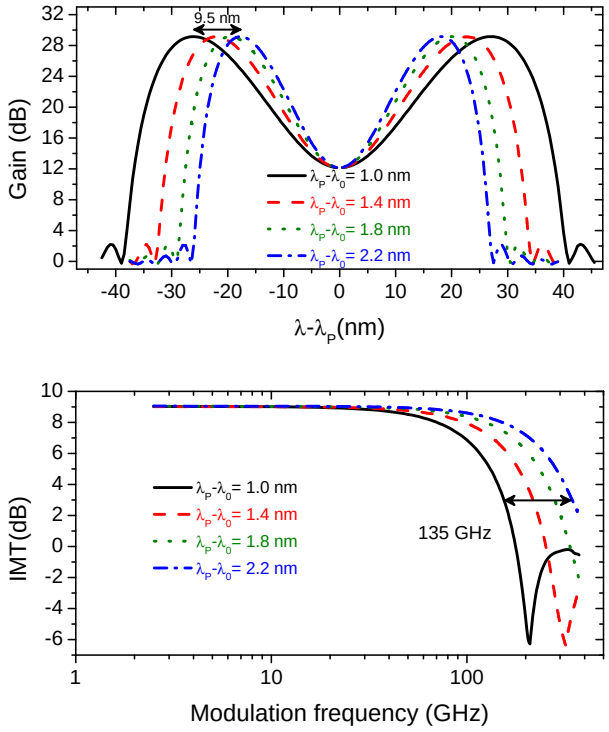

Figure 4.4: Signal gain spectra (top) and IMT as a function of MF (bottom) for four different pump ZDW separations.

Changing the dispersion parameters of the fiber at the pump wavelength can modify the phase matched wavelength at which maximum gain occurs and, accordingly, the walk-off delay, without changing the gain magnitude itself. Tuning the pump closer to the ZDW results in the maximum gain wavelength shifting further away from the pump, hence in a broader gain spectrum. The wider the gain spectrum, the larger the walk-off and the lower the cut-off frequency. The gain spectra for four different values of separation between the pump wavelength and the ZDW ($\Delta\lambda_{p0}$) are presented in Fig. 4.4(top). The maximum gain wavelength shifts toward the pump wavelength by 9.5 nm as the pump is tuned further away from the ZDW from 1 nm to 2.2 nm. The IMT at the maximum gain for the corresponding four values of $\Delta\lambda_{p0}$ are shown in Fig. 4.4(bottom). For low-MFs, the IMT to the signal can be estimated

by $2\gamma P_p L$ [72]. Therefore, the IMT is identical for all signals at the maximum gain since the pump non-linear self phase shift $\gamma P_p L$ is identical for a fixed pump power. On the other hand, the cut-off frequencies are different as a result of the different walk-off delays induced by the different dispersion values at the pump wavelength. The amplifier with the widest spectrum presents the lowest cut-off frequency. In our example, a 1.2 nm increase of $\Delta\lambda_{p0}$ reduces the cut-off frequency by 135 GHz from 251 GHz to 116 GHz. The other way to shift the walk-off (at maximum gain) between the pump and signal is through variations of the pump non-linear self phase shift $\gamma P_p L$, which will change the parametric gain as well. In order to illustrate this effect, the IMT to the signal has been simulated for different pump powers and depicted in Fig. 4.5 for $\Delta\lambda_{p0} = 1.4$ nm.

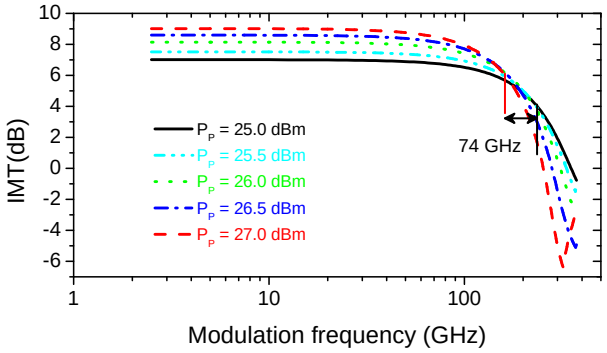

Figure 4.5: IMT as a function of MF for different input pump powers when $\Delta\lambda_{p0} = 1.4$ nm. Higher pump powers increase the walk-off delay, which result in the cut-off frequency shifting to lower values.

At low MFs, the higher the pump power is set, the more the intensity modulation of the pump transfers to the signal. The cut-off frequency is lower for higher input pump powers as the walk-off delay is proportional to the pump power. The IMT decreases from 9 dB to 7 dB at low MFs, and the cut-off frequency increases by 74 GHz from 161 GHz to 235 GHz when the pump power decreases from 27 dBm to 25 dBm. Overall, wide band amplifiers designed with high pump power and small pump ZDW separation have lower cut-off frequencies

4.5 IMT in Non-Linear Regime

As it was previously mentioned, the pump IM transfers efficienly to the signal at low MFs. One way to reduce this detrimental effect is to op-

erate in the gain saturated regime. Since the parametric gain responds quasi-instantaneously to the input signal power variations, the induced fluctuations to the signal can be suppressed during propagation through the fiber when the amplifier enters its saturation mode. The analytical solution of the low frequency IMT presented in [72] is based on the main assumption that the amplifier operates in the linear gain regime and the pump power does not deplete. Accordingly, the modulation of the pump remains unchanged over the length of the amplifier in spite of the presence of parametric gain [72]. As the pump power becomes depleted and higher order FWM products are generated as a result of the increase in signal input power, it is necessary to rely on full numerical simulations in order to capture the complete dynamics of the interacting waves. In this section, in order to understand the mechanism of the IMT to the signal under saturation, we first investigate the IMT evolution along the fiber, then study the effect of the gain saturation on the low frequency IMT over the entire gain spectrum.

4.5.1 IMT Evolution Along the Fiber

The power evolution during propagation along the fiber of the pump and the signal located at the maximum gain can be seen in Fig. 4.6(top). The input pump power is 27 dBm and $\Delta\lambda_{p0}$ = 1.4 nm. Signals with four input power levels are considered. $P_s(0)$ = -30 dBm corresponds to the unsaturated gain when the amplifier has the maximum gain of 29.1dB. $P_s(0)$ = -9.6 dBm and -6.0 dBm result in gain compression of 1.5 dB and 3 dB, respectively and $P_s(0)$ = -1.4 dBm corresponds to the situation when the signal reaches its maximum output power and the pump reaches its maximum depletion at the output of the 500 m HNLF. Here, the power is plotted in linear scale and the output signal gain in dB is indicated beside the figure for each $P_s(0)$.

Fig. 4.6(bottom) illustrates the IMT in linear scale along the fiber for the four saturation levels. The modulation depth is 5% and the MF is 10 GHz. The pump intensity modulation starts transferring to the signal at the early stages of the fiber and grows through the fiber along with the amplification of the signal. But the IMT to the signal decreases towards the output of the fiber when the amplifier enters saturation, and notably reaches a maximum value before the fiber end. One can clearly observe that the maximum modulation transfer to the signal corresponds to the steep growth of the signal power along the fiber. Afterwards, the IMT starts decreasing close to where the signal power evolution along the fiber changes curvature. In this region, the output signal is stable against the power fluctuations of the input pump. It means that the high

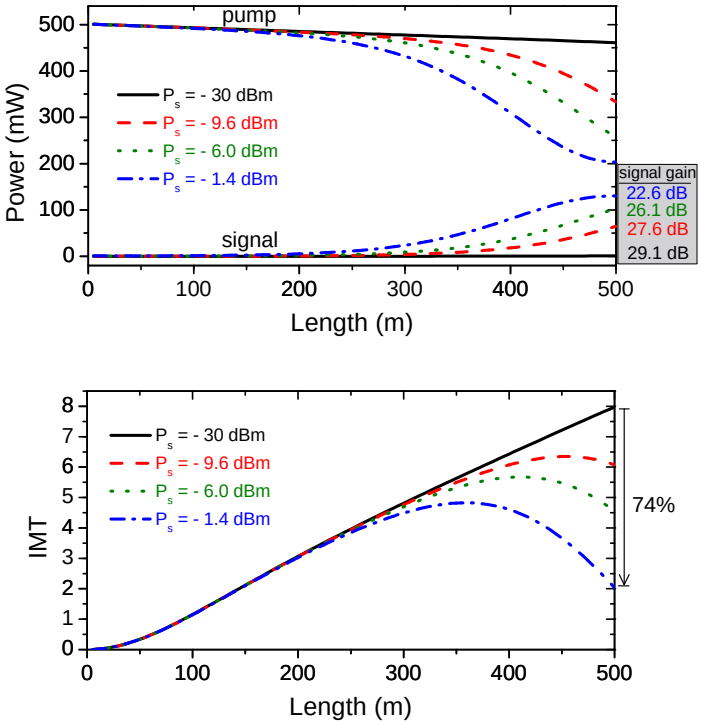

Figure 4.6: Power evolution of the pump and signal (top) and IMT to the signal (bottom) along the fiber for different signal input power levels. P_p = 27 dBm and $\triangle\lambda_{p0}$ = 1.4 nm.

intensity levels of the signal experience gain saturation, while the lower levels are still linearly amplified, resulting in compression of the signal fluctuations and IMT reduction (this point will be further discussed later in this section and illustrated in Fig. 4.7). A reduction of more than 70% of the IMT compared to the unsaturated case can be obtained at the HNLF output under strong saturation when the signal input power is equal to $P_s(0)$ = -1.4 dBm. Therefore, operating in saturation makes it possible to decrease the IMT to the signal as the maximum IMT is typically reached for shorter fiber lengths.

The pump and signal output power as well as the IMT are shown as a function of signal input power in Fig. 4.7. As the output signal saturation starts and the pump becomes depleted, the IMT clearly decreases. The IMT to the signal is suppressed by 43% and 74% compared to the unsaturated case when the maximum gain drops by 3 dB and when the signal output power is at its maximum level, respectively. Waveforms of the pump and signal in the time domain can illustrate how the intensity

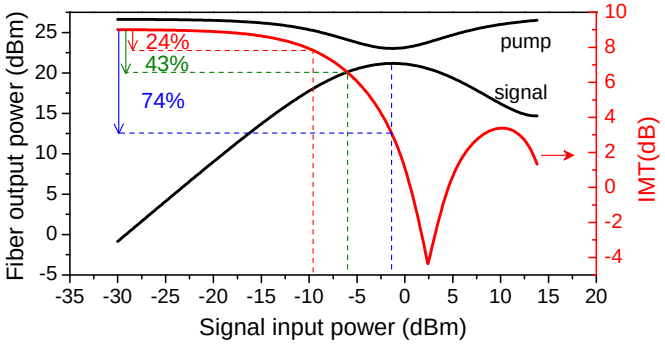

Figure 4.7: Pump and signal output powers (left axis) and IMT (right axis) as a function of the signal input power.

modulation of the pump transfers to the signal along the fiber.

The waveforms of the input pump and amplified signals at 1540.5 nm under different saturation conditions are plotted in Fig. 4.8. In these graphs, the evolution of the waveforms is illustrated by representing the power of the signal over four periods as a function of time and propagation length in the fiber. Fig. 4.8(a,b) shows the pump and signal waveforms along the fiber, respectively, for $P_s(0)$ = -30 dBm. The modulation depth of the pump is constant along the fiber since the pump remains undepleted with such a low value of signal input power. The fluctuations of the signal power distinctly follow the pump fluctuations and are significantly enhanced at the output of the amplifier in this unsaturated gain case. Under gain saturation, Fig. 4.8(c-e), the IMT maximum is pushed from the fiber end at 500 m to 455 m, 410 m and 360 m for $P_s(0)$ = -9.6 dBm, -6.0 dBm and -1.4 dBm, respectively and the IMT at the fiber output is consequently reduced.

4.5.2 IMT Spectrum

After analyzing the IMT along the fiber at the maximum gain signal, we now turn to the study of the IMT over the signal gain spectrum. The whole gain and IMT spectra as a function of the signal input power are shown in Fig. 4.9 in two contour plots. Comparison of these two plots enables to determine the optimum parameter region for the signal wavelength and input power in order to achieve specific gain and IMT. The gain is obviously decreased by increasing the signal input power due to pump depletion. Amplifiers with higher gain saturate first as the saturation power of the FOPAs is inversely proportional to the gain [61]. The IMT clearly increases rapidly with increasing pump signal wavelength

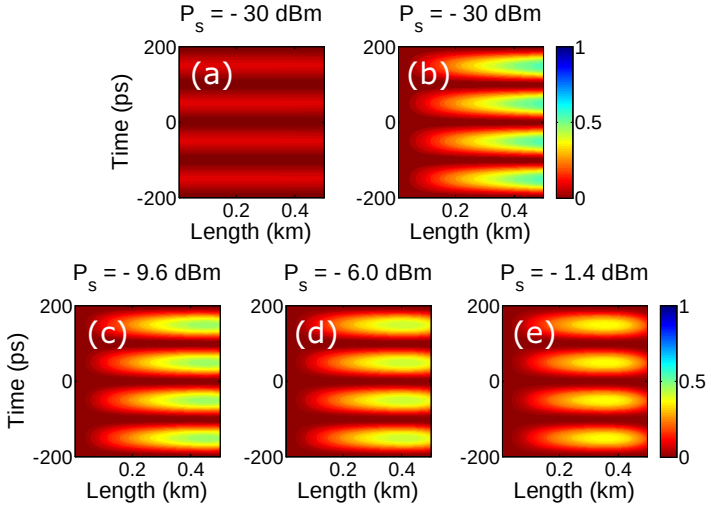

Figure 4.8: Waveforms along the fiber for the pump (a) and signal (b) for P_s = -30 dBm. Evolution of the waveform of the signal for P_s = -9.6 dBm (c), P_s = -6.0 dBm (d) and P_s = -1.4 dBm (e).

separation. In the linear regime, the IMT to the signal depends on the gain variation with respect to the pump power fluctuations at each signal wavelength [72]. Signal wavelengths at the outer slopes of the gain spectrum suffer the most from pump to signal IMT as the pump power dependence of the gain makes that part of the spectrum more sensitive to the pump intensity fluctuations. In the non-linear gain regime, the IMT is considerably reduced as the signal input power increases and the gain saturates. The IMT reduction is more pronounced at the wavelengths corresponding to the maximum unsaturated gain since the gain at these wavelengths saturates first. For signal wavelengths at 1540.5 nm and 1585.5 nm, corresponding to the maximum unsaturated gain, the IMT is decreased by 2.4 dB from 9 dB to 6.6 dB when the gain is reduced by 3 dB (corresponding to $P_s(0)$ = -6.0 dBm), and by 5.9 dB to 3.1 dB when the pump reaches its minimum at the fiber output (corresponding to $P_s(0)$ = -1.4 dBm).

In order to quantify the induced improvement of the quality of the amplified signal by operation of the FOPA in saturation, the following definition for the signal to noise ratio (SNR) of the signal is used:

$$SNR = \frac{P_{avg}(L)}{\sqrt{\left\langle (P(L,t) - P_{avg}(L))^2 \right\rangle}}. \tag{4.8}$$

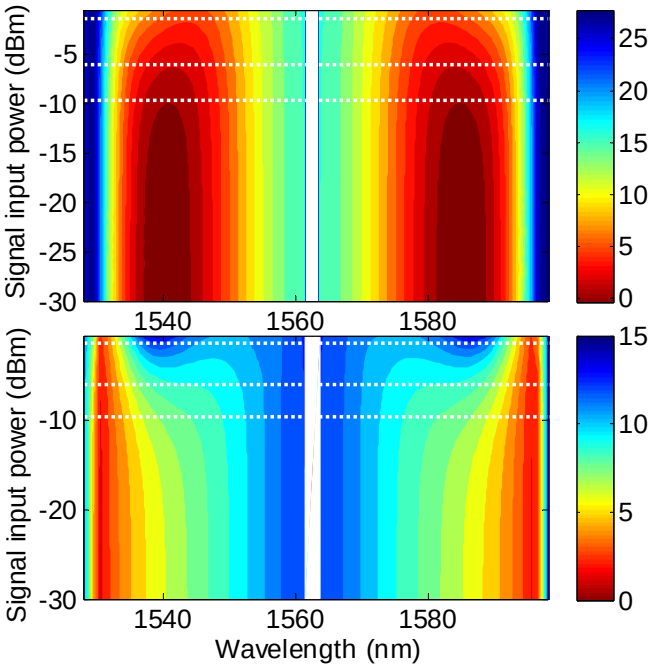

Figure 4.9: Signal gain (top) and IMT (bottom) spectra as a function of signal input power (in dB units). The dashed lines show the power levels at $P_s(0)$ = -9.6 dBm, -6 dBm and -1.4 dBm. The signal wavelengths located further away from the pump experience an enhanced IMT.

The signal SNR and the gain are shown as a function of input signal power in Fig. 4.10. The SNR is 5.5 dB when the amplifier is unsaturated and improves by 2.3 dB and 5.9 dB from 5.5 dB to 7.8 dB and 11.4 dB when the gain is reduced by 3dB and when $P_s(0)$ = -1.4 dBm, respectively. Here, 5.9 dB improvement of the SNR indicates that the power fluctuations of the signal located at the maximum gain are compressed by about four times compared to the unsaturated signal.

4.6 Experimental Result for Pump-to-Signal IMT

Experiments have been performed in order to verify the IMT improvement in single pump FOPAs under saturation. The presented experiment in this section has been carried out by Valentina Cristofori, DTU Fotonik [J-3, C-8]. The experimental setup is depicted in Fig. 4.11. A CW tunable laser source (TLS) is used as pump source (λ_p = -1.4 dBm) and is subsequently phase modulated to broaden its spectrum in order to increase the SBS threshold using three combined radio frequencies. The

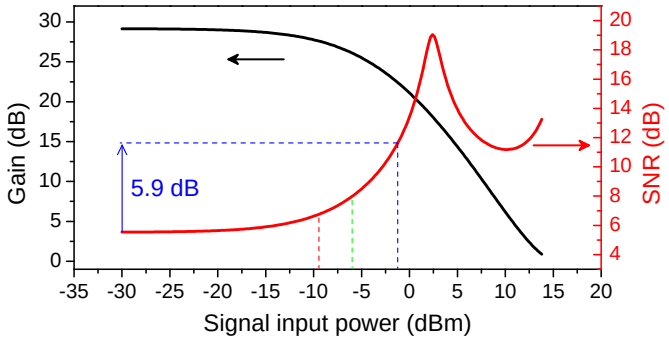

Figure 4.10: Signal gain (left axis) and SNR (right axis) as a function of the signal input power.

frequencies (f_1 = 100 MHz, f_2 = 300 MHz, f_3 = 600 MHz) are chosen outside the range of amplitude modulation frequencies imposed on the pump (10 GHz) in order not to impact the IMT measurements results.

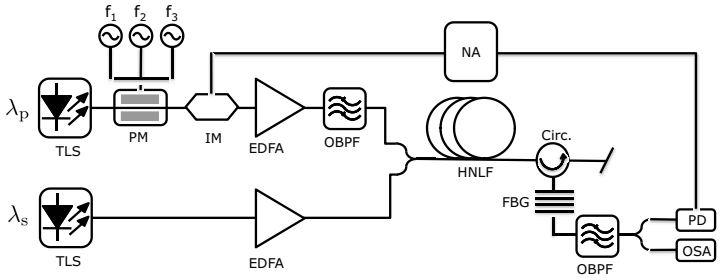

Figure 4.11: Experimental setup for FOPA pump to signal IMT measurement.

To this end, the SBS suppression has been optimized for frequency tones away from the amplitude modulation frequency of the pump so that sufficient small signal gain is achieved in order to assess the effect of saturation. The SBS threshold is 25 dBm and is defined as the HNLF input power at which the output power stops increasing linearly with the input power. The pump is then intensity modulated with a sinusoidal radio frequency signal in a Mach-Zehnder intensity modulator (MZM), and amplified up to 27.5 dBm in an EDFA. It is ensured that the IM is operated at a quadrature point with a sufficiently small modulation index to avoid the creation of harmonics. A tunable OBPF with 2 nm full width at half maximum bandwidth is used to suppress the out of band amplified spontaneous emission induced by the EDFA. The pump and signal are combined via a 90/10% coupler in a 400 m long HNLF,

with a ZDW of 1559.2 nm, a non-linear coefficient of 11.9 $W^{-1}{\cdot}km^{-1}$ and a dispersion slope of 0.018 $ps{\cdot}nm^{-2}{\cdot}km^{-1}$. To determine the IMT, the pump modulation index is measured at the output of the IM and subsequently compared to the modulation depth of the amplified signal measured at the output of the HNLF, after suppression of the pump and the idler by means of a fiber Bragg grating (FBG) at the pump wavelength (used as a notch filter in transmission) and an OBPF tuned to the signal wavelength. The modulation depths are measured with a network analyzer (NA) and a photodiode (PD). The peak to peak output power variation is extracted from the S-parameters provided by the NA, while the average power is obtained from the value of the photocurrent.

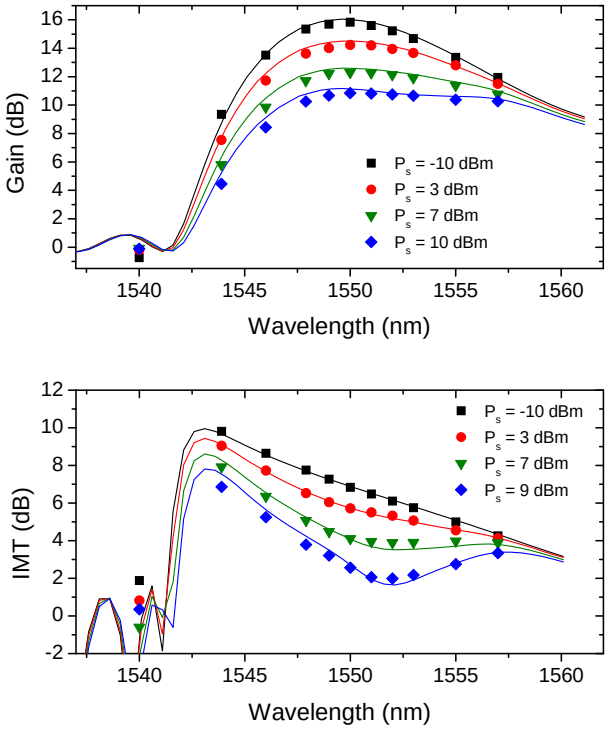

Figure 4.12: Measured signal gain (top) and IMT (bottom) spectra for different saturation levels. The solid lines show the calculated values while the symbols represent the measurements.

In Fig. 4.12(top) the signal gain is shown as a function of the signal wavelength for different signal input power levels. The measurements (symbols) are compared with numerical simulations (solid lines). As expected from the theory, the measurements show a decrease of the amplifier gain as the signal power is increased. The saturation effect is notable

already for $P_s = +7$ dBm and it becomes stronger for +10 dBm, for which the maximum gain decreases from the unsaturated value (from 15.8 dB to 10.8 dB) and the gain spectrum becomes flatter. The IMT to the signal is characterized under the same saturation levels and illustrated in Fig. 4.12(bottom). In very good agreement with the simulations, the IMT is seen to increase with increasing wavelength detuning between the signal and pump. The transfer is significant at the maximum gain wavelength, which is the main region of interest in FOPAs. However, it is clearly noted that the IMT decreases for higher signal powers as the gain saturates. The IMT at the maximum gain (1550 nm) is decreased from an unsaturated value of 6.8 dB by 23%, 47% and 63% to 5.7 dB, 4.1 dB and 2.6 dB when the gain drops by 1.6 dB, 3.5 dB and 5 dB, respectively.

4.7 Summary

In conclusion, the pump to signal IMT in single pump FOPAs has been numerically and experimentally studied. More specifically, the modulation frequency dependence of the IMT, its evolution along the fiber and its gain saturated behavior have been investigated in details. The IMT is maximum and independent of the pump modulation frequency for low frequencies (less than about 50 GHz) and starts decreasing when the modulation period is comparable to the pump signal walk-off delay. The IMT cut-off frequency in one pump FOPAs is about 100-200 GHz, which can be shifted depending on the value of the fiber dispersion parameters at the pump wavelength or the pump non-linear self-phase shift. In the case of low MFs, the IMT to the signal can be suppressed by operating in the gain saturation mode. With sufficiently large saturation, the IMT reaches its maximum value before the end of the HNLF. A large reduction of the IMT of more than 50% has been measured for a signal wavelength corresponding to the maximum unsaturated gain. Operation in the saturated regime improves the output SNR compared to the unsaturated regime by more than 5 dB. Quantifying the IMT to the signal enables to assess the degradation of the amplified signal.

Chapter 5

Fiber Optical Parametric Chirped Pulse Amplification

5.1 Introduction

Chirped-pulse amplification (CPA) is a well known scheme for distortionless amplification of ultra-short high peak power pulses. The conceptual schematic of CPA is illustrated in Fig. 5.1. Input pulses prior to amplification are at first stretched using a dispersive element in order to lower their peak power. The temporally stretched pulses is then safely amplified without the onset of damaging nonlinear effects in the amplifier. Finally, the amplified pulse is recompressed close to its original pulse duration by using an element with the opposite sign of dispersion.

CPA in the optical domain was proposed and experimentally demonstrated by Strickland and Mourou in 1985 in order to generate subpicosecond pulses [75], with energies at the Joule level where the amplification was achieved by direct laser amplification. A different implementation of CPA which made use of parametric amplification was proposed in 1992 [76]. This scheme is called optical parametric chirped-pulse amplifi-

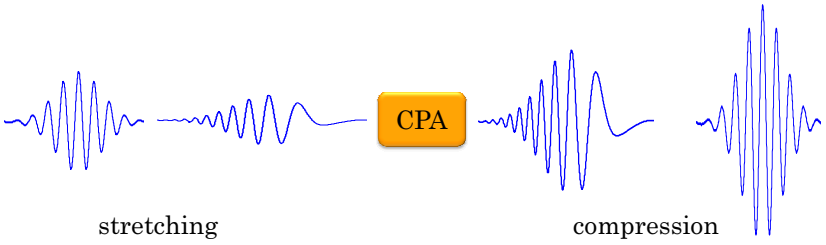

Figure 5.1: Conceptual schematic of chirped-pulse amplification.

cation (OPCPA). OPCPA is based on three-wave mixing in second-order non-linear crystals in order to parametrically amplify ultra-short pulses. This scheme has been widely used for the generation of high peak power pulses in an amplifier with a very flexible gain in terms of bandwidth, spectral tunability and amount of gain [77].

Parametric amplification in optical fibers has many similarities with the parametric amplification in non-linear crystals while it can be realized in a more compact size with long-term stability. OPCPA in optical fibers, called fiber OPCPA (FOPCPA), was first proposed and numerically simulated by Hanna et al. in 2006 [78]. Later in 2010, the first FOPCPA was experimentally demonstrated by Caucheteur et al. in an all-fiber configuration [79] where 6.4 ps Fourier-transform-limited pulses in the telecommunication window were stretched to 190 ps, amplified in a CW-pumped FOPA by $\sim$ 25 dB, and recompressed into their initial duration without any significant spectral or temporal distortions. A chirped fiber Bragg grating (CFBG) was used to stretch and compress the signal pulses. Operation of FOPCPA around 1 μm using photonic crystal fibers (PCFs) as the gain medium was verified in [80], where 200 fs pulses were stretched to $\sim$ 4.5 ns using a diffraction grating, amplified by $\sim$ 35 dB in a pulsed-pump FOPA, and recompressed to $\sim$ 400 fs.

FOPCPA for sub-picosecond pulses in the telecommunication window was demonstrated in [81], where 750 fs signal pulses were stretched to 40 ps, amplified by 30 dB in a pulsed-pump FOPA, and recompressed to 808 fs using a set of standard single mode fiber (SSMF) and dispersion compensating fiber (DCF) as stretcher and compressor.

This chapter discusses an experimental demonstration of FOPCPA for few picosecond pulses in section 5.2 and sub-picosecond pulses in section 5.3. More specifically, in the telecommunication window, the dynamics of FOPCPA is investigated for few picosecond pulses in the linear and non-linear regimes with focus on pulse distortion which occurs in the non-linear regime . The first experimental demonstration of pulse distortion in non-linear regime, which was already predicted only numerically, is presented in section 5.2 [C-6]. Moreover, FOPCPA of pulses as short as 400 fs, compatible with Tbaud communication systems, is demonstrated in the linear regime for the first time [C-2, C-3, J-2].

5.2 FOPCPA for Few Picosecond Pulses

From the aforementioned demonstrations, it is fair to conclude that FOPCPA is a promising amplification scheme for pico- and femto-second pulses in optical fibers. In this section, the dynamics of FOPCPA is in-

vestigated for pulses as short as 2-6 ps. Chirped pulses are generated by intensity and phase modulation of a CW laser and passed through some SSMF for additional compression. The amplifier is a single-pump FOPA which is mainly the same as the one which was experimentally under study for asymmetric gain spectrum in saturation in section 3.2 with almost the same wavelength allocation for the pump and signal at maximum gain. The different saturation rates for the signal and idler at the two sides of the spectrum allows us to investigate not only the dynamics of FOPCPA for the idler but also the effect of the accumulated dispersion in FOPAs on the chirped wavelength converted pulses since they experience several times more dispersion than the signal according to the specific gain spectrum of the amplifier.

Since parametric amplification is an ultra-fast process with gain strongly dependent on the input signal power [82], the output of an FOPCPA depends on the temporal profile of the input chirped signal, an effect that is revealed in the amplified signal after recompression. The amplified signal distortion can be investigated operating in the non-linear gain regime to highlight the effect of the parametric gain response. Recent numerical studies have reported the appearance of excess noise in the form of pedestals around the recompressed signal in the non-linear gain regime [80, 83]. In this section, we have experimentally compared FOPCPAs for differently chirped pulses under transition from linear to saturated gain regime and investigated the signal distortion after recompression. Moreover, the effect of accumulated dispersion in the amplifier on the pulse broadening in saturation is studied. This investigation is not only interesting from a fundamental point of view, but is also particularly important with regard to performance, since operation in saturation is attractive for signal noise suppression and regeneration.

5.2.1 Experimental Setup

The experimental setup is shown in Fig. 5.2. The pump signal is a continuous wave at 1557.5 nm that is phase modulated using a 10 Gbit/s 2^7-1 pseudorandom binary sequence to suppress stimulated Brillouin scattering (SBS), amplified by an erbium-doped fiber amplifier (EDFA) up to 28.5 dBm and filtered by a 1 nm bandwidth optical band pass filter (OBPF). The chirped signal pulses are generated from a tunable laser followed by an intensity modulator (IM) and a phase modulator (PM) synchronously driven by sinusoidal electrical signals at 40 GHz. The pulses are then amplified, filtered by a 5 nm bandwidth OBPF and the power at the input to the amplifier is controlled by an optical variable attenuator (OVA). A 10/90% coupler combines the pump and

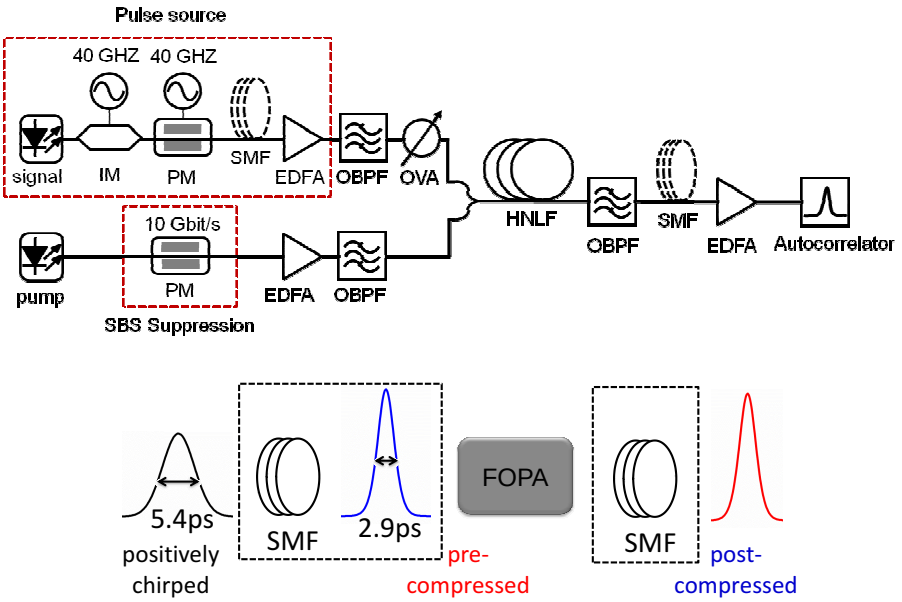

Figure 5.2: Experimental setup for FOPCPA.

signal into a 500 m highly non-linear fiber (HNLF) with non-linear coefficient of 10.7 $W^{-1}{\cdot}km^{-1}$, dispersion slope of 0.0185 $ps{\cdot}nm^{-2}{\cdot}km^{-1}$, loss of 0.7 $dB{\cdot}km^{-1}$ and zero-dispersion wavelength (ZDW) at 1550.4 nm. The amplified signal is finally filtered by a 5 nm bandwidth OBPF. The output of the PM is a positively chirped (PC) pulse, with 5.4 ps pulsewidth as measured by an autocorrelator, which calculates the full width at half maximum (FWHM) of the pulse under the assumption of a $sech^2$ pulse shape. Compressing the output of the PM by 250 m of SSMF will result in negatively chirped pulses (hereafter referred to as pre-compressed pulses) with 2.9 ps width, as indicated in the inset of Fig. 5.3(left).

5.2.2 Pulse Distortion in Saturated FOPCPA

Gain Saturation for Differently Chirped Signals

The dynamics of amplification of chirped pulses in an FOPCPA are investigated for the generated broad PC and narrow pre-compressed pulses. Furthermore, the broad PC pulses are post-compressed after filtering the amplified signal (using the same amount of SMF as the pre-compression) in order to evaluate the quality of the amplified signal when moving from the linear to the non-linear gain regime. Considering $sech^2$ shape for the pulses, the ratio between the peak power, P_{peak}, and average power, P_{avg},

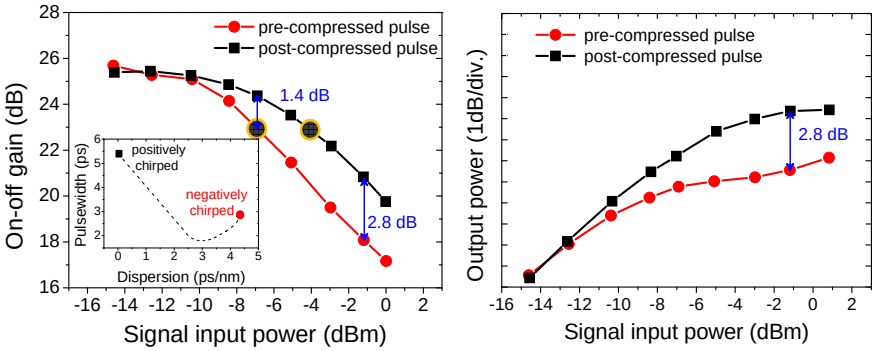

Figure 5.3: On-off gain as a function of signal input power for the pre- and post-compressed signals.

can be calculated from

$$P_{peak} = 0.88 \frac{\text{pulse energy}}{\text{temporal FWHM}} = 0.88 \frac{P_{avg}}{\text{repetition rate} \times \text{temporal FWHM}} \quad (5.1)$$

which is equal to 6.1 dB for the PC and 8.8 dB for the pre-compressed pulses. Thus, at the input of the HNLF, the peak power difference between the PC (and also the post-compressed pulses) and the pre-compressed is 2.7 dB.

The signal gain and output power at 1547 nm (which corresponds to the phase matched wavelength, resulting in maximum small signal gain) has been characterized as a function of the signal input power for the pre- and post-compressed pulses in Fig. 5.3.

In the linear gain regime, both signals have the same gain but by increasing the signal input power, the gain for shorter pre-compressed pulses saturates faster than the broader post-compressed pulses. In fact, the gain saturation depends on the signal peak power as the parametric gain responds fast to the input signal time variations. The gain difference at P_s = -7 dBm is 1.4 dB and it even increases to 2.8 dB for P_s = -1.2 dBm.

Signal Pulse Broadening

The pulse broadening evolution under saturation for three situations is illustrated in Fig. 5.4: the PC, pre- and post-compressed pulses. The measurements show that the pulses are temporally broadened when operating in gain saturation. The broadening rate, however, is different for different chirp values.

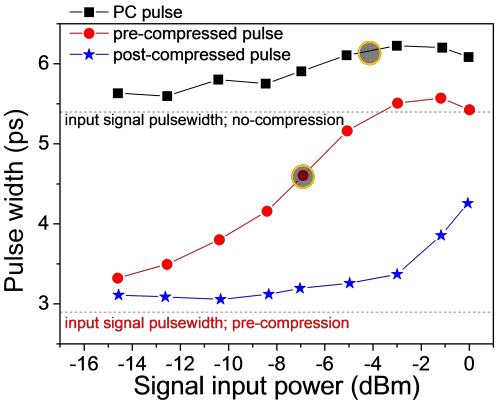

Figure 5.4: Pulsewidth as a function of signal input power for broad PC, narrow pre-compressed and post-compressed pulses.

At first the effect of amplification and saturation is compared between PC and post-compressed signals which have identical pulsewidths at the input of the HNLF. Both pulses therefore experience the same amplification and nonlinear-effects in the FOPA. Both preserve their pulsewidth in the linear regime while, by going to saturation, the post-compressed pulses starts broadening for $P_s > -3$ dBm which indicates the existence of an added incompressible noise to the pulses under gain saturation.

Comparing the post-compressed pulseswith the narrow pre-compressed pulses shows that both pulses have the same pulsewidth only for very low average input signal powers to the HNLF. In fact, their pulsewidth difference at the input of the fiber resulting in a 2.7 dB difference in their peak power for a same average power, causes a fast saturation and then broadening for the narrow pre-compressed pulses. This conclusion stands also for the broad PC pulses. Comparing the pulse broadening for the same level of saturation for PC and pre-compressed pulses, depicted with yellow circles in Fig. 5.3(left), pulse broadening is faster for the shorter pre-compressed pulses by going to saturation, depicted with yellow circles in Fig. 5.4.

The pulse shapes at different saturation levels are shown in the three cases in Fig. 5.5. The pulse shapes for narrow pre-compressed pulse show strong pedestals in deep saturation (middle plot).

Furthermore the comparison between pre- and post-compression in the linear regime shows the same pulse shape, as shown in Fig. 5.5 (solid curves in the middle and bottom plots). The pulse broadening is mild in the case of post-compression and the pulse shape can be maintained for higher signal input powers. This can be related to the lower non-linear interaction during amplification for temporally broad pulses. The ampli-

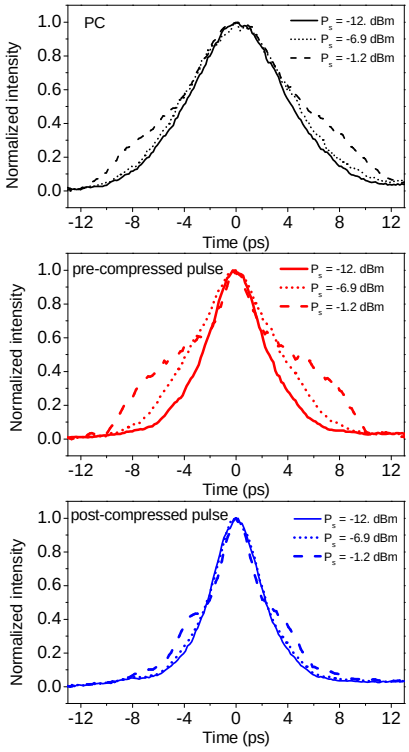

Figure 5.5: Autocorrelation traces for the PC (top), pre-compressed (middle) and post-compressed pulses (bottom) under different saturation levels.

fied pulse preserves its shape and width up to P_s = -3 dBm (blue stared curve in Fig. 5.4), i.e. when the gain is saturated by more than 3 dB. For higher saturation levels, e.g. P_s = -1.2 dBm in Fig. 5.5, the PC signal demonstrates that the pedestals emerging around the amplified signal (top plot) cannot be removed by post-compression (bottom plot). The experiments thus confirm the results shown only numerically in [80, 83]. As it is discussed based on the simulated spectrograms in [80], the added noise to the signal in saturation appears as two unchirped wave packets around the signal which are merged with the signal in time domain. The unchirped noise cannot be recompressed and show its effect as pedestals around the signal after recompression.

The power spectra at the output of the HNLF for the PC and pre-compressed pulses are depicted in Fig. 5.6 for the highly saturated case, i.e. P_s = -1.2 dBm. The effect of cross-phase modulation can be clearly seen on the pump wave for the narrow pre-compressed pulses.

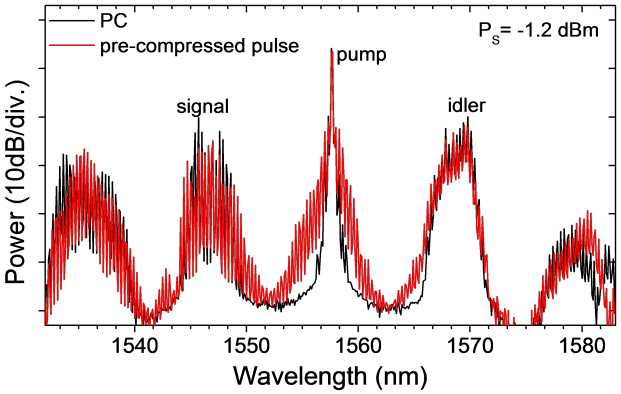

Figure 5.6: Power spectrum at the output of the HNLF for P_s = -1.2 dBm for the positively-chirped pulses and the pre-compressed ones.

For the chirped signal pulses under study in this section, the pulse evolution is dominated mainly by the amount of the chirp, and thus the pulse width, rather than the chirp sign. With the signal located in the weak normal-dispersion region of the HNLF (3.4 nm below the zero-dispersion wavelength), the chirp sign does not play a leading role. However, depending on the amount of dispersion accumulated by the signal under FOPCPA, the pulse quality can also be affected. This effect is studied in the following, looking at the idler.

Idler Pulse Broadening

In order to study the effect of accumulated dispersion on the pulse broadening, FOPCPA for the pre-compressed signal with 2.9 ps width at the input to the HNLF , is compared with its corresponding generated idler. The signal is located at 1547 nm, close to the wavelength of maximum gain, and the idler is located at 1568.5 nm. The conversion efficiency of the idler is compared with the signal on-off gain in Fig. 5.7(left). In the linear gain regime, both signal and idler have the same gain, but by going to the nonlinear regime the gain saturation differs for them as an effect of third-order dispersion [J-4], as it can also be seen from the output powers in Fig. 5.7(right). The gain asymmetry in saturation, here for the pulsed signals, is even more noticeable than for the monochromatic waves studied in section 3.2. The gain difference at P_s = -7 dBm is 2.6 dB and even increases to 5.2 dB for P_s = -1.2 dBm.

The pulse broadening evolution under saturation for the signal and idler is illustrated in Fig. 5.8(left). The measurements show that the

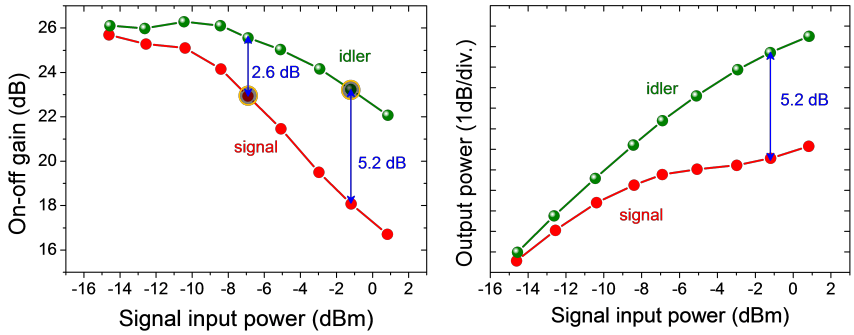

Figure 5.7: FOPCPA for idler corresponding to the pre-compressed signal. Left: comparison of on-off gains. Right: comparison of output powers.

main impact of saturation on the pulse shape manifests itself as pulse broadening. However, the broadening rate is different for the signal and idler. In the linear regime, the output signal pulsewidth is almost the same as the input one, while the idler pulsewidth shows compression with respect to the input signal. Considering the point that the generated idler is the phase conjugated of the signal and thus positively chirped (C>0), and propagates in the anomalous dispersion region of the HNLF (i.e. wgere β<0), the compression of the idler pulsewidth can be explained since the accumulated dispersion at the idler wavelength is more than that experienced by the signal. The idler is located 18.1 nm from the ZDW while the signal is separated only by 3.4 nm. The pulse shapes of the idler for different saturation levels are shown in Fig. 5.8(right). Comparing the idler with the signal at the same P_s levels, one can see the idler can maintain its pulse shape when the signal is highly saturated and distorted (Fig. 5.5 (middle)).

From the results presented, one may interpret that pulse broadening for the signals with shorter pulsewidths is faster in transition from the linear to non-linear regime as it can be seen in Fig. 5.4. On the other hand, the comparison between the pulse broadening for the signal and idler in Fig. 5.8 reveals that the broadening for the idler with shorter pulsewidth is not faster than that for the signal. Indeed, the saturation rate is not the same for the signal and idler, but one can compare the pulse broadening for a same level of saturation. As it can be seen from Fig. 5.7(left), the gain drop for the signal at P_s = -7 dBm is almost the same as the drop in conversion efficiency for the idler at P_s = -1.2 dBm, depicted in yellow circle in the figure. Comparing the pulse broadening at these levels, different pulsewidth and broadening can be clearly seen from

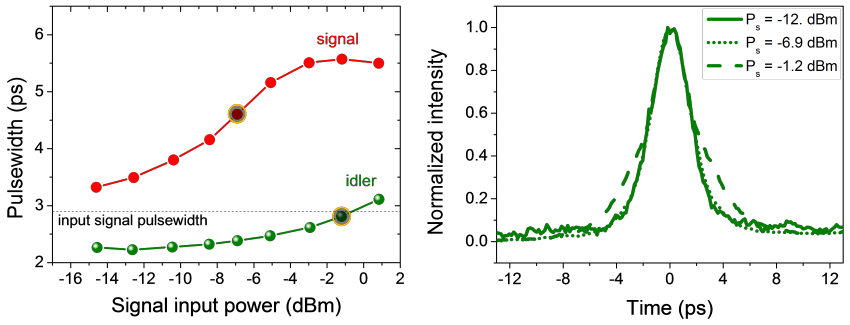

Figure 5.8: Left: comparison of pulsewidth broadening between the pre-compressed signal and its corresponding idler. Right: autocorrelation trace of the idler under different saturation levels.

Fig. 5.8(left). This may be understood from the accumulated dispersion experienced by the idler which is several times more than that of the signal. The initial pulse compression taking place for the idler oppositely drives the pulse broadening in saturation.

The conclusion is that two factors contribute to pulse broadening in FOPCPAs under saturation: one is the pulse width and the other is the accumulated dispersion in the amplifier at the pulse wavelength. The narrower the pulsewidth, the faster the pulse broadening. However, the accumulation of enough dispersion, with opposite sign from the chirp of the pulse, slows down the pulse broadening in saturation.

5.3 FOPCPA for Sub-Picosecond Pulses

This section focuses on FOPCPA of pulses as short as 400 fs. The results of this section is from a joint collaboration where the author has a secondary authorship [J-2, C-2, C-3]. The motivation behind FOPCPA for sub-picosecond pulses in the telecommunication window is to investigate FOPCPA for amplification of ultra-short pulses compatible with Tbaud communication systems where pulses durations shorter than 500 fs exist, e.g. for 1.28 Tbit/s, 5.1 Tbit/s or even 10.2 Tbit/s [84, 85, 86].

In this experiment, the signal pulses are generated at 28 MHz repetition rate in a figure-of-eight mode-locked laser (F8L) and are then filtered with a 9 nm bandpass filter to generate Gaussian pulses at 1571.6 nm with 400 fs full-width at half maximum pulsewidth. The pulses are stretched to approximately 50 ps in 309 m of SSMF, amplified to 26 dBm in a FOPA consisting of 500 m standard HNLF pumped with 28.5 dBm power. The amplified signal was filtered out and subsequently recom-

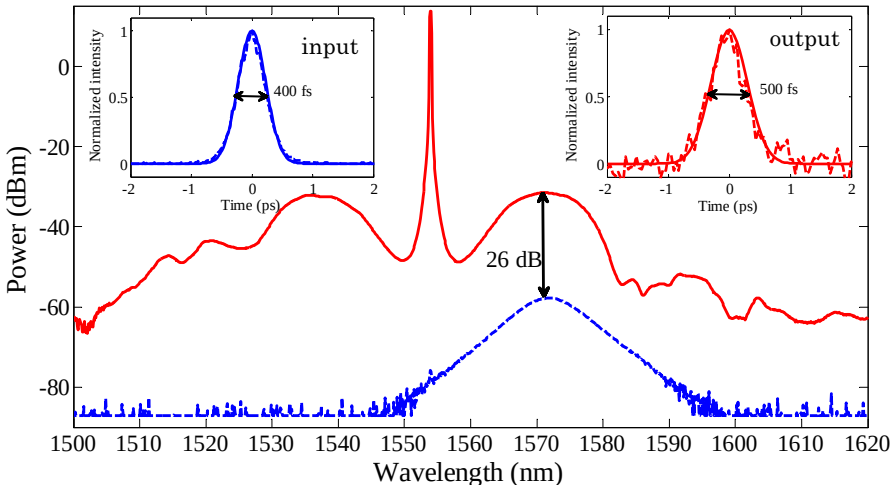

Figure 5.9: Measured optical spectra at the output of the HNLF with the pump switched off (dashed blue line) and on (solid black line). Inset: autocorrelation traces of the signal (a) at the input of the SSMF and (b) the output of the DCF [C-3].

pressed to 500 fs using a 50.5 m long DCF.

Optical spectra measured at the output of the HNLF with the pump switched off and on are shown in Fig. 5.9 together with the autocorrelation traces of the signal at the input of the SSMF and the output of the DCF. The noise on the output trace is due to the high losses in the filtering stage. The measured data has been fitted to Gaussian curves. The compressed pulse is broader with respect to the input pulse by about 100 fs. This can be due to the unflat gain spectrum as well as to a lack of compensation of high-order dispersion terms, which adds some chirp to the pulse. The peak-to-average power for the initial signal with 400 fs pulses is 49.2 dB which is lowered down to about 26.7 dB for 50 ps chirped pulses. The amplified signal after recompression has a width of 500 fs, resulting a peak-to-average power of 48.3 dB.

The optimized gain spectrum and amount of chirp applied to the signal prior to amplification are the two challenges in order to amplify the signal with the least amount of distortion. The FOPA is designed for a fairly flat gain at the signal wavelength mainly due to the high power of the pump and the pump wavelength being close to the ZDW of the HNLF. On the other hand, it is necessary to find a compromise between the stretching factor and the saturation of the amplifier. A too low stretching factor, i.e. a too high peak power, saturates the amplifier, while a too high stretching factor makes the dispersion management to

compress back the pulse after amplification impractical. In this experiment, the length of the SSMF is chosen somehow to lower down the peak power of the input signal to just below the onset of saturation checked from the output spectrum of the HNLF.

5.4 Summary

In this chapter, FOPCPA has been experimentally investigated for few picosecond and subpicosecond pulses. Parametric amplification of different chirped pulses in the linear and saturation regime was investigated. The chirped pulses show different rates of broadening in transition from the linear to non-linear regime. Pulse broadening depends on the initial pulsewidth, amount of chirp and accumulated dispersion in the amplifier. The shorter the pulse, the faster the broadening. However the broadening rate can be slowed down if the pulse has a potential for compression based on its sign of chirp, and the accumulated dispersion acquired in the amplifier.

The strongly chirped signals have higher saturation powers, which result in reduced pulse distortion for higher signal input powers. The amplified chirped signals in highly saturated amplifiers show excess distortion under the form of pedestals around the amplified signal after recompression.

Amplification of short, nearly transform-limited pulses of 9 nm bandwidth and 400 fs pulse duration has been demonstrated in a FOPCPA. The 400 fs pulses was first stretched to 50 ps, just enough to be at the limit of linear amplification, amplified by 26 dB in a fairly flat gain single-pump FOPA, and then compressed back to 500 fs.

Chapter 6

Cascaded In-Line Fiber Optical Parametric Amplifiers

6.1 Introduction

Fiber optical parametric amplifiers (FOPAs) are a promising choice for amplification of data signals outside the erbium-doped fiber amplifiers (EDFAs) band in long-distance optical transmission systems. As it was discussed in chapter 2, the gain of FOPAs depends on pump power, fiber non-linearity and fiber dispersion properties, and can therefore be tailored with respect to the wavelength configuration of the interacting waves and be centered at about any arbitrary wavelength. Other unique aspects of FOPAs, such as the possibility for regeneration using gain saturation and frequency conversion make them even more attractive for multi-functional applications [87, 31]. Until now, FOPAs have been mostly used as stand-alone amplifiers or all-optical signal processing elements, and only recently have studies on the implementation of these amplifiers in transmission links been under focus [43, 88, 89, 90]. In Ref. [43] the performance of single-pump FOPAs in dense wavelength-division multiplexed systems was investigated using a recirculating loop with the FOPA actually used outside of the loop, either as a booster amplifier or at the end of the transmission line. In Ref. [89], the reduction of non-linear phase noise by an all-optical amplitude limiter using saturation of four-wave mixing in a fiber has been investigated in a recirculating loop transmission. However no gain was provided to the signal in the parametric amplitude regenerator. The use of FOPAs as in-line amplifiers in a multi-span link has never been reported so

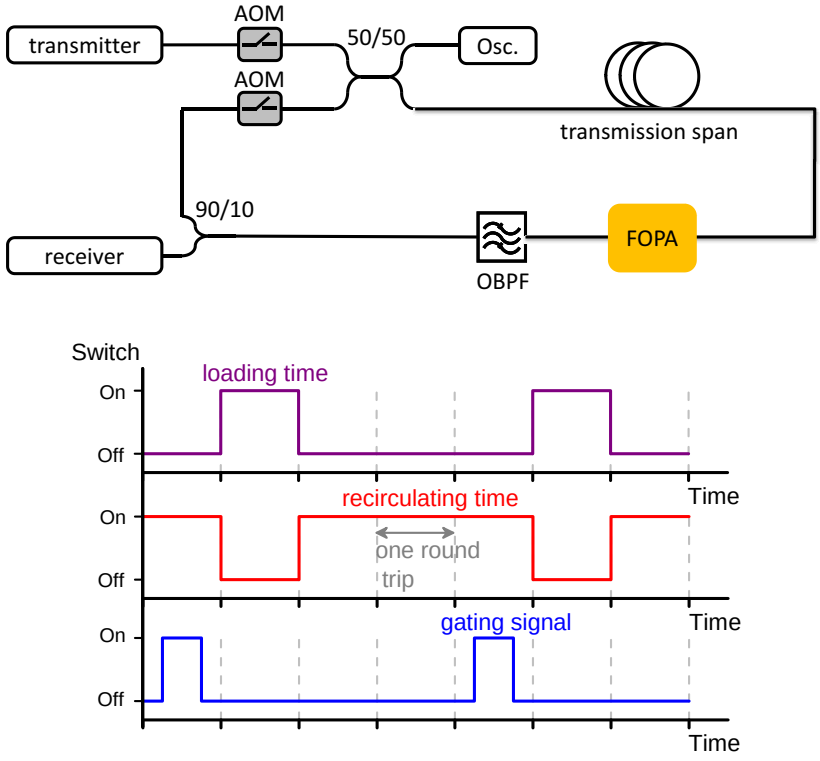

Figure 6.1: Schematic of recirculating loop transmission (top) and the loop timing diagram (bottom).

far. In this chapter, the performance of cascaded single-pump FOPAs using a multi-span recirculating loop transmission has been experimentally investigated for the first time, where a FOPA with 20 dB on-off gain is located in the transmission line. The cascadability of the FOPA is demonstrated for 40 Gbit/s carrier-suppressed return-to-zero (CSRZ) on-off keying (CSRZ-OOK) and CSRZ differential-phase shift keying (CSRZ-DPSK) modulated signals. Error-free performance is achieved for both modulation formats over a 320 km dispersion managed link, thus demonstrating a first step towards the implementation of FOPAs as in-line amplifiers [C-5].

6.2 Recirculating Loop Transmission

In order to cascade FOPAs in the laboratory, a recirculating loop transmission is used. In this scheme, the modulated signal is sent into a recirculating loop which consists of two acousto-optic modulators (AOMs),

fiber span and the amplifier, as shown in Fig. 6.1(top). The data signal is sent to the loop via a 50/50% coupler, circulated a given number of round trips in the loop, and continuously sent via a 90/10% coupler to the receiver. Circulations in the loop are controlled by the two AOMs. The two switches allow us to load and unload data into the loop periodically, as it can be seen in the loop timing diagram depicted in Fig. 6.1(bottom), the data is sent to the receiver via a 90/10% coupler for characterization. All devices at the receiver are synchronized with the loop and gate the signal at the last round trip.

In the experiment presented in the following section, one round trip time, which can be measured from the oscilloscope located at the second output port of the 50/50% coupler, is about 455 μs which accounts for the total fiber length included in the loop. The gating window is chosen equal to 50% of a round trip time and applied at the middle of the last round trip time window.

6.3 Experimental Setup for Cascaded FOPAs

The experimental setup is shown in Fig. 6.2. A recirculating loop is used to realize the cascadability investigation of FOPAs. At the transmitter, a 67% RZ-OOK or RZ-DPSK signal is generated from a continuous wave (CW) laser at 1545 nm using cascaded Mach-Zehnder modulators (MZMs) used as pulse carver and data modulator, respectively. The data modulator is driven with a 2^{31}-1 pseudo-random binary sequence (PRBS) at 40 Gbit/s. The modulation format is selected by adjusting the bias and peak-to-peak voltage applied to the data modulator. The modulated signal is then amplified by an EDFA followed by an optical bandpass filter (OBPF) with 3 nm bandwidth and its power at the loop input is adjusted by an optical variable attenuator (OVA). Gating of the bit-error ratio (BER) test-set and the oscilloscope enable the characterization of the signal after the last round-trip in the loop. The transmission link consists of an 80 km long standard single-mode fiber (SSMF) and a matching length of 13 km dispersion compensating fiber (DCF).

The FOPA, placed between the SSMF and the DCF, is realized by combining the signal with a CW pump that has been phase modulated with four radio-frequency (RF) tones of frequencies 111 MHz, 675 MHz, 1 GHz and 2.25 GHz for stimulated Brillouin scattering (SBS) mitigation, before being amplified by a high-power EDFA. The pump and signal are combined in a Mach-Zehnder interferometer add/drop multiplexer with fiber Bragg gratings (FBGs) reflective at the pump wavelength in each arm. This solution enables to simultaneously achieve less

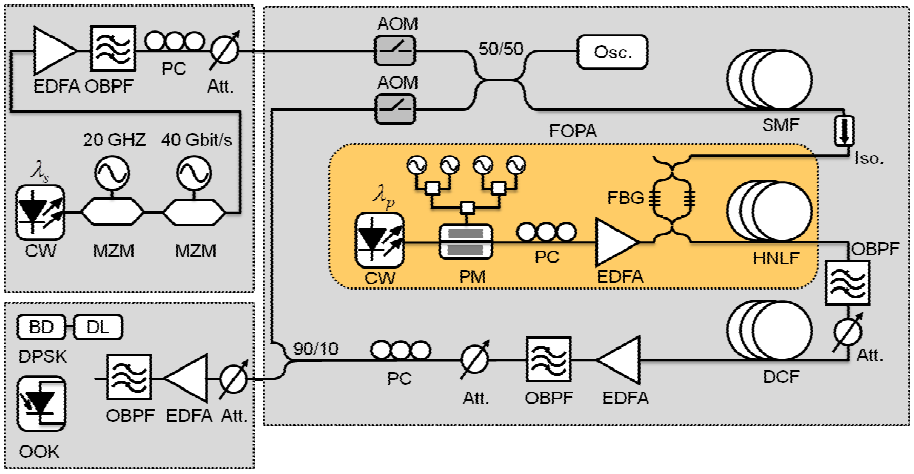

Figure 6.2: Experimental setup for cascaded FOPAs.

than 1 dB coupling loss for the transmitted signal/reflected pump and to filter the out-of-band amplified spontaneous emission noise from the pump. The parametric amplification, with 20 dB on-off small signal gain at 1545 nm, takes place in a 500 m long highly non-linear fiber (HNLF) with zero-dispersion wavelength at 1550.4 nm, non-linear coefficient of 10.7 $W^{-1}{\cdot}km^{-1}$, dispersion slope of 0.0185 $ps{\cdot}nm^{-2}{\cdot}km^{-1}$, and attenuation of 0.7 $dB{\cdot}km^{-1}$. The pump and signal power at the HNLF input are 28 dBm and -18 dBm, respectively. The amplified signal is then filtered out by two cascaded thin-film OBPFs with 3 nm and 5 nm bandwidths in order to sufficiently suppress the pump. An EDFA with 28 dB gain and 15 dBm saturated output power is used after the DCF in order to compensate the loss of the rest of the elements in the loop, such as filters, loop switch and couplers. Finally the power in the loop is balanced with an OVA.

The FOPA design used in the present demonstration is polarization sensitive. Therefore it is ensured that a stable principal state of polarization is found for the recirculating loop thanks to polarization controllers (PCs) placed before the loop switch. Polarization matching between the signal and pump is ensured in order to provide maximum parametric gain. This is achieved thanks to another PC placed in the pump path within the FOPA. The receiver consists of an EDFA preamplifier, and a photodiode with 45 GHz bandwidth in the case of OOK, or a 1 bit fiber delay interferometer (DI) followed by a balanced detector (BD), also with 45 GHz bandwidth, for DPSK. A loop-compatible clock recovery circuit is also employed at the receiver.

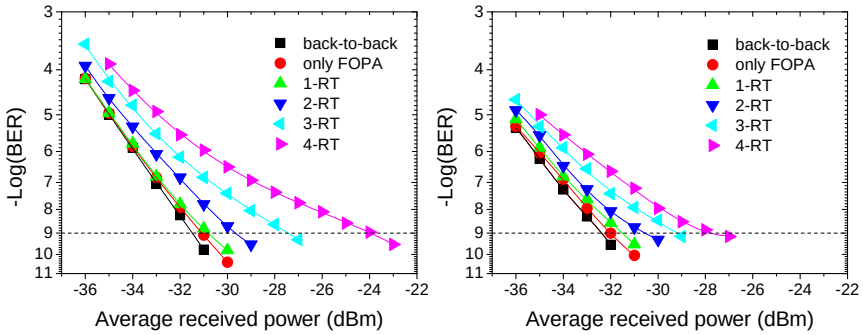

Figure 6.3: BER characteristics of 40 Gbit/s CSRZ-OOK (a) and CSRZ-DPSK (b).

6.4 Experimental Results

The performance of the cascaded FOPA is studied for CSRZ-OOK and CSRZ-DPSK modulation at 40 Gbit/s. The optimized average signal power at the input of the SSMF and DCF are 1.4 dBm and -5 dBm, respectively. Bit-error-ratio (BER) measurements are carried out as a function of the average received power. The BER performance of the cascaded FOPA for several round trips (RTs) as well as for the FOPA alone (without transmission span) are presented in Fig. 6.3. Error-free performance is achieved for both modulation formats up to four round trips (RTs), corresponding to 320 km transmission.

The power penalty as a function of the number of RTs has been extracted for a BER of 10^{-9}, as shown in Fig. 6.4. The eye diagrams, taken at the input of the receiver, are also illustrated in the insets of the figure. '0' round trip corresponds to the penalty of the FOPA itself when placed between the transmitter and the receiver, which is less than 0.5 dB. When increasing the transmission distance by increasing the number of round trips, the power penalty increases while the pulse shape is well preserved, which suggests that noise accumulation is responsible for signal degradation for both modulation formats. For longer transmission distances the CSRZ-DPSK format shows a lower power penalty thanks to its well known robustness towards the effects of fiber non-linearities. The penalty difference compared with the CSRZ-OOK format is 2.7 dB after 4 round trips.

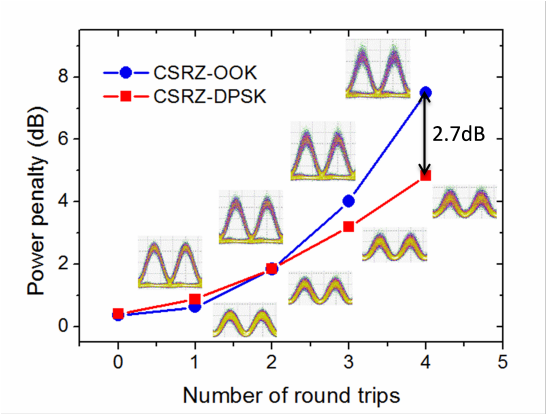

Figure 6.4: Power penalty as a function of number of round trips and corresponding eye diagrams for 40 Gbit/s CSRZ-OOK and CSRZ-DPSK signals.

6.5 Comparison with EDFAs

In this section the performance of the loop is compared with the situation where the FOPA is replaced by an EDFA with $\sim$ 22 dB gain. At first, we look at the OSNR degradation of the FOPA and the EDFA before comparing their performances in the loop. Fig. 6.5 shows the power spectrum of the CSRZ-DPSK signals. At the left side of the figure, the input signal to the loop is compared with the amplified signal at the output of the HNLF when the FOPA is out of the loop. The OSNR degradation of the FOPA can be measured from the input and output extracted OSNRs (36.4 dB and 31.3 dB, respectively) which equals 5.1 dB. At the right side of the figure, the input signal to the loop, the output after the first RT when the FOPA is placed in the loop, and after the first RT when the FOPA in the loop is replaced by the EDFA are compared. The OSNR degradation of the loop in total can be measured in this case. The OSNR degradation is increased by 1.3 dB to 6.4 dB when the FOPA is in the loop while it is 5.3 dB for the EDFA. The total OSNR degradation of the loop for one round trip is better by 1.1 dB when the FOPA is replaced by the EDFA.

The better performance of the EDFA with respect to the FOPA after one RT can be mainly due to the fact that the transmission spans are operated under different conditions for the two situations. Efficient suppression of the pump and idler requires OBPFs with large extinction ratios to circumvent crosstalk and good cascadability, which in turn may add some loss. When the FOPA is in the loop, the input power to the DCF is limited to -5 dBm due to the high-loss filtering process,

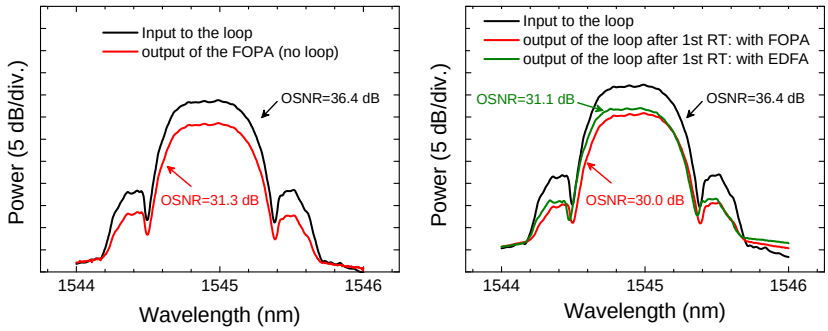

Figure 6.5: Power spectrum of the CSRZ-DPSK signal at the input and output of FOPA (left) and comparison with EDFA after first RT (right).

while this value is optimize to -1 dBm after replacing the FOPA with the EDFA, which indeed contributes to the overall improvement of the link performance. The noise added to the signal, resulting in 1.1 dB penalty in the total OSNR degradation of the loop for only one RT, will be accumulated in longer transmission distances showing its effect in the BER performance for larger numbers of RTs.

Knowing the aforementioned point, the power penalty of the system at a BER of 10^{-9} is compared for the situation when the FOPA is in the loop with the situation when it is replaced by the EDFA. One can see that the power penalty is no more than 2 dB up to 4 RTs when the EDFA is used. Considering the aforementioned suboptimal launched power to the DCF in the loop, this comparison prevents us to conclude that the performance of the FOPA is detrimental by more than twice compared to the EDFA. The following section discusses the possible practical improvements that can be applied when the FOPA is used as an in-line amplifier.

6.6 Practical Advances to Improve the System Performance

Even though the first cascadability of in-line FOPAs has been demonstrated in this experiment, it is clear that further practical advances are needed to make the scheme comparable with EDFAs. We believe that FOPAs have the potential to serve as in-line amplifiers provided some practical improvements are fulfilled. In this section, possible ways to improve the operation of FOPAs as in-line amplifiers in a recirculating loop are discussed. There are indeed some limitations in this demonstration

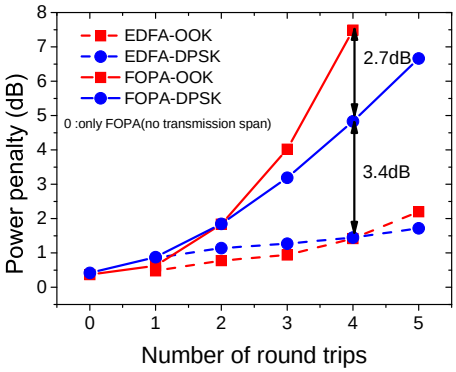

Figure 6.6: Comparison of the power penalty for the FOPA and EDFA.

which can be overcome.

6.6.1 Optimization of the Recirculating Loop Transmission

The length of transmission span in a loop affects the performance of the loop. In general, the more spans are included in each round trip, the better the performance of the loop. The transmission span in this experiment consisted of 80 km SSMF and 13 km DCF with total loss of about 27 dB. The transmission span can be optimized in terms of length as well as fiber type. One can think about a loop with a higher number of SMF+DCF spans. Moreover, the overall loss of the spans can also be reduced by using non-zero dispersion shifted fibers (NZDSFs) and inverse dispersion fibers (IDFs). Lower loss in the loop helps to easily balance the power of the recirculated signal to the loop, and also to balance the input powers to the spools of SSMF/NZDSF and DCF/IDF. Specifically for the setup in the presented experiment, the other source of loss was the one introduced by the filters located after the HNLF, which could be easily reduced using lower loss elements such as WDM couplers.

6.6.2 Optimization of the FOPA

Effect of the pump OSNR As we saw in chapter 4, the intensity noise introduced from the pump has an adverse effect on the signal quality. By increasing the pump OSNR, which can be fulfilled by increasing the launched power to the high-power EDFA implemented in the FOPA, one can minimize the pump-to-signal intensity noise transfer.

The effect of pump OSNR is investigated here for the situation where

the FOPA is placed alone between the transmitter and receiver. The effect of the pump OSNR on the BER performance for both CSRZ-OOK and CSRZ-DPSK signals is shown in Fig. 6.7. As it can be seen, a 0.7 dB increase in pump OSNR improves the BER performance by about 1 dB in case of OOK and 0.3 dB for DPSK signals. The experiment in this chapter was performed for pump OSNR of 52 dB, which could have been increased to promote the overall performance of the system in larger number of round trips. Such an effect may be negligible for well-designed single FOPAs, but are of an accumulative nature if FOPAs are cascaded as in-line amplifiers.

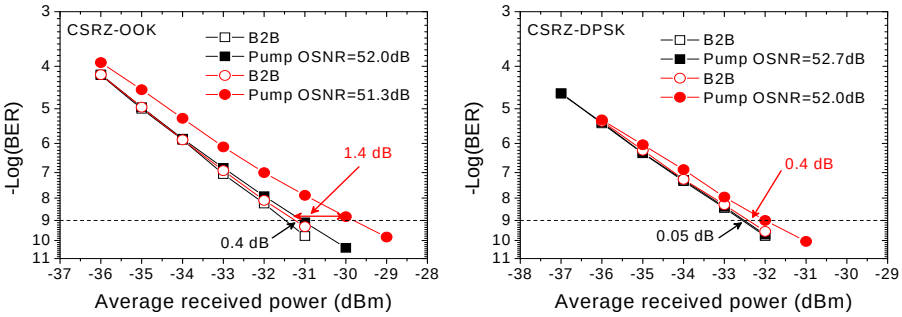

Figure 6.7: Effect of pump OSNR on the BER performance of 40 Gbit/s CSRZ-OOK signal (left) and CSRZ-DPSK signal (right).

Polarization sensitivity Most importantly, since parametric amplification is strongly polarization sensitive, a polarization-independent scheme needs to be implemented if the FOPA is used as in-line device. Using either polarization diversity or dual-pump FOPAs with orthogonally-polarized pumps should be implemented to overcome polarization-induced gain changes while providing sufficient signal gain.

6.7 Summary

The performance of cascaded single-pump FOPAs has been experimentally investigated for the first time using recirculating loop transmission. The feasibility of exploiting FOPAs as in-line amplifiers was investigated for 40 Gbit/s CSRZ-OOK and CSRZ-DPSK signals. Both modulation formats show error-free performance up to 320 km. The choice of CSRZ-DPSK signals allows to reduce the power penalty by 2.7 dB compared to CSRZ-OOK. Possible sources of impairments and possible ways to

improve the performance of FOPAs as in-line amplifiers have also been discussed.

Chapter 7

Amplification and Regeneration of a 640 Gbit/s RZ-DPSK Signal

7.1 Introduction

This chapter explores the use of single-pump fiber optical parametric amplifiers (FOPAs) for amplification and regeneration of high-speed optical time division multiplexed (OTDM) signals. In the OTDM systems all information is carried on a single wavelength channel: short optical pulse streams, called tributaries, are generated from a pulse source (typically at 10 GHz or 40 GHz, called base-rate), split up into several branches and separately data modulated. After adjusting a proper time delay between the branches, the tributaries are combined and form a temporally interleaved serial data signal at a data rate several times higher than the base-rate, depending on the number of split branches. High-speed data signals beyond the bandwidth limitation of electronics is achievable using this technique. A single wavelength channel at 1.28 Tbit/s obtained by time-division multiplexing of 128 single polarization on-off keying (OOK) data channels at 10 Gbit/s [84] as well as a total capacity of 5.1 Tbit/s using differential quadrature phase shift keying (DQPSK) data-modulation and polarisation-multiplexing [85] have been demonstrated. The total capacity on a single-channel has even been pushed to 10.2 Tbit/s by combining multi-level modulation using 16-ary quadrature-amplitude modulation (16-QAM) [86].

The spectral bandwidth of the generated OTDM signal depends on the pulsewidth of the multiplexed pulses at the base-rate. The shorter the multiplexed pulses, the broader the OTDM spectrum, which de-

mands optical signal processors with compatible operation bandwidths. This chapter discusses the use of FOPAs for amplification and regeneration of OTDM signals. All-optical amplification and regeneration of high-speed signals using FOPAs are presented in the following parts of this section. Section 7.2 describes the experimental setup for amplification and regeneration of a 640 Gbit/s OTDM signal. The static gain spectrum of the designed FOPA is discussed in section 7.3. Amplification performance and all-optical regeneration of the 640Gbit/s signal are presented in sections 7.4 and 7.5, respectively. The use of FOPAs for regeneration of wavelength division multiplexed signals are proposed and discussed in section 7.6 and at last the conclusion is drawn in section 7.7.

7.1.1 Parametric Amplification of OTDM Signals

So far, the highest capacity amplified in a single-pump FOPA has consisted of 26 wavelength-division-multiplexed (WDM) return-to-zero differential-phase-shift-keying (RZ-DPSK) modulated signals at 43.7 Gbit/s [43]. Crosstalk mainly limits the amplification performance of WDM signals in parametric amplifiers due to four-wave mixing (FWM) between the channels [91, 92]. In contrast, OTDM signals can be more secured against crosstalk as all the channels are time interleaved. The first amplification of a single channel OTDM signal at 640 Gbit/s using a single-pump FOPA [C-4, J-1] is discussed in the section 7.4 of this chapter.

7.1.2 Phase-Preserving Amplitude Regeneration of OTDM Signals

Optical signals are degraded during propagation through the long-haul transmission links due to various impairments, such as amplified spontaneous emission (ASE) noise added by in-line amplifiers, nonlinear effects e.g. cross-phase modulation, and chromatic dispersion imposed by the transmission medium and other dispersive elements. These impairments introduce amplitude jitter, extinction ratio (ER) degradation and timing jitter to the transmitted signal. A regenerator is required to remove the added noise and restore the quality of the signal. Regeneration with functionalities including reamplification and reshaping are referred to as 2R regeneration, which contributes in removal of amplitude jitter and ER enhancement plus amplification, while 3R regeneration is able to also retime the signal as well and overcome the timing jitter. All-optical signal regeneration is one of the desired functionalities to extend the trans-

mission distance in high-capacity optical networks without resorting to optical-electrical-optical conversions, which are increasingly challenging to implement at ultra-high bit rates.

Different schemes for all-optical regeneration (AOR) using optical fibers as the non-linear medium have been demonstrated. An effective regeneration scheme was proposed by P.V. Mamyshev in 1998 [93]. This scheme works based on self-phase modulation and off-centered filtering in a simple configuration and is able to regenerate return-to-zero OOK (RZ-OOK) signals both for "0" and "1" bits. Using this scheme, phase modulated signals also can be regenerated after modulation conversion to OOK [94].

Regarding AOR for phase modulated signals, amplitude and phase noise reduction can be achieved using phase-sensitive FOPAs [28, 29, 30]. Amplitude only regeneration of phase modulated signals, while the phase is preserved, is still effective as it prevents the conversion of the amplitude fluctuations to the phase fluctuations through the fiber nonlinearities, called nonlinear phase noise [23], and thus is able to improve the transmission performance of the signal.

Phase-insensitive FOPAs operating in the saturation regime have been realized for optical level equalization and amplitude noise suppression [21, 22], which are accompanied with gain for the signal. The scheme preserves the wavelength and phase of the signal. Based on the power transfer function of the signals in FOPAs, amplitude noise removal for OOK signals, based on saturated FOPAs, takes place only for "1" bits due to the two levels of amplitude involved in OOK modulation[1]. On the other hand, amplitude noise suppression for phase modulated signals, i.e. DPSK and DQPSK formats, where all the symbols have an equal average power, is achievable in gain saturated FOPAs [24, 26, 97] without ideally affecting the phase information of the signal.

Phase-preserving amplitude regeneration (PPAR) of optical signals has been demonstrated in different schemes. PPAR based on optical injection locking for 10 Gbit/s binary phase-shift keyed (BPSK) signals [98], or on a semiconductor optical amplifier for 40 Gbit/s DPSK signals [99], have been recently reported. So far, the highest bit rate at which single-channel all-optical regeneration has been achieved is 640 Gbit/s, using a periodically-poled lithium niobate (PPLN) waveguide [100]. Regeneration of a total capacity of 640 Gbit/s has also been demonstrated based on saturated FWM in a highly-nonlinear fiber (HNLF) [101], al-

[1]For amplitude regeneration of OOK signals based on gain saturated FOPAs, higher-order FWM products (HFPs) instead of the signal itself can be used as they have faster amplification rate than the signal which results in more step-like transfer function [95, 96].

beit using wavelength and polarization multiplexing. In both cases, regeneration was realized for OOK data signals and accompanied with no amplification. FOPAs can simultaneously amplify and regenerate degraded signals thanks to the ultra-fast process of their gain saturation, which makes them highly suitable for high bit-rate applications [102]. However, the regeneration of high-speed short pulses based on saturated FOPAs can be challenging, mainly due to the limited uniform gain bandwidth available in single-pump FOPAs and the generation of undesirable higher-order FWM products falling in the bandwidth of the data signal in dual-pump FOPAs, as it was discussed in chapters 2 and 3. Section 7.5 of this chapter reports the first demonstration of PPAR for a 640 Gbit/s DPSK OTDM signal based on gain-saturation in a single-pump FOPA [C-1, J-1].

7.2 Experimental Setup

The experimental setup for amplification and regeneration of a 640 Gbit/s RZ-DPSK signal is illustrated in Fig. 7.1. It consists of a 640 Gbit/s transmitter, a FOPA, a non-linear optical loop mirror (NOLM) demultiplexer and a 10 Gbit/s receiver. At the transmitter, 10 GHz short pulses are generated from an erbium glass oscillating pulse-generating laser (ERGO-PGL) at 1542 nm with $\sim$ 1.5 ps full width at half maximum (FWHM) pulse width. The short pulses are amplified and launched into a 400 m dispersion-flattened highly non-linear fiber (DF-HNLF) to broaden their spectrum through self-phase modulation and supercontinuum (SC) generation. The broadened signal is filtered at 1553 nm and 1542 nm with 14 nm and 5 nm optical bandpass filters (OBPFs) to generate two 10 GHz pulse trains to be used as the data signal and the NOLM demultiplexer control pulses, respectively. The data signal is encoded at 10 Gbit/s in the RZ-DPSK modulation format using a 2^7-1 pseudo-random binary sequence (PRBS) and then time multiplexed up to 640 Gbit/s using a PRBS-preserving passive fiber-delay multiplexer. The dispersion accumulated in the transmitter is compensated and the signal is spectrally shaped using an optical signal processor (SP), amplified and input to the FOPA for amplification characterization. In case of regeneration characterization, the pink box is included in the setup: the signal is combined with amplified spontaneous emission (ASE) noise via a 90/10 % coupler and then launched to the FOPA and the OSNR of the signal is adjusted by a variable attenuator placed after the noise source.

At the FOPA, the pump is a continuous wave (CW), which is phase

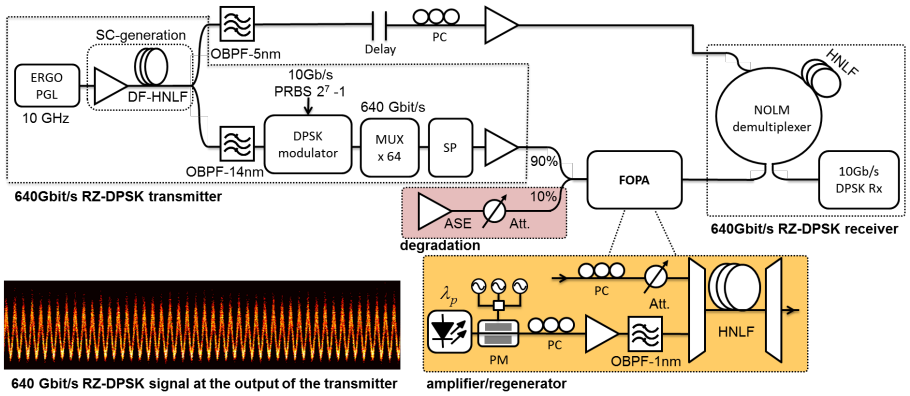

Figure 7.1: Experimental setup for amplification of a 640 Gbit/s RZ-DPSK signal using a FOPA.

modulated by three frequency tones (106 MHz, 288 MHz and 1 GHz) in order to suppress stimulated Brillouin scattering. The pump is then amplified and filtered with a 1 nm OBPF, to remove out-of-band ASE noise, and coupled with the signal into the HNLF used as gain medium by a WDM coupler. The OSNR of the pump is 54 dB and its input power to the HNLF is 27 dBm. The HNLF is 500 m long, with zero-dispersion wavelength (ZDW) at 1569 nm, dispersion slope of 0.016 ps·nm^{-2}·km^{-1}, non-linear coefficient of 11.4 W^{-1}·km^{-1} and loss of 0.7 dB·km^{-1}. At the output of the FOPA, the amplified signal is filtered by cascading two WDM couplers to suppress the pump wave without affecting the signal spectrum. The amplified 640 Gbit/s OTDM signal is demultiplexed in the NOLM, operating based on cross-phase modulation induced by the 10 GHz control pulses in a 50 m HNLF, resulting in 10 Gbit/s RZ-DPSK signals. Finally, the demultiplexed signals are demodulated and detected using a 1-bit delay interferometer and a balanced photodetector.

7.3 Static Gain Spectrum

In order to amplify or regenerate high-speed OTDM signals consisting of very short pulses using FOPAs, an amplifier with flat gain and free from any overlap with higher-order FWM products (HFPs) in saturation is desirable. Concerning the gain flatness in single-pump FOPAs, for a given HNLF, the gain bandwidth can be tuned by tuning the wavelength and power of the pump, which determine the balance between the linear ($\Delta\beta$) and non-linear ($2\gamma P_p$) phase-mismatch terms $\Delta\beta + 2\gamma P_p = 0$. As it was discussed in chapter 2, pumping the amplifier close to the ZDW can broaden the gain spectrum over 10 nm at the expense of losing gain.

The other factor that needs to be ensured in processing of short pulses in FOPAs is the proper frequency separation between the pump and signal. The signal spectral bandwidth needs to be separated enough from the pump so that the new generated waves, resulting from interaction between the pump and a part of the signal spectrum close to the pump, does not overlap with the other side of the signal spectrum.

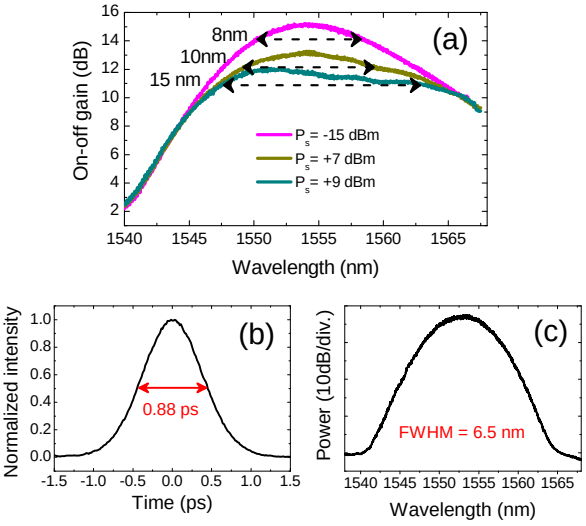

Figure 7.2: (a) Static gain spectra for different signal input powers; (b) Autocorrelation trace and (c) Spectrum of the 640 Gbit/s OTDM signal at the input of the FOPA.

At first, static gain spectra are measured using a swept CW probe signal for different signal input powers to the HNLF (P_s), as shown in Fig. 7.2(a). The pump wavelength was set 2.5 nm above the ZDW at 1571.5 nm in order to provide a fairly flat gain spectrum around the signal wavelength centered at 1553 nm. The 1 dB gain bandwidths for P_s = -15 dBm, +7 dBm and +9 dBm are 8 nm, 10 nm and 15 nm, respectively. The flatter gain spectrum for higher input signal powers is due to the fact that saturation occurs faster for the parts of the signal spectrum with the highest gain.

The autocorrelation trace and spectrum of the 640 Gbit/s signal input to the FOPA are shown in Fig. 7.2(b)(c). The input signal has a Gaussian pulse shape with 620 fs temporal (880 fs autocorrelation) and 6.5 nm spectral FWHM. The signal is centered at 1553 nm which has 18.5 nm wavelength separation from the pump. This wavelength separation is about equal to three times the signal spectral FWHM. This separation can ensure no overlap of the new generated waves in satura-

tion within twice the signal spectral FWHM.

7.4 Amplification of a 640 Gbit/s RZ-DPSK Signal

Once an amplifier with sufficient flat gain bandwidth is designed, amplification of a 640 Gbit/s signal consisting of pulses as short as 620 fs is investigated in this section for the first time. The amplification performance for the 640 Gbit/s RZ-DPSK signal is studied at different gain levels in order to find out the effect of gain shaping in the saturated regime.

7.4.1 Effect of Gain Shaping

The output spectra of the FOPA for different signal input power levels are shown in Fig. 7.3(a). The maximum gain is achieved for the signal with -10 dBm average input power and is about 15 dB (net gain measured between the FOPA input and output, as defined in Fig. 7.1). The average output power and signal gain, measured in a 14 nm spectral window, are shown as a function of the average signal input power in the inset of Fig. 7.3(b). The signal gain is decreased by 1.7 dB by increasing the signal input power up to +6 dBm.

To investigate the effect of the gain shaping on the amplified signal, the difference between the input spectrum to the FOPA and the amplified spectrum was examined for different signal input powers, within the FWHM range of the input signal spectrum (i.e. 6.5 nm) as shown in Fig. 7.3(c). The extracted peak-to-peak deviation of this power difference is represented in Fig. 7.3(d). As the signal input power increases and the gain spectrum becomes flatter, the peak-to-peak deviation consequently decreases, resulting in reduced spectral shaping. The notable point here is the clear spectral shaping of the amplified signal for input signal powers above -2 dBm, while the signal gain (calculated based on the average input and output powers) does not show significant saturation at this power. At this power, the effect of the localized saturation of the FOPA gain does not result in a gain drop for the signal average power but does significantly alter the shape of the gain spectrum. It appears that, at a signal power of about -2 dBm, it is possible to achieve both high average gain and a flat gain spectrum for this FOPA configuration.

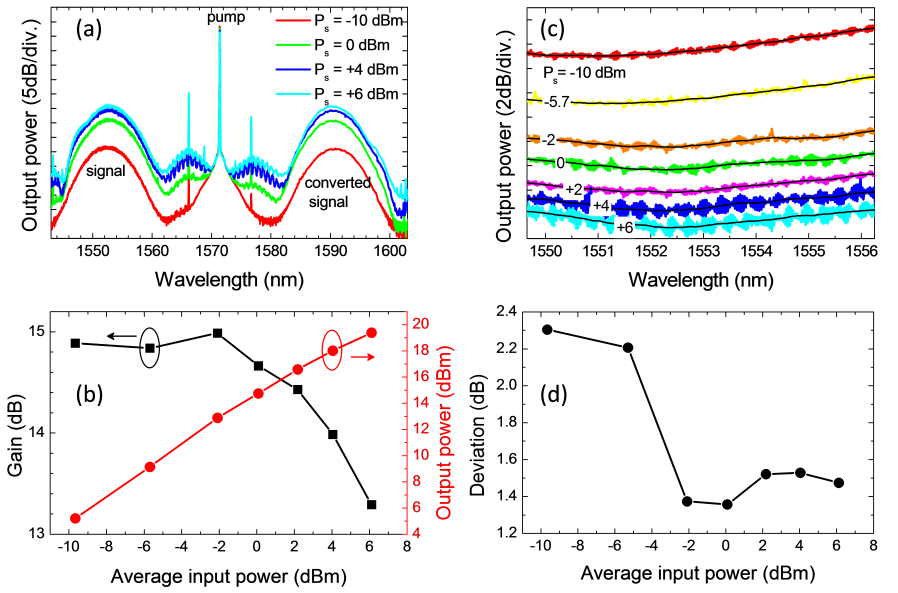

Figure 7.3: (a) Output spectra of the FOPA for different signal input powers. (b) Signal output power and signal gain as a function of signal input power to the FOPA. (c) Differences between the FOPA input and output signal power spectra within the FWHM range of the input signal spectrum. (d) Peak-to-peak values of the power spectrum differences.

7.4.2 Bit-Error-Ratio Performance

Fig. 7.4(a) shows the results of bit-error-ratio (BER) measurements for the 10 Gbits/s demultiplexed signal as a function of the average received power at the input of the demultiplexer. The back-to-back curve was measured when the pump was off and the input signal power to the HNLF was set to +5 dBm. The receiver sensitivity at a BER of 10^{-9} of all the 64 demultiplexed channels is shown in Fig. 7.4(b). Sensitivities for all the channels are spread within ~ 2 dB. The rest of the measurements are performed for channel number 2 with -17.1 dBm back-to-back sensitivity. Amplification with 15 dB net gain and less than 1 dB power penalty compared to back-to-back is successfully achieved for P_s = -10 dBm. The performance of the system is even closer to the back-to-back case when the signal input power is increased, reaching about 0.1 dB penalty for P_s = +6 dBm. In fact, the signal is more affected by the intensity noise transfer from the pump in the unsaturated gain regime. Increase of the signal input power to the FOPA reduces the pump-to-signal noise transfer [J-3, J-5] and flattens the gain spectrum, as shown above, re-

sulting in better signal performance at the expense of 1.7 dB of signal gain. The eye diagrams of the 10 Gbit/s demultiplexed and demodulated signal at a BER of 10^{-9} are also shown in Fig. 7.4(c) for back-to-back and amplified signals with 15 dB and 13.3 dB gain, corresponding to P_s = -10 dBm and +6 dBm, respectively.

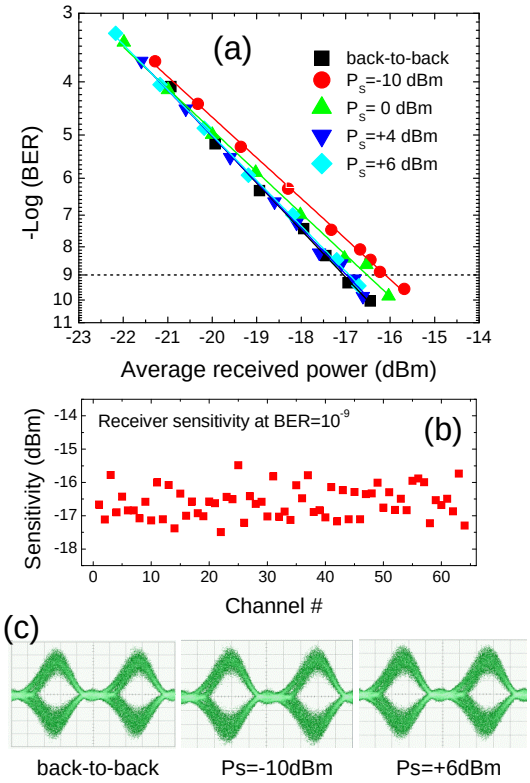

Figure 7.4: (a) BER measurements for a 10 Gbit/s DPSK channel demultiplexed from the 640 Gbit/s signal; (b) Receiver sensitivity at a BER of 10^{-9} in back-to-back configuration; (c) Eye-diagrams of demultiplexed and demodulated signals for back-to-back and after amplification with -10 dBm and +6 dBm input power.

7.5 Regeneration of a 640 Gbit/s RZ-DPSK Signal

In a transmission link, amplitude noise can be converted to nonlinear phase noise through the Kerr non-linearity of the transmission fibers (self-phase and cross-phase modulations) which adversely affects the phase information of the signal [23]. Therefore, PPAR of phase encoded signals can mitigate the accumulation of nonlinear phase noise

in a transmission link. The effectiveness of phase-preserving amplitude regenerators for DPSK signals is proved by placing the regenerator either before some transmission spans [98, 103, 104] or before the receiver [24, 25, 26, 35, 105]. Amplitude regeneration, before going for further transmission, prevents the translation of the amplitude noise to phase noise during transmission. On the other hand, when PPAR is located at the receiver, the effect of the amplitude regeneration is actually verified through the contribution of the amplitude noise on the output current of the balanced receiver [35].

In this section, PPAR of a 640 Gbit/s RZ-DPSK signal using a single-pump FOPA is demonstrated for the first time. The designed FOPA with a 10 nm saturated gain bandwidth with flatness better than 1 dB is used for amplification and PPAR of the 620 fs short OTDM signals. Regeneration is studied for degraded signals with different levels of input OSNR.

7.5.1 Degraded Input Signal

The regeneration is evaluated for signals with different OSNR levels to the FOPA. The clean and degraded input signal spectra to the FOPA, which are measured by an optical spectrum analyzer with 0.1 nm resolution bandwidth, are shown in Fig. 7.5. The OSNR was calculated by integration of the signal and noise powers over a 20 nm bandwidth, represented in yellow in Fig. 7.5, and normalizing the noise power to a 0.1 nm bandwidth reference

$$\mathrm{OSNR} = \frac{P_{signal}}{P_{noise} \times \frac{\Delta\nu_{ref.}}{\Delta\nu_{power}}} \tag{7.1}$$

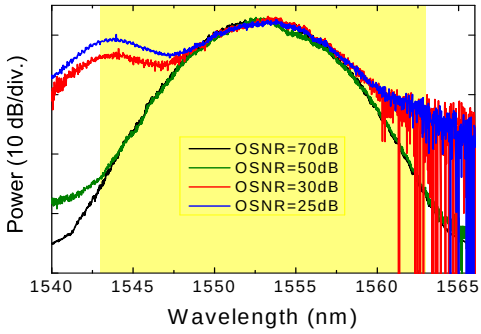

Figure 7.5: Spectra of the 640 Gbit/s OTDM signals input to the FOPA for different OSNRs. Yellow region: the bandwidth in which the OSNR is evaluated.

The clean signal corresponds to the case with no loaded noise and has an OSNR of 70 dB. Three levels of degradation are set at the input of the regenerator, corresponding to reduced OSNR values of 50 dB, 30 dB and 25 dB. For the highly degraded signals with 30 dB and 25 dB of OSNRs, output of a high-power EDFA is used as ASE source while for the lower levels a preamplifier EDFA is used resulting in differences mainly seen on the short-wavelength side of the signal spectra.

7.5.2 Bit-Error-Ratio Performance

Fig. 7.6 shows the results of BER measurements for the 10 Gbit/s demultiplexed signal as a function of the average received power (measured at the input of the demultiplexer). The back-to-back curve was measured for the noise-free signal when the pump was off and the input signal power to the HNLF was set to +5 dBm. The rest of the measurements are performed for channel number 2 with -17.1 dBm back-to-back sensitivity. When the signal is not regenerated, the input signal average power is set to -10 dBm and to +6 dBm for regeneration. The slightly degraded signal, with OSNR = 50 dB, shows almost no sensitivity difference (<0.3 dB) before and after regeneration, indicating that no regeneration is needed for this input OSNR level. When the input OSNR is reduced to 30 dB, the regeneration improves the received sensitivity by 2.2 dB, showing the effectiveness of the scheme at improving the quality of the degraded signal. For more degraded signals, i.e. OSNR = 25 dB, the distortion is too high to be regenerated and no error-free performance was possible.

The spectra measured at the output of the FOPA HNLF for the amplified clean signal, the degraded signal with OSNR = 30 dB and the corresponding regenerated signal are depicted in Fig. 7.7. Amplification of 13.3 dB has been measured for the regenerated signal.

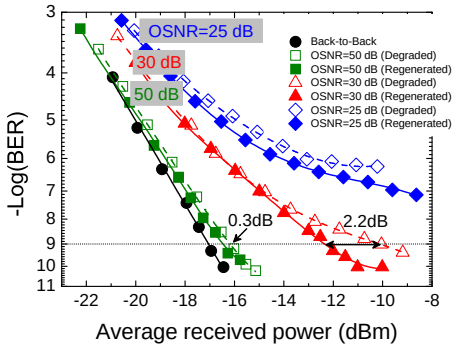

Figure 7.6: BER measurements for a 10 Gbit/s DPSK channel demultiplexed from the degraded 640 Gbit/s signal for different levels of input OSNR, as well as after regeneration.

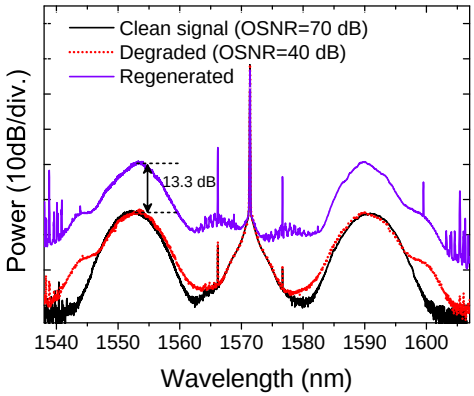

Figure 7.7: Output spectra of the FOPA for the amplified clean signal (OSNR=70 dB), degraded signal (OSNR=40 dB) and corresponding regenerated signal with 13.3 dB amplification.

7.6 All-Optical Regeneration of WDM Signals Based on FOPAs

This section describes the proposed idea in the invention [P-1]. This invention presents a novel scheme for AOR of high-capacity WDM channels based on a saturated single-pump FOPA. The author had her contribution in building the regenerator part of the proposed scheme. The implementation of the scheme is under realization currently at the High-Speed Communication Group, DTU Fotonik.

Unlike OTDM signals, WDM signals are parallel and regeneration

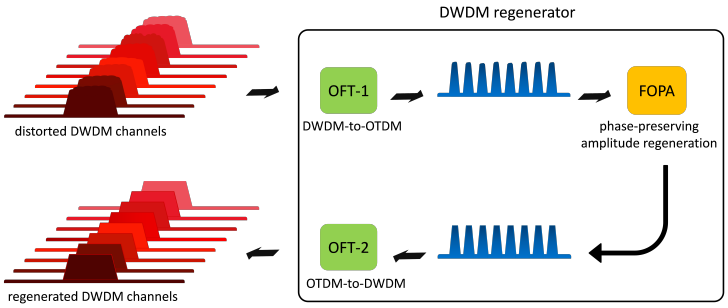

Figure 7.8: Basic principle of the DWDM regenerator using OFT-based DWDM-to-OTDM conversion and FOPA-based optical phase-preserving amplitude regeneration, followed by OFT-based OTDM-to-DWDM conversion.

of such signals, without splitting them up into individual wavelengths and allocating a regenerator to each WDM channel, is generally challenging. In order to avoid the inter-channel nonlinear interaction in a multi-channel WDM regenerator, different schemes have been demonstrated based on space-division multiplexing, bi-directional propagation, polarization multiplexing and time interleaving the WDM channels [106, 107, 108].

Contrary to parallel WDM channels, AOR of high-speed OTDM signals is less challenging as the data signals are serial and do not overlap in time, which allows FOPAs to see them independently. AOR for WDM channels is applicable after converting the parallel WDM channels into a serial OTDM signal as shown schematically in Fig. 7.8. WDM-to-OTDM conversion can be realized using different techniques. Using the optical Fourier transformation (OFT) technique, WDM-to-OTDM conversion has been demonstrated at high bit rates: a 640-Gbit/s OTDM signal has been mapped to 100 GHz WDM channel spaced grid [109] or even converted onto a 25 GHz dense WDM (DWDM) grid [110].

Based on the saturated-FOPA, PPAR for phase encoded signals can be achieved using this scheme. After regeneration, using a second unit of OTDM-to-WDM conversion [111] would enable converting back the serial OTDM signals to parallel WDM channels. The invention [P-1] proposes scheme for all-optical regeneration of DWDM data signals simultaneously without splitting them up in individual wavelength channels. The scheme allows for high capacity handling due to the ultra-fast operation of all the three involved units: an optical serializer (DWDM-to-OTDM), a FOPA-based AOR and an optical de-serializer (OTDM-to-DWDM).

7.7 Summary

In this chapter amplification and PPAR of a 640 Gbit/s RZ-DPSK OTDM signal in a single-pump FOPA has been demonstrated for the first time to our knowledge. The performance of the amplifier for different gain levels has been investigated. The effect of parametric gain saturation for the 620 fs interleaved pulses has been investigated by characterizing the effect of gain shaping. For the 6.5 nm FWHM spectrally broad signal, we found that the gain saturation manifests its effect through the shaping of the signal spectrum rather than through output average power, which typically stands for a monochromatic or spectrally narrow signals. Parametric amplification of the 640 Gbit/s RZ-DPSK signals was evaluated by BER characterization. Error-free performance with 15 dB net gain has been achieved with less than 1 dB power penalty, which was further reduced to almost no penalty when the gain was saturated by 1.7 dB.

PPAR has also been demonstrated for the 640 Gbit/s RZ-DPSK OTDM signal based on a gain optimized single-pump FOPA. For the degraded signal with 40 dB reduced OSNR, the receiver sensitivity has been improved by 2.2 dB by the regenerator, simultaneously providing 13.3 dB of gain.

Finally, the potential of the gain saturated FOPA for PPAR of DWDM systems has been discussed. Using the OFT technique and converting parallel DWDM channels into a serial OTDM signals, one would be able to regenerate multiple channel DWDM systems with DPSK and QPSK modulation formats.

Chapter 8

Conclusion

In this Ph.D. project, optical amplification and regeneration based on fiber optical parametric amplifiers (FOPAs) have been investigated for three signal regimes: continuous wave signals, few-picosecond short pulse trains and data-modulated signals up to 640 Gbit/s. The chapter summarizes the results and presents the outlook to some future works.

Gain saturated spectra in single- and dual-pump FOPAs the gain saturation behavior of single- and dual-pump FOPAs has been studied in chapter 3.

- In gain saturated single-pump FOPAs, an unexpected spectral asymmetry has been observed experimentally. Based on the comprehensive simulations, the resulting asymmetric gain spectrum has been found to be due to the effect of the third-order dispersion in strong saturation, where the output spectrum of the amplifier consists of a large number of generated higher-order FWM products (HFPs) which result in the formation of very short optical pulses. Interplay between the excited HFPs and the emitted dispersive waves (DWs) at the short-wavelength side of the spectrum results in faster saturation for that part of the gain spectrum. The simulations for a wide range of second- and third-order dispersion values reveal that dispersion plays an important role in the asymmetry feature of the saturated gain spectrum such that the asymmetry factor exhibits local maxima when the DWs overlap with the HFPs and shows a maximum for overlap with the first HFP (1HFP).

  In this study, the effect of the dispersion profile of the fiber on the conversion efficiency of HFPs has been studied while the nonlinear phase shift, $\gamma P_p L$, was considered as a fixed value. It means that, in our investigation 1) the amplification bandwidth has been

varied through changes in the dispersion terms of the highly nonlinear fiber (HNLF) and 2) the saturation level has been changed by the launched signal power to the HNLF. However, the amplification bandwidth and saturation level in FOPAs can be varied in a different manner, by altering the $\gamma P_p L$ term.

The amplification bandwidth can be tuned by the pump power, P_p, as well as the nonlinear coefficient, γ, which results in displacing the generated DWs' frequencies. For a fixed value of the signal input power, the saturation level can be altered by a change in any of the variables in the $\gamma P_p L$ term, which affects the frequency of the DWs as well as the asymmetry factor. Even though the asymmetric feature of the gain saturated single-pump FOPAs has been investigated for a fixed value of the $\gamma P_p L$ term, one would expect that the same conclusion would stand for the fixed dispersion term and varying the $\gamma P_p L$ term, due to the balance needed between the dispersion and nonlinearities for the phase-matching condition.

Apart from the fundamental study and insight one gains from the investigation of the saturation behavior in single-pump FOPAs, the characterization of the generated HFPs with optimum conversion efficiency can contribute in applications such as modulation format conversion and optical regeneration. Since the phase of the generated 1HFPs is the double of the signal phase, an m-level phase-shift keying (PSK) signal can be converted to an m/2-level PSK signal at the frequency of the 1HFP [112, 113]. Conversion of differential quadrature PSK (DQPSK) to differential PSK (DPSK) data at 10 and 160 Gbaud, and conversion of differential 8-level PSK (D8PSK) to DQPSK data at 40 Gbaud has been demonstrated using the 1HFPs [113]. Since the growth rate of the 1HFPs is faster than the signals, 1HFPs have more step-like power transfer function, which can be used for amplitude regeneration of intensity modulated signals [114, 96]. Therefore, knowledge about an efficient generation of 1HFPs based on the dispersion profile of the nonlinear medium, can contribute to the aforementioned applications.

- Dual-pump FOPAs in saturation have been studied in order to investigate their gain flatness in linear and saturated regime for short-pulse amplification and regeneration. The generation of HFPs in dual-pump FOPAs limits the applicable bandwidth for allocation of a signal with wide spectral width. In the saturation regime, when the signal is located between the two pumps in 1/3 of the pump frequency separation, the most powerful generated HFP falls

on the signal which strictly limits the operation bandwidth for the signal.

Pump-to-signal intensity modulation transfer in single-pump FOPAs The pump-to-signal intensity modulation transfer (IMT) in single-pump FOPAs has been numerically and experimentally studied in chapter 4, as one of the major noise sources in FOPAs. In contrast with previous researches, the IMT in single-pump FOPAs has been investigated in terms of the modulation frequency, its evolution along the fiber and its gain saturated behavior. The IMT is maximum and independent of the pump modulation frequency for low frequencies (less than about 50 GHz) and starts decreasing when the modulation period is comparable to the pump signal walk-off delay. The IMT cut-off frequency in single-pump FOPAs is about 100-200 GHz, which can be shifted depending on the value of the fiber dispersion parameters at the pump wavelength or the pump non-linear self-phase shift. In the case of low MFs, the IMT to the signal can be suppressed by operating in the gain saturation mode. With sufficiently large saturation, the IMT reaches its maximum value before the end of the HNLF. The largest reduction of IMT is for signal wavelengths around the maximum unsaturated gain. A large reduction of the IMT of more than 50% has been measured for a signal wavelength corresponding to the maximum unsaturated gain.

Fiber optical parametric chirped pulse amplification of picosecond and and sub-picosecond pulses Fiber optical parametric chirped pulse amplification (FOPCPA) has been experimentally studied for few picosecond and sub-picosecond short pulses in chapter 5.

- FOPCPA for different chirped signals in the linear and non-linear gain regime has been investigated for a few picosecond short pulses. The chirped pulses show different rates of broadening in transition from the linear to the non-linear regime. Pulse broadening depends on the initial pulsewidth, amount of chirp and accumulated dispersion in the amplifier. The shorter the pulsewidth, the faster the broadening. However the broadening rate can be slowed down if the pulse has a potential for compression based on its sign of chirp, and the accumulated dispersion acquired in the amplifier. The strongly chirped signals have higher saturation powers, which result in reduced pulse distortion for higher signal input powers. The amplified chirped signals in highly saturated amplifiers show excess distortion under the form of pedestals around the amplified signal after recompression.

- Amplification of short nearly transform-limited pulses of 9 nm bandwidth and 400 fs pulse duration has been demonstrated in a single-pump FOPA. The 400 fs pulses was first stretched to 50 ps, just enough to be at the limit of linear amplification, amplified by 26 dB in a fairly flat gain single-pump FOPA and then compressed back to 500 fs.

Single-pump FOPAs as in in-line amplifier Single-pump FOPAs are placed in a recirculating loop transmission in chapter 6 in order to investigate their performance as in-line amplifiers for 40 Gbit/s CSRZ-OOK and CSRZ-DPSK signals. Both modulation formats show error-free performance up to 320 km. The choice of CSRZ-DPSK signals allows to reduce the power penalty by 2.7 dB compared to CSRZ-OOK. Possible sources of impairments and possible ways to improve the performance of FOPAs as in-line amplifiers have also been discussed.

The performance of a single FOPA is comparable with a single erbium-doped fiber amplifier (EDFA). This point is promising for use of FOPAs as inline amplifiers for providing amplification outside the bandwidth of the EDFAs. To use FOPAs as in-line device, polarization-independent operation is needed to be considered. Pump-to-signal modulation transfer is the other limiting factor which needs to be controlled by choosing a narrow linewidth laser pump, properly filtering the pump wave and optimum operation for SBS threshold enhancement.

Parametric amplification and all-optical phase-preserving amplitude regeneration of a 640 Gbit/s RZ-DPSK signal Amplification and phase-preserving amplitude regeneration (PPAR) of a 640 Gbit/s RZ-DPSK optical time division multiplexed (OTDM) signal in a single-pump FOPA has been demonstrated in chapter 7.

- A gain-flattened single-pump FOPA has been designed for amplification and regeneration of pulses with 620 fs temporal and 6.5 nm spectral width. The performance of the amplifier for different gain levels has been investigated by characterizing the effect of gain shaping. It was found that for such temporally narrow pulses the gain saturation manifests its effect through the shaping of the signal spectrum rather than through the output average power which typically stands for a monochromatic or spectrally narrow signals. Error free performance with 15 dB net gain has been achieved with less than 1 dB power penalty, which was further reduced to almost no penalty when the gain was saturated by 1.7 dB.

- Based on the gain optimized single-pump FOPA, PPAR has been demonstrated for the 640 Gbit/s RZ-DPSK OTDM signal. For the degraded signal with 40 dB reduced OSNR, the receiver sensitivity has been improved by 2.2 dB by the regenerator, simultaneously providing 13.3 dB of gain.

- The potential of PPAR based on saturated FOPAs for dense wavelength division multiplexing (DWDM) channels has been discussed. Using optical Fourier transformation (OFT) technique and converting parallel DWDM into a single wavelength serial OTDM signal, one could regenerate the multichannel DWDM systems for DPSK and QPSK modulation formats.

Based on the designed flat gain single-pump FOPA, amplification of OTDM signals at Tbaud data rate is possible using polarization multiplexing combined width high spectral efficiency modulation formats, i.e. DQPSK and 16-QAM. As long as the amplifier operates in the unsaturated regime, amplification of amplitude, phase or combined phase and amplitude modulated signals can be safe in FOPAs. However the gain saturation may result in distortion for data modulated signals with multiple amplitude levels, i.e OOK and 16-QAM [115].

PPAR based on gain saturated FOPAs is suitable for phase modulated signals, i.e. for DPSK and DQPSK modulations, where all the bits have the same average power. The same design as the discussed regenerator can be used for DQPSK signals and thus double the handling capacity to 1.28 Tbit/s. PPAR for polarization-multiplexed signals may be achieved in a more complex setup using gain-saturated polarization independent FOPAs [60].

List of Acronyms

AOR	All-Optical Regeneration
ASE	Amplified Spontaneous Emission
BER	Bit-Error-Ratio
BPSK	Binary Phase-Shift Keyed
CFBG	Chirped Fiber Bragg Grating
CPA	Chirped-Pulse Amplification
CW	Continuous Wave
DPSK	Differential Phase-Shift Keying
DQPSK	Differential Phase-Shift Keying
DW	Dispersive Wave
DWDM	Dense Wavelength Division Multiplexing
EDFA	Erbium-Doped Fiber Amplifier
FOD	Forth-Order Dispersion
FOPCPA	Fiber Optical Parametric Chirped-Pulse Amplification
FWHM	Full Width at Half Maximum
FWM	Four-Wave Mixing
GVD	Group-Velocity Dispersion
HFP	Higher-Order FWM Product
HNLF	Highly-Nonlinear Fiber
IDF	Inverse Dispersion Fiber

IMT	Intensity Modulation Transfer
MF	Modulation Frequency
MI	Modulation Instability
NF	Noise Figure
NLSE	Nonlinear Schrödinger Equation
NZDSF	Non-Zero Dispersion Shifted Fiber
OBPF	Optical Band Pass Filter
OFT	Optical Fourier Transformation
OPCPA	Optical Parametric Chirped-Pulse Amplification
OSNR	Optical Signal-to-Noise Ratio
OTDM	Optical Time Division Multiplexed
PBS	Polarization Beam Splitter
PC	Polarization Controller
PCF	Photonic Crystal Fiber
PI-FOPA	Phase-Insensitive FOPA
PM	Phase Modulation
PMD	Polarization Mode Dispersion
PPAR	Phase-Preserving Amplitude Regeneration
PPLN	Periodically- Poled Lithium Niobate
PRBS	Pseudorandom Binary Sequence
PS-FOPA	Phase-Sensitive FOPA
PTDC	Parametric Tunable Dispersion Compensator
QAM	Quadrature-Amplitude Modulation
RF	Radio-Frequency
RIN	Relative Intensity Noise
RZ	Return-to-Zero

SBS	Stimulated Brillouin Scattering
SOD	Second-Order Dispersion
SOP	State of Polarization
SPM	Self-Phase Modulation
SRS	Stimulated Raman Scattering
SSFM	Split Step Fourier Method
SSMF	Standard Single-Mode Fiber
SVEA	Slowly Varying Envelope Approximation
THG	Third-Harmonic Generation
WDM	Wavelength Division Multiplexed
XPM	Cross-Phase Modulation
ZDW	Zero-Dispersion Wavelength

Bibliography

[1] R. Stolen, "Phase-matched-stimulated four-photon mixing in silica-fiber waveguides," *IEEE Journal of Quantum Electronics*, vol. 11, no. 3, pp. 100–103, 1975.

[2] K. K. Wong, K. Shimizu, K. Uesaka, G. Kalogerakis, M. E. Marhic, and L. G. Kazovsky, "Continuous-wave fiber optical parametric amplifier with 60-dB gain using a novel two-segment design," *IEEE Photonics Technology Letters*, vol. 15, no. 12, pp. 1707–1709, 2003.

[3] T. Torounidis, P. A. Andrekson, and B.-E. Olsson, "Fiber-optical parametric amplifier with 70-dB gain," *IEEE Photonics Technology Letters*, vol. 18, no. 10, pp. 1194–1196, 2006.

[4] T. Torounidis and P. Andrekson, "Broadband single-pumped fiber-optic parametric amplifiers," *IEEE Photonics Technology Letters*, vol. 19, no. 9, pp. 650–652, 2007.

[5] J. Boggio, S. Moro, E. Myslivets, J. R. Windmiller, N. Alic, and S. Radic, "155-nm continuous-wave two-pump parametric amplification," *IEEE Photonics Technology Letters*, vol. 21, no. 10, pp. 612–614, 2009.

[6] J. C. Boggio, C. Lundstrom, J. Yang, H. Sunnerud, and P. Andrekson, "Double-pumped fopa with 40 dB flat gain over 81 nm bandwidth," in *European Conference on Optical Communication*, 2008, p. Tu.3.B.5.

[7] Z. Tong, C. Lundström, P. Andrekson, C. McKinstrie, M. Karlsson, D. Blessing, E. Tipsuwannakul, B. Puttnam, H. Toda, and L. Grüner-Nielsen, "Towards ultrasensitive optical links enabled by low-noise phase-sensitive amplifiers," *Nature Photonics*, vol. 5, no. 7, pp. 430–436, 2011.

[8] J. L. Blows and S. E. French, "Low-noise-figure optical parametric amplifier with a continuous-wave frequency-modulated pump," *Optics Letters*, vol. 27, no. 7, pp. 491–493, 2002.

[9] K. Tanizawa, J. Kurumida, M. Takahashi, T. Yagi, and S. Namiki, "In-line polarization-insensitive parametric tunable dispersion compensator for WDM signals," *Journal of Lightwave Technology*, vol. 30, no. 11, pp. 1750–1756, 2012.

[10] M. Galili, E. Palushani, H. C. Hansen Mulvad, H. Hu, and L. K. Oxenløwe, "Wavelength preserving optical serial-to-parallel conversion," in *Optical Fiber Communication Conference*, 2013, p. OM2G.4.

[11] J. Boggio, A. Guimarães, F. Callegari, J. Marconi, M. Rocha, M. debarros, and H. Fragnito, "Parametric amplifier for mid-span phase conjugation with simultaneous compensation of fiber loss and chromatic dispersion at 10 Gb/s," *Microwave and Optical Technology Letters*, vol. 42, no. 6, pp. 503–505, 2004.

[12] B.-P. Kuo, E. Myslivets, A. O. Wiberg, S. Zlatanovic, C.-S. Brès, S. Moro, F. Gholami, A. Peric, N. Alic, and S. Radic, "Transmission of 640-Gb/s RZ-OOK channel over 100-km SSMF by wavelength-transparent conjugation," *Journal of Lightwave Technology*, vol. 29, no. 4, pp. 516–523, 2011.

[13] J. Hansryd and P. A. Andrekson, "O-TDM demultiplexer with 40-dB gain based on a fiber optical parametric amplifier," *IEEE Photonics Technology Letters*, vol. 13, no. 7, pp. 732–734, 2001.

[14] G.-W. Lu, K. Abedin, T. Miyazaki, and M. Marhic, "RZ-DPSK OTDM demultiplexing using fibre optical parametric amplifier with clock-modulated pump," *Electronics letters*, vol. 45, no. 4, pp. 221–222, 2009.

[15] Y. Liang, Y. Zhou, P. C. Chui, and K. K. Wong, "160-Gb/s OTDM de-multiplexing based on a pulsed pump optical parametric amplifier," in *Optical Fiber Communication Conference*, 2009, p. OMH3.

[16] C. Schubert, S. Diez, J. Berger, R. Ludwig, U. Feiste, H. Weber, G. Toptchiyski, K. Petermann, and V. Krajinovic, "160-Gb/s all-optical demultiplexing using a gain-transparent ultrafast-nonlinear interferometer (GT-UNI)," *IEEE Photonics Technology Letters*, vol. 13, no. 5, pp. 475–477, 2001.

[17] T. Torounidis, M. Westlund, H. Sunnerud, B. Olsson, and P. Andrekson, "Signal generation and transmission at 40, 80, and 160 Gb/s using a fiber-optical parametric pulse source," *IEEE Photonics Technology Letters*, vol. 17, no. 2, pp. 312–314, 2005.

[18] A. Vedadi, A. M. Ariaei, M. M. Jadidi, J. A. Salehi *et al.*, "Theoretical study of high repetition rate short pulse generation with fiber optical parametric amplification," *Journal of Lightwave Technology*, vol. 30, no. 9, pp. 1263–1268, 2012.

[19] A. Vedadi, M. A. Shoaie, C.-S. Brès *et al.*, "Near-nyquist optical pulse generation with fiber optical parametric amplification," *Optics Express*, vol. 20, no. 26, pp. B558–B565, 2012.

[20] X. Wang, J. Xu, and K. K. Wong, "All-optical 3R regeneration using fiber optical parametric oscillator and amplifier," in *National Fiber Optic Engineers Conference*, 2012, p. JW2A.80.

[21] K. Inoue, "Optical level equalisation based on gain saturation in fibre optical parametric amplifier," *Electronics Letters*, vol. 36, no. 12, pp. 1016–1017, 2000.

[22] K. Inoue and T. Mukai, "Experimental study on noise characteristics of a gain-saturated fiber optical parametric amplifier," *Journal of Lightwave Technology*, vol. 20, no. 6, p. 969, 2002.

[23] J. P. Gordon and L. F. Mollenauer, "Phase noise in photonic communications systems using linear amplifiers," *Optics Letters*, vol. 15, no. 23, pp. 1351–1353, 1990.

[24] C. Peucheret, M. Lorenzen, J. Seoane, D. Noordegraaf, C. V. Nielsen, L. Gruner-Nielsen, and K. Rottwitt, "Amplitude regeneration of RZ-DPSK signals in single-pump fiber-optic parametric amplifiers," *IEEE Photonics Technology Letters*, vol. 21, no. 13, pp. 872–874, 2009.

[25] X. Guo, K. P. Lei, X. Fu, H. K. Tsang, and C. Shu, "Amplitude regeneration of 80-Gb/s polarization-multiplexed RZ-DPSK signals in a dual-orthogonal-pump fiber optical parametric amplifier," in *Optical Fiber Communication Conference*, 2013, p. OTu2D.1.

[26] F. Futami, R. Okabe, S. Ono, S. Watanabe, R. Ludwig, C. Schmidt-Langhorst, and C. Schubert, "All-optical amplitude noise suppression of 160-Gb/s OOK and DPSK data signals using a parametric fiber switch," in *Optical Fiber Communication Conference*, 2007, p. OThB3.

[27] M. Matsumoto, "Optical parametric regeneration for phase-modulated signals," in *Conference on Lasers and Electro-Optics*, 2011, p. CWD3.

[28] R. Slavík, F. Parmigiani, J. Kakande, C. Lundström, M. Sjödin, P. A. Andrekson, R. Weerasuriya, S. Sygletos, A. D. Ellis, L. Grüner-Nielsen *et al.*, "All-optical phase and amplitude regenerator for next-generation telecommunications systems," *Nature Photonics*, vol. 4, no. 10, pp. 690–695, 2010.

[29] J. Kakande, A. Bogris, R. Slavík, F. Parmigiani, D. Syvridis, P. Petropoulos, and D. J. Richardson, "First demonstration of all-optical QPSK signal regeneration in a novel multi-format phase sensitive amplifier," in *European Conference on Optical Communication*, 2010, p. PD3.3.

[30] J. Kakande, A. Bogris, R. Slavík, F. Parmigiani, D. Syvridis, P. Petropoulos, D. Richardson, M. Westlund, and M. Sköld, "QPSK phase and amplitude regeneration at 56 Gbaud in a novel idler-free non-degenerate phase sensitive amplifier," in *Optical Fiber Communication Conference*, 2011, p. OMT4.

[31] S. Petit, T. Kurosu, M. Takahashi, T. Yagi, and S. Namiki, "Low penalty uniformly tunable wavelength conversion without spectral inversion over 30 nm using SBS-suppressed low-dispersion-slope highly nonlinear fibers," *IEEE Photonics Technology Letters*, vol. 23, no. 9, pp. 546–548, 2011.

[32] S. Namiki, "Wide-band and -range tunable dispersion compensation through parametric wavelength conversion and dispersive optical fibers," *Journal of Lightwave Technology*, vol. 26, no. 1, pp. 28–35, 2008.

[33] Y. Zhou, B. P. Kuo, K. Cheung, S. Yang, P. Chui, and K. Wong, "Wide-band generation of picosecond pulse using fiber optical parametric amplifier and oscillator," *IEEE Journal of Quantum Electronics*, vol. 45, no. 11, pp. 1350–1356, 2009.

[34] M. Gao, J. Kurumida, and S. Namiki, "43-Gb/s operation of wavelength-tunable optical parametric regenerator," *IEEE Photonics Technology Letters*, vol. 23, no. 11, pp. 718–720, 2011.

[35] ——, "Wavelength-tunable optical parametric regenerator," *Optics Letters*, vol. 35, no. 20, pp. 3468–3470, 2010.

[36] G. P. Agrawal, *Nonlinear Fiber Optics*, 3rd ed. Academic Press, 2006.

[37] M. Hirano, T. Nakanishi, T. Okuno, and M. Onishi, "Silica-based highly nonlinear fibers and their application," *IEEE Journal of Selected Topics in Quantum Electronics*, vol. 15, no. 1, pp. 103–113, 2009.

[38] K. Tai, A. Hasegawa, and A. Tomita, "Observation of modulational instability in optical fibers," *Physical Reviewe Letters*, vol. 56, no. 2, pp. 135–138, 1986.

[39] A. Hasegawa, "Generation of a train of soliton pulses by induced modulational instability in optical fibers," *Optics Letters*, vol. 9, no. 7, pp. 288–290, Jul 1984.

[40] A. M. Heidt, "Efficient adaptive step size method for the simulation of supercontinuum generation in optical fibers," *Journal of Lightwave Technology*, vol. 27p, no. 18, pp. 3984–3991, 2009.

[41] O. V. Sinkin, R. Holzlöhner, J. Zweck, and C. R. Menyuk, "Optimization of the split-step fourier method in modeling optical-fiber communications systems," *Journal of lightwave technology*, vol. 21, no. 1, p. 61, 2003.

[42] M. Karlsson, "Four-wave mixing in fibers with randomly varying zero-dispersion wavelength," *Journal of the Optical Society of America B: Optical Physics*, vol. 15, no. 8, pp. 2269–2275, 1998.

[43] N. Dahdah, D. S. Govan, M. Jamshidifar, N. J. Doran, and M. E. Marhic, "Fiber optical parametric amplifier performance in a 1-Tb/s DWDM communication system," *IEEE Journal of Selected Topics in Quantum Electronics*, vol. 18, no. 2, pp. 950–957, 2012.

[44] M. Marhic, A. Rieznik, and H. Fragnito, "Investigation of the gain spectrum near the pumps of two-pump fiber-optic parametric amplifiers," *Journal of the Optical Society of America B: Optical Physics*, vol. 25, no. 1, pp. 22–30, 2008.

[45] K. Shiraki, M. Ohashi, and M. Tateda, "Suppression of stimulated brillouin scattering in a fibre by changing the core radius," *Electronics letters*, vol. 31, no. 8, pp. 668–669, 1995.

[46] J. Hansryd, F. Dross, M. Westlund, P. Andrekson, and S. Knudsen, "Increase of the sbs threshold in a short highly nonlinear fiber

by applying a temperature distribution," *Journal of lightwave technology*, vol. 19, no. 11, pp. 1691–1697, 2001.

[47] M. Ohashi and M. Tateda, "Design of strain-free-fiber with nonuniform dopant concentration for stimulated brillouin scattering suppression," *Lightwave Technology, Journal of*, vol. 11, no. 12, pp. 1941–1945, 1993.

[48] N. Yoshizawa and T. Imai, "Stimulated brillouin scattering suppression by means of applying strain distribution to fiber with cabling," *Lightwave Technology, Journal of*, vol. 11, no. 10, pp. 1518–1522, 1993.

[49] M. Takahashi, M. Tadakuma, and T. Yagi, "Dispersion and brillouin managed hnlfs by strain control techniques," *Journal of Lightwave Technology*, vol. 28, no. 1, pp. 59–64, 2010.

[50] D. Cotter, "Transient stimulated brillouin scattering in long single-mode fibres," *Electronics Letters*, vol. 18, no. 12, pp. 504–506, 1982.

[51] A. Kobyakov, S. Kumar, D. Q. Chowdhury, A. B. Ruffin, M. Sauer, S. R. Bickham, and R. Mishra, "Design concept for optical fibers with enhanced sbs threshold," *Opt. Express*, vol. 13, no. 14, pp. 5338–5346, 2005.

[52] L. Grüner-Nielsen, D. Jakobsen, S. Herstrøm, B. Pálsdóttir, S. Dasgupta, D. Richardson, C. Lundström, S. L. Olsson, and P. A. Andrekson, "Brillouin suppressed highly nonlinear fibers," in *European Conference on Optical Communication*, 2012, p. We.1.F.1.

[53] C. Lundstrom, R. Malik, L. Gruner-Nielsen, B. Corcoran, S. Olsson, M. Karlsson, and P. A. Andrekson, "Fiber optic parametric amplifier with 10 dB net gain without pump dithering," *IEEE Photonics Technology Letters*, vol. 25, no. 3, pp. 234–237, 2013.

[54] A. Durecu-Legrand, A. Mussot, C. Simonneau, D. Bayart, T. Sylvestre, E. Lantz, and H. Maillotte, "Impact of pump phase modulation on system performance of fibre-optical parametric amplifiers," *Electronics Letters*, vol. 41, no. 6, pp. 350–352, 2005.

[55] Q. Lin and G. P. Agrawal, "Vector theory of four-wave mixing: polarization effects in fiber-optic parametric amplifiers," *Journal of the Optical Society of America B: Optical Physics*, vol. 21, no. 6, pp. 1216–1224, 2004.

[56] T. Hasegawa, K. Inoue, and K. Oda, "Polarization independent frequency conversion by fiber four-wave mixing with a polarization diversity technique," *IEEE Photonics Technology Letters*, vol. 5, no. 8, pp. 947–949, 1993.

[57] K. K. Wong, M. E. Marhic, K. Uesaka, and L. G. Kazovsky, "Polarization-independent one-pump fiber-optical parametric amplifier," *IEEE Photonics Technology Letters*, vol. 14, no. 11, pp. 1506–1508, 2002.

[58] ——, "Polarization-independent two-pump fiber optical parametric amplifier," *IEEE Photonics Technology Letters*, vol. 14, no. 7, pp. 911–913, 2002.

[59] T. Richter, R. Elschner, A. Gandhe, K. Petermann, and C. Schubert, "Parametric amplification and wavelength conversion of single-and dual-polarization DQPSK signals," *IEEE Journal of Selected Topics in Quantum Electronics*, vol. 18, no. 2, pp. 988–995, 2012.

[60] S. Watanabe, F. Futami, R. Okabe, T. Kato, R. Ludwig, C. Schmidt-Langhorst, and C. Schubert, "Polarization-independent all-optical amplitude limiter using two-stage gain-saturated fiber parametric amplifiers," in *OptoElectronics and Communications Conference*, 2009, p. TuD3.

[61] P. Kylemark, H. Sunnerud, M. Karlsson, and P. A. Andrekson, "Semi-analytic saturation theory of fiber optical parametric amplifiers," *Journal of Lightwave Technology*, vol. 24, no. 9, pp. 3471–3479, 2006.

[62] K. Inoue and T. Mukai, "Signal wavelength dependence of gain saturation in a fiber optical parametric amplifier," *Optics Letters*, vol. 26, no. 1, pp. 10–12, 2001.

[63] N. Akhmediev, M. Karlsson *et al.*, "Cherenkov radiation emitted by solitons in optical fibers," *Physical Review A*, vol. 51, no. 3, pp. 2602–2607, 1995.

[64] A. K. Abeeluck and C. Headley, "Continuous-wave pumping in the anomalous-and normal-dispersion regimes of nonlinear fibers for supercontinuum generation," *Optics Express*, vol. 30, no. 1, pp. 61–63, 2005.

[65] M. Droques, B. Barviau, A. Kudlinski, M. Taki, A. Boucon, T. Sylvestre, and A. Mussot, "Symmetry-breaking dynamics of the modulational instability spectrum," *Optics Letters*, vol. 36, no. 8, pp. 1359–1361, 2011.

[66] K. Inoue and T. Mukai, "Spectral hole in the amplified spontaneous emission spectrum of a fiber optical parametric amplifier," *Optics Letters*, vol. 26, no. 12, pp. 869–871, 2001.

[67] J. L. Blows and P.-f. Hu, "Cross-talk-induced limitations of two-pump optical fiber parametric amplifiers," *Journal of the Optical Society of America B: Optical Physics*, vol. 21, no. 5, pp. 989–995, 2004.

[68] G. Kalogerakis, M. E. Marhic, and L. G. Kazovsky, "Multiple-wavelength conversion with gain by a high-repetition-rate pulsed-pump fiber opa," *Journal of Lightwave Technology*, vol. 23, no. 10, p. 2954, 2005.

[69] G. Kalogerakis, K. Shimizu, M. E. Marhic, K.-Y. Wong, K. Uesaka, and L. G. Kazovsky, "High-repetition-rate pulsed-pump fiber opa for amplification of communication signals," *Journal of Lightwave Technology*, vol. 24, no. 8, pp. 3021–3027, 2006.

[70] Z. Tong, A. Bogris, M. Karlsson, and P. A. Andrekson, "Full characterization of the signal and idler noise figure spectra in single-pumped fiber optical parametric amplifiers," *Optics Express*, vol. 18, no. 3, pp. 2884–2893, 2010.

[71] P. Kylemark, M. Karlsson, and P. A. Andrekson, "Gain and wavelength dependence of the noise-figure in fiber optical parametric amplification," *IEEE Photonics Technology Letters*, vol. 18, no. 11, pp. 1255–1257, 2006.

[72] M. E. Marhic, G. Kalogerakis, K. K.-Y. Wong, and L. G. Kazovsky, "Pump-to-signal transfer of low-frequency intensity modulation in fiber optical parametric amplifiers," *Journal of Lightwave Technology*, vol. 23, no. 3, p. 1049, 2005.

[73] F. Yaman, Q. Lin, G. P. Agrawal, and S. Radic, "Pump-noise transfer in dual-pump fiber-optic parametric amplifiers: Walk-off effects," *Optics Letters*, vol. 30, no. 9, pp. 1048–1050, 2005.

[74] P. Kylemark, P. O. Hedekvist, H. Sunnerud, M. Karlsson, and P. A. Andrekson, "Noise characteristics of fiber optical parametric

amplifiers," *Journal of Lightwave Technology*, vol. 22, no. 2, p. 409, 2004.

[75] D. Strickland and G. Mourou, "Compression of amplified chirped optical pulses," *Optics Communications*, vol. 55, no. 6, pp. 447–449, 1985.

[76] A. Dubietis, G. Jonušauskas, and A. Piskarskas, "Powerful femtosecond pulse generation by chirped and stretched pulse parametric amplification in BBO crystal," *Optics Communications*, vol. 88, no. 4, pp. 437–440, 1992.

[77] A. Dubietis, R. Butkus, and A. P. Piskarskas, "Trends in chirped pulse optical parametric amplification," *IEEE Journal of Selected Topics in Quantum Electronics*, vol. 12, no. 2, pp. 163–172, 2006.

[78] M. Hanna, F. Druon, P. Georges *et al.*, "Fiber optical parametric chirped-pulse amplification in the femtosecond regime," *Optics Express*, vol. 14, no. 7, pp. 2783–2790, 2006.

[79] C. Caucheteur, D. Bigourd, E. Hugonnot, P. Szriftgiser, A. Kudlinski, M. Gonzalez-Herraez, and A. Mussot, "Experimental demonstration of optical parametric chirped pulse amplification in optical fiber," *Optics Letters*, vol. 35, no. 11, pp. 1786–1788, 2010.

[80] D. Bigourd, L. Lago, A. Kudlinski, E. Hugonnot, and A. Mussot, "Dynamics of fiber optical parametric chirped pulse amplifiers," *Journal of the Optical Society of America B: Optical Physics*, vol. 28, no. 11, pp. 2848–2854, 2011.

[81] Y. Zhou, Q. Li, K. K. Cheung, S. Yang, P. Chui, and K. K. Wong, "All-fiber-based ultrashort pulse generation and chirped pulse amplification through parametric processes," *IEEE Photonics Technology Letters*, vol. 22, no. 17, pp. 1330–1332, 2010.

[82] M. E. Marhic, *Fiber optical parametric amplifiers, oscillators and related devices.* Cambridge University Press, 2008.

[83] C. Manzoni, J. Moses, F. X. Kärtner, and G. Cerullo, "Excess quantum noise in optical parametric chirped-pulse amplification," *Optics Express*, vol. 19, no. 9, pp. 8357–8366, 2011.

[84] H. Hansen Mulvad, L. Oxenlwe, M. Galili, A. Clausen, L. Gruner-Nielsen, and P. Jeppesen, "1.28 Tbit/s single-polarisation serial OOK optical data generation and demultiplexing," *Electronics Letters*, vol. 45, no. 5, pp. 280–281, 2009.

[85] H. H. Mulvad, M. Galili, L. K. Oxenløwe, H. Hu, A. T. Clausen, J. B. Jensen, C. Peucheret, and P. Jeppesen, "Demonstration of 5.1 Tbit/s data capacity on a single-wavelength channel," *Optics Express*, vol. 18, no. 2, pp. 1438–1443, 2010.

[86] T. Richter, E. Palushani, C. Schmidt-Langhorst, R. Ludwig, L. Molle, M. Nolle, and C. Schubert, "Transmission of single-channel 16-QAM data signals at terabaud symbol rates," *Journal of Lightwave Technology*, vol. 30, no. 4, pp. 504–511, 2012.

[87] M. Gao, J. Kurumida, and S. Namiki, "Wide range operation of regenerative optical parametric wavelength converter using ASE-degraded 43-Gb/s RZ-DPSK signals," *Optics Express*, vol. 19, no. 23, pp. 23 258–23 270, 2011.

[88] B. Corcoran, S. L. Olsson, C. Lundstrom, M. Karlsson, and P. Andrekson, "Phase-sensitive optical pre-amplifier implemented in an 80km DQPSK link," in *Optical Fiber Communication Conference*, 2012, p. PDPA5A.4.

[89] M. Matsumoto and K. Sanuki, "Performance improvement of DPSK signal transmission by a phase-preserving amplitude limiter," *Optics Express*, vol. 15, no. 13, pp. 8094–8103, 2007.

[90] S. L. Olsson, B. Corcoran, C. Lundström, M. Sjödin, M. Karlsson, and P. A. Andrekson, "Phase-sensitive amplified optical link operating in the nonlinear transmission regime," in *European Conference on Optical Communication*, 2012, p. Th.2.F.1.

[91] M. Jamshidifar, A. Vedadi, and M. E. Marhic, "Reduction of four-wave-mixing crosstalk in a short fiber-optical parametric amplifier," *IEEE Photonics Technology Letters*, vol. 21, no. 17, pp. 1244–1246, 2009.

[92] R. Elschner, T. Richter, and C. Schubert, "Characterization of FWM-induced crosstalk for WDM operation of a fiber-optical parametric amplifier," in *European Conference on Optical Communications*, 2011, p. Mo.1.A.2.

[93] P. Mamyshev, "All-optical data regeneration based on self-phase modulation effect," in *European Conference on Optical Communication*, vol. 1, 1998, pp. 475–476.

[94] M. Matsumoto, "A fiber-based all-optical 3R regenerator for DPSK signals," *IEEE Photonics Technology Letters*, vol. 19, no. 5, pp. 273–275, 2006.

[95] S. Radic, C. McKinstrie, R. Jopson, J. Centanni, and A. Chraplyvy, "All-optical regeneration in one-and two-pump parametric amplifiers using highly nonlinear optical fiber," *IEEE Photonics Technology Letters*, vol. 15, no. 7, pp. 957–959, 2003.

[96] N. M. Shah and M. Matsumoto, "2R regeneration of time-interleaved multiwavelength signals based on higher order four-wave mixing in a fiber," *IEEE Photonics Technology Letters*, vol. 22, no. 1, pp. 27–29, 2010.

[97] T. Richter, R. Ludwig, J. Fischer, S. Watanabe, R. Okabe, T. Kato, and C. Schubert, "All-optical level equalization of data packets using a fiber-optic parametric amplifier," in *European Conference on Optical Communication*, 2010, p. We.8.A.7.

[98] L. M. Jones, F. Parmigiani, V. Rancano, M. A. Ettabib, P. Petropoulos, and D. J. Richardson, "Transmission performance of phase-preserving amplitude regenerator based on optical injection locking," in *Optical Fiber Communication Conference*, 2013, p. OW4C.4.

[99] C. Porzi, G. Serafino, A. Bogoni, and G. Contestabile, "All-optical regeneration of 40 Gb/s NRZ-DPSK signals in a single SOA," in *National Fiber Optic Engineers Conference*, 2013, p. JW2A.55.

[100] A. Bogoni, X. Wu, S. R. Nuccio, and A. E. Willner, "640 Gb/s all-optical regenerator based on a periodically poled lithium niobate waveguide," *Journal of Lightwave Technology*, vol. 30, no. 12, pp. 1829–1834, 2012.

[101] J. Wang, H. Ji, H. Hu, J. Yu, H. C. Hansen Mulvad, M. Galili, E. Palushani, P. Jeppesen, W. Wang, and L. K. Oxenløwe, "Simultaneous regeneration of 4×160-Gbit/s WDM and PDM channels in a single highly nonlinear fiber," in *Optical Fiber Communication Conference*, 2013, p. OW4C.7.

[102] J. Hansryd, P. A. Andrekson, M. Westlund, J. Li, and P.-O. Hedekvist, "Fiber-based optical parametric amplifiers and their applications," *IEEE Journal of Selected Topics in Quantum Electronics*, vol. 8, no. 3, pp. 506–520, 2002.

[103] M. Matsumoto, "Nonlinear phase noise reduction of DPSK signals by an all-optical amplitude limiter using fwm in a fiber," in *European Conference on Optical Communication*, 2006, p. Tu1.3.5.

[104] D. Endres, C. Stephan, K. Sponsel, G. Onishchukov, B. Schmauss, and G. Leuchs, "Experimental comparison of all-optical phase-preserving amplitude regeneration techniques," in *International Conference on Transparent Optical Networks*, 2010, p. Th.A1.6.

[105] G. K. Lei, C. Shu, and H. Tsang, "Amplitude noise reduction, pulse format conversion, and wavelength multicast of PSK signal in a fiber optical parametric amplifier," in *National Fiber Optic Engineers Conference*, 2012, p. JW2A.79.

[106] L. Provost, P. Petropoulos, and D. J. Richardson, "Optical WDM regeneration: status and future prospects," in *Optical Fiber Communication Conference*, 2009, p. OWD7.

[107] P. G. Patki, M. Vasilyev, and T. I. Lakoba, "Multichannel all-optical regeneration," in *IEEE Photonics Society Summer Topical Meeting Series*. IEEE, 2010, pp. 172–173.

[108] F. Parmigiani, L. Provost, P. Petropoulos, D. J. Richardson, W. Freude, J. Leuthold, A. D. Ellis, and I. Tomkos, "Progress in multichannel all-optical regeneration based on fiber technology," *IEEE Journal of Selected Topics in Quantum Electronics*, vol. 18, no. 2, pp. 689–700, 2012.

[109] E. Palushani, H. H. Mulvad, M. Galili, H. Hu, L. Oxenlowe, A. T. Clausen, and P. Jeppesen, "OTDM-to-WDM conversion based on time-to-frequency mapping by time-domain optical fourier transformation," *IEEE Journal of Selected Topics in Quantum Electronics*, vol. 18, no. 2, pp. 681–688, 2012.

[110] H. C. H. Mulvad, E. Palushani, H. Hu, H. Ji, M. Lillieholm, M. Galili, A. Clausen, M. Pu, K. Yvind, J. M. Hvam *et al.*, "Ultra-high-speed optical serial-to-parallel data conversion by time-domain optical fourier transformation in a silicon nanowire," *Optics Express*, vol. 19, no. 26, 2011.

[111] H. H. Mulvad, H. Hu, M. Galili, H. Ji, E. Palushani, A. Clausen, L. Oxenlowe, and P. Jeppesen, "DWDM-to-OTDM conversion by time-domain optical fourier transformation," in *European Conference on Optical Communication*, 2011, p. Mo.1.A.

[112] G.-W. Lu and T. Miyazaki, "Optical phase erasure based on FWM in HNLF enabling format conversion from 320-Gb/s RZDQPSK to 160-Gb/s RZ-DPSK," *Optics Express*, vol. 17, no. 16, pp. 13 346–13 353, 2009.

[113] G.-W. Lu, E. Tipsuwannakul, T. Miyazaki, C. Lundstrom, M. Karlsson, and P. A. Andrekson, "Format conversion of optical multilevel signals using FWM-based optical phase erasure," *Journal of Lightwave Technology*, vol. 29, no. 16, pp. 2460–2466, 2011.

[114] C. Ito, I. Monfils, and J. Cartledge, "All-optical 3R regeneration using higher-order four-wave mixing in a highly nonlinear fiber with a clock-modulated optical pump signal," in *IEEE Lasers and Electro-Optics Society Annual Meeting*. IEEE, 2006, p. TuH2.

[115] F. D. Ros, R. Borkowski, D. Zibar, and C. Peucheret, "Impact of gain saturation on the parametric amplification of 16-QAM signals," in *European Conference on Optical Communication*. Optical Society of America, 2012, p. We.2.A.3.

ISBN: 978-87-93089-28-0

Published by:
DTU Fotonik
Department of Photonic Engineering
Technical University of Denmark
Ørsteds Plads, building 343
DK-2800 Kgs. Lyngby

Zohreh Lali-Dastjerdi was born in Isfahan, Iran in 1980. She received the Bachelor of Science in Physics, major in Solid State, from Shahid Chamran University, Ahvaz, Iran in 2003 and the Master of Science degree in Physics, major in Laser, from Vali-e-Asr University of Rafsanjan, Iran in 2006. She worked as an instructor at Basic Sciences Group of Azad University, Shoushtar, Iran for three years. In April 2010 she joined the High-Speed Optical Communications Group at DTU Fotonik, Department of Photonics Engineering, Technical University of Denmark as a Ph.D. Student. Her Ph.D. project has been supervised by Prof. Christophe Peucheret, Prof. Karsten Rottwitt and Assoc. Prof. Michael Galili.

The Ph.D. project has been accomplished in June 2013 and the thesis has been defended on 27th of August 2013. The evaluation committee consisted of Prof. Peter Andrekson (Chalmers University of Technology, Sweden), Assoc. Prof. Arnaud Mussot (University Lille 1, France) and Assoc. Prof. Jesper Lægsgaard (DTU Fotonik).